DEVELOPMENT OF A NOVEL ORTHOPEDIC MICROFASTENER

A Thesis

by

MUKUL MUKUND AGNIHOTRI

Submitted to the Office of Graduate Studies of
Texas A&M University
in partial fulfillment of the requirements for the degree of

MASTER OF SCIENCE

December 2005

Major Subject: Mechanical Engineering

DEVELOPMENT OF A NOVEL ORTHOPEDIC MICROFASTENER

A Thesis

by

MUKUL MUKUND AGNIHOTRI

Submitted to the Office of Graduate Studies of
Texas A&M University
in partial fulfillment of the requirements for the degree of

MASTER OF SCIENCE

Approved by:

Co-Chairs of Committee,	Wayne N.P. Hung
	Terry Creasy
Committee Member,	Jyhwen Wang
Department Head,	Dennis O'Neal

December 2005

Major Subject: Mechanical Engineering

ABSTRACT

Development of a Novel Orthopedic Microfastener. (December 2005)

Mukul Mukund Agnihotri, B.Eng., University of Pune

Co-Chairs of Advisory Committee: Dr. Wayne N.P. Hung
Dr. Terry Creasy

Over the last decade, biodegradable screws and plates have received wide acceptance over metallic fasteners for orthopedic fracture fixation. A biodegradable fastener would gradually "disappear" during healing of a fractured bone or tissues, therefore avoiding a secondary operation to remove that fastener. When using a metal fastener, the current approach requires manual threading on a large bone fragment for fixation. This technique is difficult when it is required to fixate a small bone fragment. This study puts forth the development of a threadless, polymer based orthopedic fastener for small fragment fixation which would provide stability and interfragmental compression to the fracture site.

The fastener was designed with ratchets on its surface, which deflect during insertion into the drilled hole in the bone and subsequently stiffen to hold the bone fragments in place due to interference. The head of the fastener was developed analogous to a Belleville washer which deflects during insertion of the fastener and subjects the bone fragments to interfragmental compression. Finite element analysis (FEA) was conducted to design the fastener profile and assess its performance. The push-in and pull-out forces predicted by FEA were comparable to the experimental results for the prototype of the microfasteners. The push-in force was found to increase with increasing insertion depth and radial interference. The force required to initiate pull-out was maximum and was reduced with reducing fastener bone contact. An analytical model was proposed to explain the fastener bone interaction. It was found to be in good agreement with the FEA and experimental results at low levels of interference.

To my loving parents.

ACKNOWLEDGMENTS

I would like to express my sincere gratitude towards my advisor, Dr. Wayne Hung for providing me with invaluable guidance and motivation towards the successful culmination of this thesis. I appreciate the time and effort he has put into my research.

I take this opportunity to thank Dr. Jyhwen Wang for serving on my thesis committee. His knowledge and experience in finite element analysis helped a lot in getting me started with the initial stages of my research. I would also like to thank Dr. Terry Creasy for serving on my thesis committee and for permitting me to use his materials testing laboratory.

I am grateful to Dr. Angie Hill Price for providing me access to the materials testing laboratory and the profilometer for my experiments. I acknowledge Mr. Jim Sajewski at Mechanical Engineering, Mr. Frank Cervantez and Mr. John Macek at Engineering Technology for being ever ready to help out with any technical needs.

I am fortunate to be a part of a great group here at MnM lab. I would sincerely like to thank Mr. Clinton Loggins and Ms. Meagan Makarenko for helping out with development of the fastener prototype. I am thankful to Mr. Amol Dixit, Mr. Balaji Varadharajan and Mr. Mitul Kothari for making this endeavor a memorable one.

TABLE OF CONTENTS

LIST OF FIGURES

LIST OF TABLES

LIST OF SYMBOLS

b	width of spring
b_R	width of ratchet
c	elastic region of spring cross-section
d	shift in center of gravity of spring cross-section
h	thickness of spring
h_R	thickness of ratchet
l	length of spring along centroidal plane
l_R	length of ratchet along centroidal plane
m	dimensionless moment
m^*	maximum dimensionless moment
n	dimensionless axial force
r	radius of hole, $(\varnothing_{hole})/2$
r^f_i	base radius of the fastener
r^f_o	outer radius of the fastener
r_o	outer radius of hub, $(\varnothing_o)/2$
$\underline{u}$	displacement vector
x_i	radius of slot in bone
x_o	outer radius of bone
x'	$r^f_i + h_R$
x''	intermediate radius of fastener in the Region AC
y	tip displacement of spring
E	Young's modulus
E_1	elastic modulus of pin
E_2	Young's modulus of material of hub
G	shear modulus
F	reaction provided by bone to the spring
F_r	friction force

F_R transverse reaction provided by bone to the ratchet

F_S total spring force

L   length of interference

M   moment acting at spring tip

M_e moment required for yielding

M_{max} maximum moment acting at root of spring

N   axial component of reaction F

N_e axial force required for yielding

P   transverse component of reaction F

P_i interference pressure

α orientation of longitudinal axis of spring

δ radial interference

Δ dimensionless shift in center of gravity of spring cross-section

γ dimensionless elastic region of spring cross-section

κ curvature of section

κ_e curvature at yielding of section

$\varnothing$ dimensionless curvature

ξ dimensionless location along spring

μ coefficient of friction

υ Poisson's ratio

ν_1 Poisson's ratio of material of pin

ν_2 Poisson's ratio of material of hub

η dimensionless tip displacement of spring

λ material constant

$\varepsilon_{\alpha\beta}$ strain tensor

$\sigma_{\alpha\beta}$ stress tensor

σ_y yield strength

σ_t tensile stress generated in spring

σ_c compressive stress generated in spring

CHAPTER I

INTRODUCTION

Fracture of bone is one of the oldest ailments affecting mankind. The earliest evidences of fracture fixation are from the Egyptian civilization where wooden splints were used to join broken bone pieces. Practices of immobilizing bone fragments with stiffened cloth rags have also been observed.

The first instance of metallic internal fixation was in the 1770s. An iron wire was used to stabilize the broken bone. The corrosion of the wire led to tissue reaction which hampered further use of the technique till non corrosive materials were tried out. In the 1880s, noble metals were successfully used for the first time for fixation of fractures. Around the same time, metallic plates and screws had been used as implants for fracture fixation. These were coated with either gold or silver to eliminate tissue reactions [Colton, 2003; Department of Mechanical Engineering, University of California, Berkeley, 2005].

The impetus to use of metallic implants occurred with progress in synthesizing of non corrosive alloys during World War II. This led to the development and use of different types of plates, screws, wires and clamps for healing of fractures. The advantages of using biodegradable polymers instead of metals for medical implants were realized in the 1960s and fueled further research in this area. Over the last decade, there has been a significant shift towards using biodegradable implants for fracture fixation. Due to low strength of biodegradable polymers, these implants could not be used to provide secure fixation of load bearing fractures. This drawback was overcome with the introduction of biodegradable composites, having much higher strengths. Different types of screws and plates having geometries different to conventional metallic implants are currently being used.

Over the last five years, efforts have been concentrated towards providing

_____

This thesis follows the style and format of the Journal of Biomechanics.

effective fixation means for smaller fragments. Most of these methods use pins or tacks, which are threadless and miniature in sizes. These try to provide small fragment consolidation. Many of these fasteners fail to provide interfragmental compression which is one of the essential requirements for accelerated bone healing. Also these pins and tacks have different profiles with no justification available behind the use of a particular profile. Hence there is a need to develop a fastener which would be able to consolidate small fragments, while providing compressive clamping pressure on the fractured surfaces.

CHAPTER II

OBJECTIVE AND SCOPE

The main objectives of this study are stated as follows:

- To design and develop a polymer based orthopedic micro-fastener for small fragment fixation.

The main objective of this research is to design an orthopedic micro-fastener capable of fixating small bone fragments. Threaded fasteners due to their stress concentration effects, are unsuitable for small bone fragment fixation. Also, metallic fasteners have significant disadvantages with regard to fracture healing. Therefore the aim of this research is to design and develop a polymer based orthopedic micro-fastener, which would be able to stabilize small bone fragments and subject them to interfragmental compression to aid in fracture healing.

- In-vitro testing for the efficacy of the fastener

It is necessary to conduct to in-vitro testing of the fastener in order to evaluate its performance under conditions fairly similar to the actual case. The efficacy of the design can be corroborated by comparing the FE predictions with the experimental results.

This study seeks to develop a methodology towards designing and developing a polymeric orthopedic fastener which could then be applied for developing a similar fastener made of biodegradable polymers for human bone fixation.

The scope of the project lay in the following:

1. Designing and simulating the fastener

    A fastener design is to be proposed by comparing the performance of different profiles under varying parameters which define the profile. This is to be achieved by conducting finite element analysis of the fastener-bone model for push-in and pull-out action of the fastener. The simulation should also predict the interfragmental compression produced.

2. Determining the coefficient of friction between bone and polymer

    The insertion and retention strength of the fastener in the bone depends on the coefficient of friction between the bone surface and the polymer. The coefficient of friction between the bone and polymer for an interference fit, under varying levels of interference is to be determined. Bone being an inhomogeneous, anisotropic material; the surface topography of the drilled surface of the bone under varying orientations and locations needs to be examined.

3. Manufacturing a prototype of the fastener

    The polymeric fastener is to be fabricated in order to test its performance. It is essential to ensure that the chosen processes can replicate even the smaller features in the fastener.

4. In-vitro testing of the fastener

    The fastener needs to be subjected to in-vitro testing to compare the push-in and pull-out force as predicted by the finite element simulation.

5. Deriving an analytical model

An analytical model would be proposed to explain the bone and fastener interaction. The push-in and pull-out force predicted by the analytical model would be compared with the FEA and experimental results.

CHAPTER III

LITERATURE REVIEW

III.1. Structure of bone

The human skeleton is made up of more than 200 bones of different sizes and shapes [Carter and Beaupré, 2001]. The primary functions of bones are to support the muscles and organs, protect vital organs, store calcium and phosphate, and act as a source for blood cells. The structure of bone is as shown in Fig.III.1.
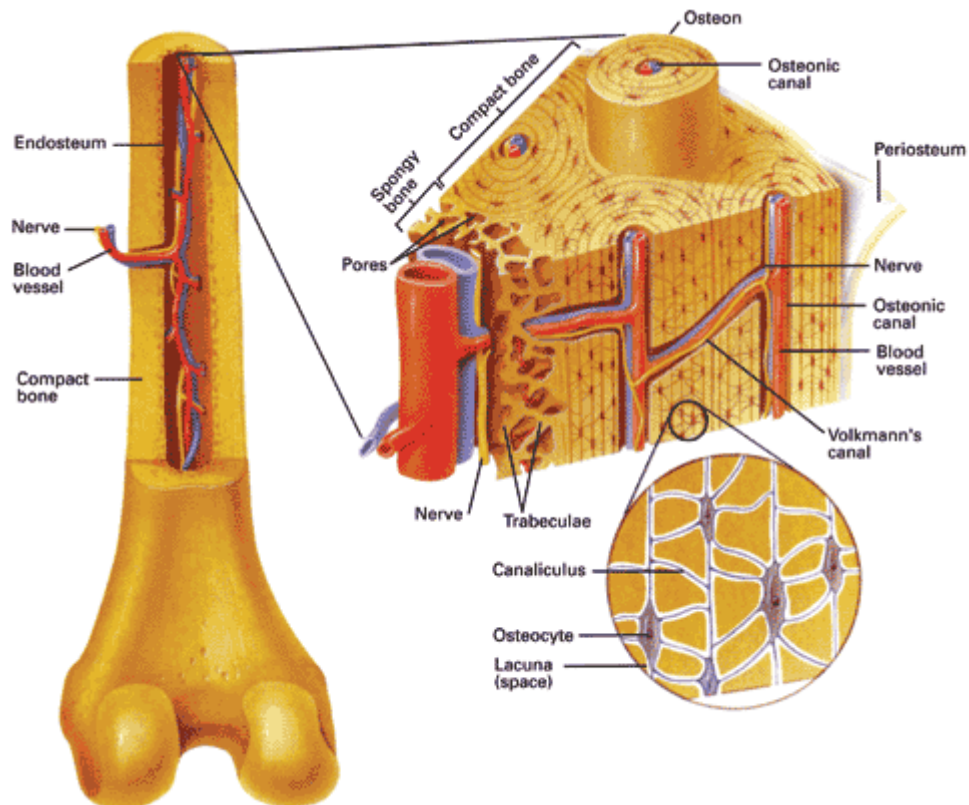
Fig.III.1. Structure of bone [Shier et al., 1996]

Bone is a growing tissue with a porous structure, which is made up of cells, blood vessels and calcium matrix. There are basically two different types of bones, namely cortical bone and cancellous bone.

Cortical bone also called as compact bone, is harder and stronger than cancellous bone and occupies the outer periphery of all the bones in the body. It has dense deposits of calcium phosphate providing it high strength. It consists of multiple bull's eye formations called as osteons or Harvesian systems, which contain blood vessels and nerves. Cancellous bone also called as the Trabecular bone or Spongy bone, is made up of a network of partitions called as trabeculae, which encloses the blood vessels. It has lesser density but higher elasticity than cortical bone. It is found at the ends of long bones or the interior of short bones [Shier et al., 1996].

Bone is a composite structure with each constituent playing a unique role in fulfilling the function of the bone. It is necessary to know the mechanical properties of the bone in order to understand its behavior under different types of loading. Bone exhibits excellent compressive strength which can be attributed to its strong cortical section. However, it is found to be weaker in tension and shear which is a cause for fracture initiation [Chao et al., 1995]. The mechanical properties of cortical bone are illustrated in Table III.1.

Table III.1. Mechanical properties of cortical bone [Reilly and Burstein, 1974; An, 1999]

Species	Density (kg/m^3)	Test	Strength (MPa)	Elastic Modulus (GPa)
Human	1900	Compression	167-215	14.7-19.7
		Tension	107-140	11.4-19.7
Bovine	1900	Compression	197-259	17.64-24.16
		Tension	135-169	16.3-26.9

III.2. Fracture of bone

Just like any other mechanical element, the bone fractures when the loading on it exceeds its strength. The type of fracture depends on nature of loading and energy released during fracture. Bending load causes fracture on the tensile side and it then propagates to the other side. Torsion produces a spiral fracture and shear stress may produce longitudinal cracks along the spiral fracture line. Impact forces tend to store a high amount of energy inside the bone, which is released due to fracture propagation, resulting in the formation of multiple bone fragments. Depending on severity, fractures are classified as simple, compound or comminuted fractures. In a simple fracture, the bone breaks into two parts. A fracture in which the bone penetrates the skin is called as compound fracture; in a comminuted fracture, the bone breaks down into small fragments.

A fractured bone loses its strength and continuity. However, nature is able to restore the original structure and strength of the bone as they were prior to fracture. The healing process involves multiple sequential phases, which can be separated into three distinct stages namely, inflammation, reparation and remodeling. Inflammation stage is most crucial, as it activates the cellular mechanism necessary for repair and protection of the healing tissue. During the reparation stage, continuity is restored by union of bone fragments through membranes. In the next stage, a bony bridge is formed between the bone fragments and it requires stabilization of the whole system [Chao et al., 1995].

The basic aim of fracture treatment is to regain the functionality of the fractured body part through reunion of the bone fragments. In order to achieve this, the fracture fixation methods should be able to realign and maintain the bone fragments in their proper position. They should also provide interfragmental compression to aid in the consolidation of the fragments [Chao et al., 1995]. Depending upon the type of fracture, either the internal or external fixation method is used.

Internal fixation methods are used when there is a need for exact reunion of the bone fragments. It is also able to provide fracture stability with pain free function of the

part. The most common internal fixation tools include screws, plates, wires, nails, pins, etc.

External fixation is employed for stabilization of compound fractures, infected non unions and soft tissue damage. The fractured bone and soft tissue can be examined and operated even after the preliminary surgery, unlike in internal fixation. Implants for external fixation include adjustable frames with clamps and screws [Müller et al., 1991].

III.3. Types of internal fixation methods

Almost all internal fixation methods produce fracture fixation through application of compression across the bone fragments. The various ways used to achieve interfragmental compression are given below.

III.3.1. Plates

A pre-bent plate can be used to provide compression between bone fragments. Tightening of the plate around the bone tends to straighten it. After removal of the tightening forces, the plate tends to undergo a springback, to regain its original shape. This pushes the two fragments closer to each other. Pre-bending is seen to increase the fixation stability and is favored for bones of small diameter and low strength [Müller et al., 1991]. Fracture fixation using a pre-bent plate is shown in Fig.III.2.
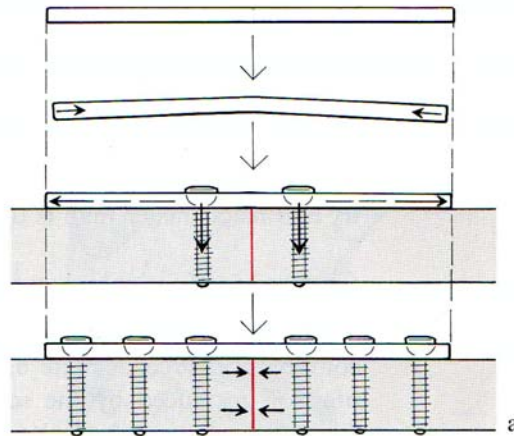
Fig.III.2. Fracture fixation with a pre-bent plate [Müller et al., 1991]
(Small arrows indicate the stresses generated due to the pre-bent plate and screws)

III.3.2. Screws

Screws can play multiple roles in fracture fixation; they can be used either to attach plates to bones or by themselves to clamp bone fragments together. Screws are classified based on their function, manner of insertion, size of the bone fragment that can be fixated securely and the type of bone into which they are to be inserted. Accordingly, they are classified as lag screws, self-tapping or non-self-tapping screws, large and small fragment screws, cortical and cancellous screws [Müller et al., 1991].

III.3.2.1. Lag screws

The ideal way of fracture fixation is to compress the bone fragments against each other, using a lag screw. A lag screw fastens only into the distal fragment and glides into the hole drilled in the proximal fragment. It can either be partially or fully threaded, but in the latter case, the pilot hole in the proximal fragment needs to be bigger than the

nominal diameter of the screw. As the screw is tightened, the fragments move towards each other, producing interfragmental compression. No compression is generated if the screw engages in both the fragments.

While inserting a lag screw, care must be taken to insert it normal to the fracture plane. If not, the fragments have a tendency to slip against each other due to shear loads. A lag screw cannot be inserted at sharp acute angles with the fracture plane as it might cause breakage of the proximal fragment due to stress concentration [Lavi, 2002]. If a single lag screw cannot be inserted normal to the fracture plane, then multiple screws with varying orientations need to be used to secure the bone fragments in place [Müller et al., 1991].

III.3.2.2. Self-tapping and non-self-tapping screws

Self-tapping screws, as the name suggests, produce threads as they are being inserted into the pilot hole. Hence, no separate tapping operation is required for inserting them. As the screw is required to produce its own thread, it tends to encounter high resistance while being inserted into the cortical bone. This might cause the screw to break, or misalign with the desired direction of insertion. Because of this, these screws are not used as lag screws. To reduce this resistance, core diameter of the screw is smaller than the diameter of the pilot hole. Non-self-tapping screws require a tapped pilot hole. It encounters much lesser force as compared to self-tapping screw.

III.3.2.3. Cortical screws

The thread on these screws has a small pitch, with small nominal to minor diameter ratio. Due to this, it is used to fixate cortical bone fragments. They are fully threaded and non-self-tapping. A typical cortical screw is shown in Fig.III.3.a.

III.3.2.4. Cancellous screws

Cancellous thread has a larger pitch than the cortical thread and high nominal to minor diameter ratio. They can be partially or fully threaded. Partially threaded screws are used as lag screws and fully threaded are used to fasten plates to bones. These screws can easily form threads inside the soft cancellous bone, increasing the holding power [Lavi, 2002]. A typical cancellous screw is shown in Fig.III.3.b.

a.   b.

Fig.III.3. a. Cortical screw; b. Cancellous screw [Orthopaedic-Implants, 2005]

III.3.2.5. Cannulated screws

Cannulated screws have a hollow shaft with a guide wire passing through it. These screws are self-drilling and self-tapping, with the guide wire maintaining the alignment of the fragments. If the guide wire is bent, the screw will not advance and might lead to breakage of the cutting tips.

III.3.2.6. Herbert screws

These are "headless" screws with threads at both ends of the shank. The pitch of the thread at the proximal end is different from that at the distal end, with no threading in

the central region of the shaft. As the screw is inserted, the difference in pitch causes the bone fragments to press against each other. However, they have been found to provide lesser compressive forces as compared to conventional screws [Ford, 1994]. A cannulated Herbert screw is shown in Fig.III.4.

Fig.III.4. Cannulated Herbert screw [GMReis, 2005]

III.3.3. Non-threaded fixation methods

Non-threaded fixation methods like Kirschner wires and staples are used to stabilize bone fragments. Kirschner wires are passed through holes drilled inside the bone fragments and then tied around them. They are also used as guide wires for cannulated screws. They are easy to use, but offer no compression to the fracture site and can cause infection if used percutaneously (inserted through the skin) [Herstik et al., 1990].

III.4. Advantages and disadvantages of metallic implants

Post World War II; there was a surge in the use of metallic orthopedic implants, mostly due to the development of novel alloys. Three classes of alloys, namely stainless steel, titanium and titanium alloys, and cobalt-chromium alloys, found wide use in the manufacturing of orthopedic implants [Cohen, 1983]. These materials have obvious advantages like high strength, availability, ease of manufacturing and low cost. They also enhance X-ray image contrast. However, metallic fixation devices are associated with certain disadvantages as stated below.

Metallic implants tend to cause pain at the fracture site due to their high hardness and stiffness. Hence, in many cases they have to be removed after the bone has healed. This requires a second surgical intervention, which subjects the patient to additional risks, mental and physical trauma, and financial burden.

High stiffness implants cause atrophy of the bone at the fracture site. Metals have a substantially higher elastic modulus than bone; steel with an elastic modulus of 200 GPa is about 8 to 12 times stiffer then cortical bone [Reilly and Burstein, 1974; An, 1999]. Hence, during the healing stage, the load is taken by the stiffer implant and the bone is not subjected to sufficient loading. The unloaded region of the bone is slowly resorbed leading to weakening of the bone at the fracture site. Strength of the healed bone tends to be lesser than the unfractured bone, which may cause subsequent fracture at the same site once the implant is removed [Tunc, 1991].

Biocompatible alloys release ions as a result of corrosion, which may cause allergies and could prove to be carcinogenic [Cohen et al., 2001]. Inflammation and blackening of the tissue in the vicinity of the implant is also observed, which could be attributed to the migration of the corrosion products [Cohen, 1983]. Relative motion between the insert and the bone produces wear particles resulting in adverse tissue reactions causing the deterioration of the bone and loosening of the implant [Hamblen, 1989]. These alloys also interfere with magnetic imaging studies causing difficulty in post operative observation [Cohen, 2001].

III.5. Biodegradable polymers

In order to reduce the risk of metallic implants as regards to corrosion and stress shielding of fractured bone, it was necessary to develop implants made out of materials that could avoid these complications. Biodegradable polymers synthesized from glycolic acid and other hydroxy groups were first developed during the early part of the twentieth century. But their affinity for water and tendency of degradation was construed as a drawback putting a halt on further research in this area. However over the last four decades, this tendency for biodegradation has turned to be a boon for the medical field. The biodegradable suture Dexon, introduced by Davis and Geck, Inc. [Middleton and Tipton, 2000] in the 1960s was the first biomedical application of these polymers.

For a biodegradable implant to be suitable for internal fixation, it should be able to satisfy certain conditions [Simon et al., 1997; Middleton and Tipton, 2000; Claes, 1992]. It should have a proper strength degradation profile, which can retain its strength till the bone begins to heal. The implant when inserted into the bone should be sufficiently strong so that it can withstand the loads exerted on it. With time, the load should be transferred from the implant to the bone to stimulate bone regrowth and healing. Hence the biodegradable implant should loose its strength causing an increase in load on to the fractured bone, which would increase its strength. Finally, when the bone has healed completely it would regain its original strength whereas the implant should lose its entire strength and undergo complete degradation. The degradation time depends on the type of polymer used. Fig.III.5 shows the ideal strength degradation profile for a biodegradable polymer.
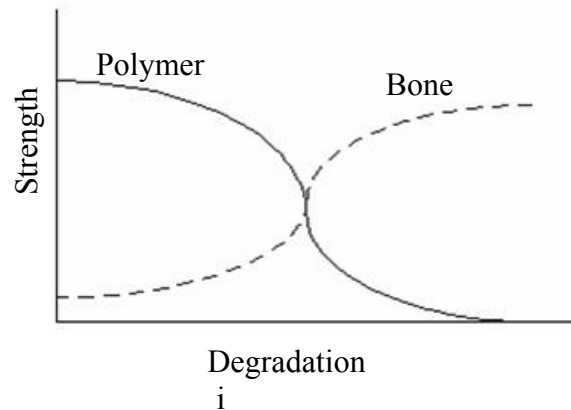
Fig.III.5. Strength profile of biodegradable polymer and bone as a function of
degradation time [Tunc, 1991]

The elastic modulus of the biodegradable polymer should be comparable to that
of bone to reduce the effect of stress shielding and pain at the fracture site due to
difference in stiffness.

The polymer must degrade due to metabolisation inside the body without leaving
any trace. It should not cause any inflammation or toxic reaction with the body. Also on
degradation, there should be no sinus formation.

These polymers should exhibit ease of manufacturability, as they are molded,
extruded or machined into different forms and shapes like screws, plates, prostheses etc.
They should exhibit sufficient shelf life and capable of sterilization without undergoing
degradation.

III.5.1. Types of biodegradable polymers

Biodegradation is achieved by using polymer linkages that are hydrophilic in
nature which leads to their instability. Polymers synthesized by ring-opening

polymerization of hydroxy acids like glycolic and lactic acid possess this tendency [Middleton and Tipton, 2000]. The most common types are enumerated below:

III.5.1.1. Polyglycolic acid (PGA)
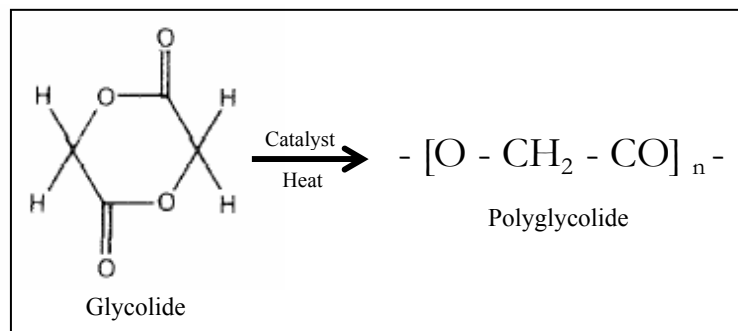
Fig.III.6. Chemical structure of glycolide [Middleton and Tipton, 2000]

High molecular weight PGA is obtained by ring opening polymerization of its monomer, as shown in Fig.III.6. PGA is a hard, tough, crystalline polymer. It has a melting point of 220 - 225°C and glass transition temperature of 35 - 40°C. PGA exhibits yield strength of 50 - 60 MPa and an elastic modulus of 7 GPa. It degrades due to hydrolysis into carbon dioxide and water which is excreted out of the body. It loses up to 50% of its strength within the first 4 weeks of implantation and degrades completely in 6 months [Simon et al., 1997; Middleton and Tipton, 2000; Claes, 1992; Rokkanen 1991; Gogolewski, 1992; Amecke et al., 1992].

III.5.1.2. Polylactic acid (PLA)
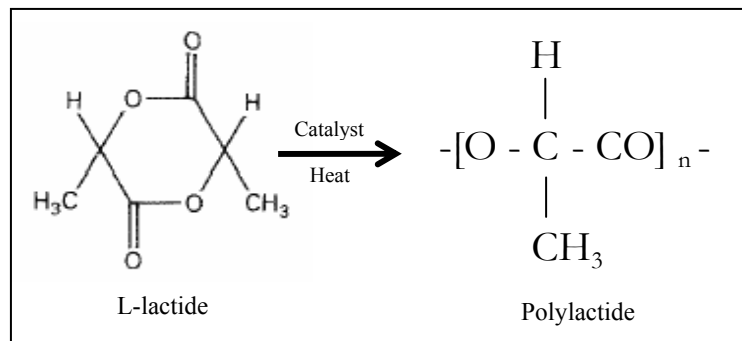
Fig.III.7. Chemical structure of lactide [Middleton and Tipton, 2000]

Lactic acid exists in two types of isomers, d-lactide and l-lactide where the latter is a naturally occurring isomer. L-lactide (LPLA) is semicrystalline in nature, has a melting point of 174 - 184°C and a glass transition temperature of 57°C. The chemical structure of L-lactide is shown in Fig.III.7. It has an elastic modulus of 3 GPa and yield strength of 60 - 70 GPa. It degrades completely within 2 years and is suitable for orthopedic applications. DL-lactide (DLPLA), which is a synthetic blend of d and l-lactide has a lower modulus (2 GPa) and degradation time (1 -1.5 years) as compared to LPLA and is favored for drug delivery applications. All isomers of PLA degrade into lactic acid which is a normal metabolic byproduct [Simon et al., 1997; Middleton and Tipton, 2000; Claes, 1992; Rokkanen 1991; Gogolewski, 1992; Amecke et al., 1992].

III.5.1.3. Polylactide-co-glycolide acid (PLGA)

Copolymers of lactide and glycolide have been developed to combine the ideal characteristics of both types. By controlling the composition of these copolymers, properties can be tailored as per the application. They have been used for orthopedics as well as drug delivery applications.

III.5.1.4. Self-reinforced composites (SRC)

For secure fixation of the bone fragments, the implant needs to have a high tensile strength. This cannot be provided by the biodegradable polymers stated above. In the late 1970s, efforts were directed towards developing reinforced biodegradable polymers, which would have an initial mechanical strength comparable to that of metals.

Different techniques were tried for reinforcing these polymers. Depending on the type of reinforcement, these composites were partially or completely degradable. The most common types of partially degradable polymers were carbon fiber reinforced with a matrix of PLA, PGA or PLGA. However the interfacial bonding between the matrix and fibers required the use of highly toxic adhesives. A porous interface led to fluid diffusion into the composite causing it to deteriorate [Simon et al., 1997]. Törmälä [1992] developed self reinforced composites with the matrix and fibers having the same chemical composition, thus eliminating the interfacial adhesives. These composites have high strength in the direction of the oriented reinforcement members.

Mechanical deformation of the non reinforced polymers results in the formation of highly oriented molecular chains which increase the strength and toughness of the polymer. Processes like wire drawing, shearing, rolling, extrusion etc. are used for attaining the molecular orientation. By controlling the process parameters like the draw ratio, the extent of orientation and hence the mechanical strength and stiffness can be controlled. Tensile strength is found to increase linearly with the draw ratio. Ultimate tensile strength of SRPLA was found to be about 400 MPa for a draw ratio of 9 [Tunc,

1991]. This is a significant increase as compared to the strength of regular PLA, which is about 60 -70 MPa.

This oriented microstructure can also be achieved by sintering a bundle of fibers made of biodegradable polymers and then shaping the specimen under pressure. By appropriate control of temperature, a self reinforced structure consisting of polymer matrix embedded with fibers of the same material can be obtained [Rokkanen, 1991; Törmälä, 1992].

Mechanical properties of different self-reinforced composites are summarized in Table III.2.

Table III.2. Mechanical properties of self-reinforced biodegradable composites
[Rokkanen, 1991; Törmälä, 1992; Simon et al., 1997]

Material	Bending Modulus (GPa)	Bending Strength (MPa)	Shear Strength (MPa)
SR-PGA rod	12-14	350-430	200-250
SR-PLLA rod	9-13	200-300	185-220

III.6. Biodegradable implants

Different types of pins, screws and plates were made out of biodegradable polymers and used successfully. Orthosorb™, a cylindrical pin developed by Johnson & Johnson Products Inc., was the first biodegradable implant to be introduced into the market [Beiser and Kanat, 1990]. It is still being used for joining small bone fragments, which are not subjected to a tensile load. However the pin is not able to provide interfragmental compression and cannot be used for load bearing bones. Subsequently,

biodegradable screws were developed for fractures, which require compressive loads for healing. Screws differing in their sizes, thread and head profiles are currently available in the market. Endo-Fix™, BioScrew™, Phantom™, Arthrex™ and Sysorb™ [Costi et al., 2001] are a few of them.

Over the last few years, there has been a trend towards using non threaded implants for fracture fixation. These implants called as "tacks" are push-in type fasteners which need to be pressed into the pilot hole drilled through the fracture site. As they dispense with the tapping operation required for threaded implants they are used for joining small bone fragments and soft tissue with bone. This technique is also cost effective as compared to threaded fasteners as it reduces the surgical time [Leinonen et al., 2003]. Commercial products include Bio-FASTak™ and TissueTak™ by Arthrex®, Bankart Tack™, SmartNail™ and The Wedge™ by BIONX Implants®.

III.7. Testing methods

The function of any fracture fixation method is to stabilize the fracture site by immobilizing the bone fragments and to provide interfragmental compression. The strength of a threaded joint is usually measured in terms of the axial force acting on the threaded member, which is required to separate the joint assuming that there are no shear forces acting on it. The same technique is used for evaluating the holding power of implants, which are inserted inside into the bone. This holding power of the implant against tensile load acting along the longitudinal axis of the implant is termed as "pull-out force" of the implant.

ASTM standardized test (ASTM F 1691 – 96) is used for determining the axial pull-out strength of medical bone screws. This method (Fig.III.8.) can be used for evaluating or comparing the strengths of different types of screws [ASTM, 2000]. The test block, either of bone or bone substitute should be fixed to an immovable base. The bone screw should be inserted through a drill bushing, which acts as a guide such that the axis of the screw is normal to the top plane of the test block. A suitable fixture

should be used to hold the head of the screw and provide a tensile load along the longitudinal axis of the screw till it breaks or separates from the test block. A data acquisition device would record the load versus load frame displacement and the maximum load would give the pull-out force of the bone screw. The effect of tightening torque has been considered in various studies [Collinge et al., 1999; Costi et al., 2001; Weiler et al., 1998] as it not only affects the strength of the joint but also cause screw breakage during insertion. By using the same principle of application of tensile load to the implant inserted into a fixed test block, the pull-out force of non threaded implants (Fig.III.9.) can also be determined (ASTM F 1540 – 95) [ASTM, 2000].
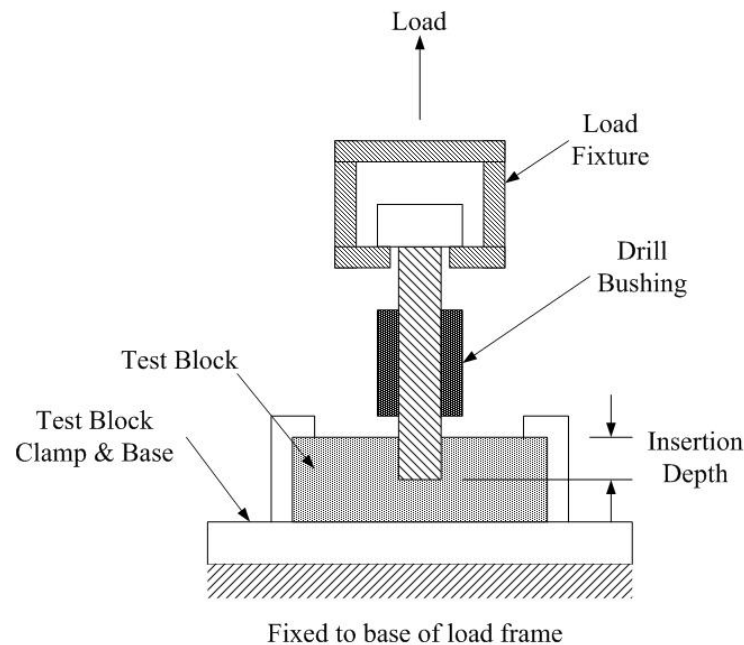
Fig.III.8. Schematic of setup for screw pull-out test ASTM F 1691 – 96 [ASTM, 2000]
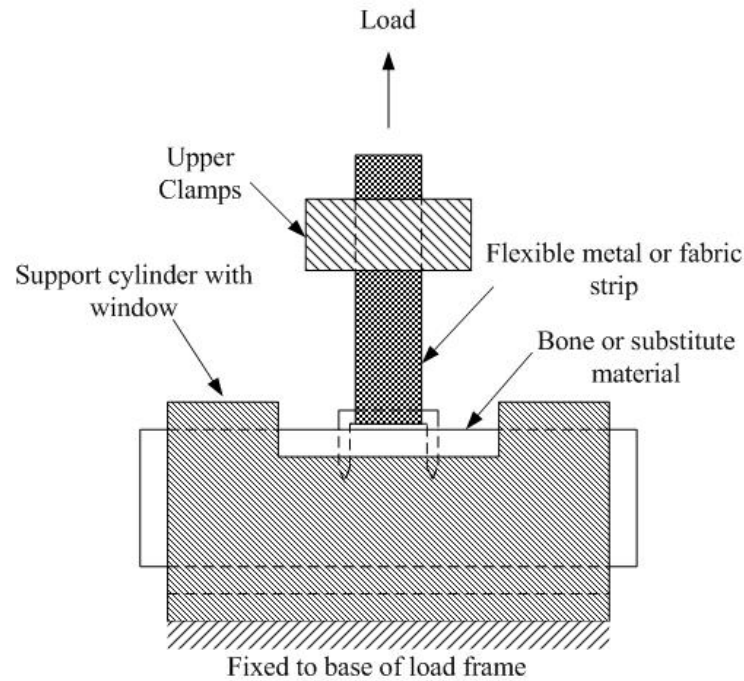
Fig.III.9. Schematic of setup for staple pull-out test ASTM F 1540 – 95 [ASTM, 2000]

It has been observed that the pull-out strength of a screw is dependent on the bone thickness and type of bone into which it is fixated [Koranyi et al., 1970, Hughes and Jordan, 1972]. It is also significantly affected by the screw diameter [Schatzker et al., 1975].

With extensive use of biodegradable implants, studies have been conducted to assess their strength and compare it with metallic implants. Collinge et al. [1999] compared the pull-out strength and torque to failure of three different types of cortical and one type of cancellous stainless steel screws, one type of titanium and PLA screws. Results showed no difference in the pull-out strength of the cortical screws, but cancellous screws offered a lesser holding power. Torque to failure for the three types of cortical stainless steel screws was almost the same. Cancellous stainless steel and

titanium screws failed at a lower torque. The PLA screws offered the least resistance to failure.

The effect of thread design and type of drive on the pull-out force, stiffness of fixation and insertion torque was conducted for five different types of biodegradable screws and compared with a titanium screw [Weiler et al., 1998]. Bovine cortical bone was used for making the bone blocks. The pull-out force of biodegradable screws was found comparable to that of the titanium screw. However, this result cannot be generalized as the screws were of different diameters. A linear correlation was observed between the stiffness of fixation (determined from the load versus displacement curve) and the thread height. This could be attributed to increased contact between the bone and the thread. The torque to failure was found to be affected by the drive design.

Costi et al. [2001] tested commercially available biodegradable screws namely, Arthrex™, BioScrew™, Endo-Fix™, Phantom™ and Sysorb™ screws to evaluate the effect of screw diameter on torsional strength and investigate the different modes of failure. All the screws were of 20 mm length but their diameters varied between 7 to 9 mm. They were threaded into polyurethane resin blocks and torque was applied manually. The failure torque and mode of failure was recorded for each screw. The Arthrex™ screw exhibited the highest torque to failure at 5.37 Nm, whereas the Endo-Fix™ required the least torque to failure of 1.07 Nm. The different modes of failure encountered were, screw failure due to shear at the resin-screw interface, radial failure of screw head, distortion of screw head geometry preventing the screw driver to get engaged with the screw and failure of the screw driver shaft. The thread profile and screw diameter were found to be the most important factors that affected the torsional strengths of the screws.

Failure strength of implant-bone joint for stainless steel and biodegradable screws of the same thread profile and size was compared by Johnson and Eda vanDyk [1996]. Bone specimen with implanted screw was held in Instron tensile testing machine so that the direction of pull-out force was parallel to axis of insertion. The average force for joint failure for steel and biodegradable screws was 436 N and 565 N, respectively.

This variation was probably due to the difference in bone density. A similar study [Caborn et al., 1997] was conducted to evaluate maximum failure load for BioScrew™ (Linvatec Corp, FL) and titanium alloy screws. The average values for these tests were 552.5 N for BioScrew and 558.3 N for titanium alloy screws.

Wouters et al. [2004] tried to determine the efficacy of a 1.1 mm diameter meniscus Arrow (Bionx Implants Ltd., Finland), which is a thread-less, push-in type of biodegradable fastener and compared its pull-out strength with a metallic screw of 2 mm diameter. In addition to axial loading, the implants were also subjected to shear loads. Average pull-out force of 68 N and shear load of 121 N was reported for the Arrow and 232 N for pull-out of the screw.

In the study by Leinonen et al. [2003], the pull-out force of biodegradable tacks (Bionx Implants Ltd., Finland) of 2 mm nominal diameter was determined and compared to that of biodegradable screws of the same size. The tacks exhibited a pull-out force of 135 N, which was higher than the screw pull-out force of 119.3 N. The tacks exhibited a higher pull-out force than the screws. Breakage of barbs on the tacks was found to be the most common cause of failure. Splitting of the tack due to misalignment with the pilot hole during insertion was another cause of failure.

III.8. Interference fit

An interference fit between a cylindrical pin and a cylindrical hub (Fig.III.10) produces interference pressure between the pin and hub. For a cylindrical interference fit, the relationship between the radial interference and the resulting interference pressure is given below [Shigley et al., 2004].
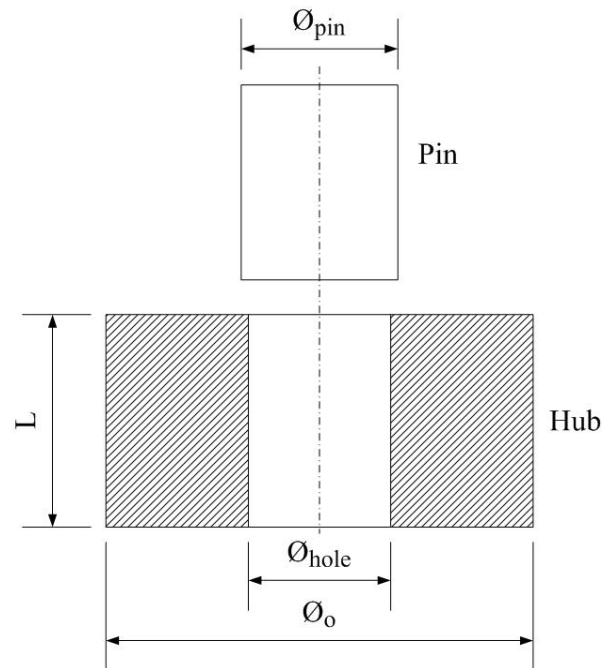
Fig.III.10. Interference between pin and hub

Define:

r   radius of hole, $(\varnothing_{hole})/2$

r_o outer radius of hub, $(\varnothing_o)/2$

E_1 elastic modulus of pin

E_2 Young's modulus of material of hub

F_r friction force

L   length of interference

P_i interference pressure

δ   radial interference, $(\varnothing_{pin}-\varnothing_{hole})/2$

μ   coefficient of friction

v_1 Poisson's ratio of material of pin

v_2 Poisson's ratio of material of hub

$$P_i = \frac{\delta}{\frac{r}{E_2}\left(\frac{r_o^2 + r^2}{r_o^2 - r^2} + v_2\right) + \frac{r}{E_1}\left(1 - v_1\right)} \tag{III.1}$$

The friction force (F_r) between the pin and the hub is given by:

$$F_r = P_i\left(2\pi r L\right)\mu \tag{III.2}$$

The change in friction force with length of contact is given by:

$$\frac{dF_r}{dL} = P_i(2\pi r)\mu \tag{III.3}$$

Thus the coefficient of friction (μ) can be evaluated by:

$$\mu = \frac{\dfrac{dF_r}{dL}}{P_i(2\pi r)} \tag{III.4}$$

Hence, if the interference pressure can be determined from the geometry of the pin and hub, then it is possible to determine the coefficient of friction between the two materials.

CHAPTER IV

DESIGN OF FASTENER

IV.1. Design of fastener

The objective of this work was to develop an orthopedic fastener that would provide an alternative for small fragment fracture fixation. The design constraints considered during the design process were as follows:

1. The fastener should be able to fixate small fragments. The base dimension of a fragment that could be fixated was assumed to be 10 to 20 mm. The fastener should be able to hold the fragments in place and subject them to interfragmental compression.

2. The final prototype of the fastener would be biodegradable and non-removable.

3. As the fastener would be polymer based and not metallic, it would ideally be used for non-load bearing fracture sites like skull, phalanges etc.

4. It should be designed to achieve a reduction in surgical time with ease of operation.

5. The profile of the fastener should be amenable to the available micromanufacturing methods. The profile should be such that a scaled down version would be able to fixate even smaller fragments.

Conventional small fragment fixation methods use mini screws made from metals or biodegradable polymers. These possess drawbacks in fixation of small bone fragments due to the stress concentration effect of threads. Also, the tapping action increases the surgical complexity and time. Recently threadless fasteners also called as "tacks" have been developed and used to overcome these drawbacks [Cohen et al., 2001]. These possess barbs or ratchets on the shaft of the fastener which help to provide fracture stability. Published literature that justifies the use of a particular type of ratchet design has yet to be found. Hence different ratchet designs were compared based upon their force requirement for insertion and withdrawal from a hole.

IV.1.1. Design of ratchet

The fastener was designed to have an interference fit with the hole drilled in bone. Ratchets provided on the shaft of the fastener deflect while being inserted into a drilled hole and subsequently stiffen to lock the fastener in place. The efficacy of fixation methods is usually measured in terms of the pull-out force and the insertion torque. Since this fastener was designed to be threadless, push-in force instead of insertion torque was taken as a measure of performance. The push-in and pull-out force of a fastener is the force acting along its longitudinal axis that is required for pushing in or pulling out the fastener respectively, from a hole drilled inside bone [Leinonen et al., 2003]. For an interference fit, the friction force (push-in or pull-out force) depends on the length of interference between the pin and hub. Thus the push-in and pull-out force per unit length of interference was taken as a measure of comparison, to make it independent of the interference length. Commercially available tacks vary in their ratchet designs, but no data was available which provided the exact configuration of different designs. Hence analogous designs were considered and compared, based on the above stated parameters by using finite element analysis.

Only 2D designs were considered, due to manufacturing constraints. The same shaft radius (1.5 mm) and outer radius (2.5 mm) were maintained on all the designs, so that same interference levels were achieved in each case. All the designs were assumed to be of unit thickness. The design F is shown in Fig.IV.1. (Refer to Appendix A for designs A to E).
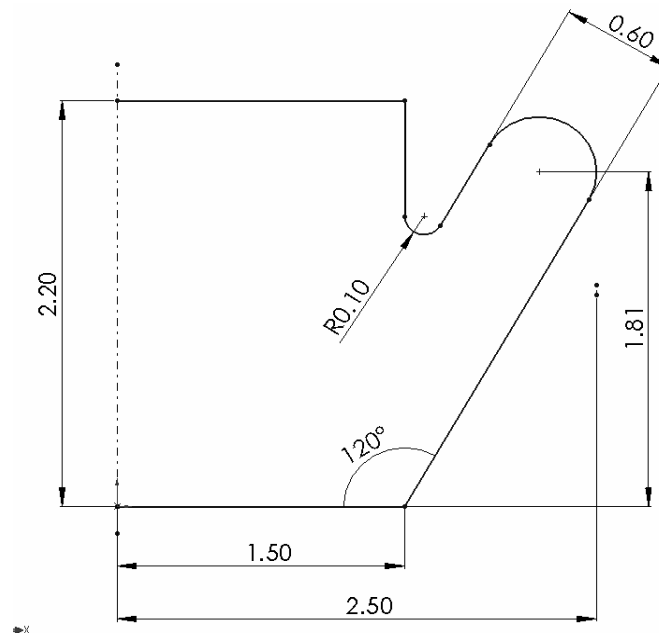
Fig.IV.1. Ratchet design F

IV.1.2. FEA of different ratchet designs

The fastener bone interaction was modeled using ABAQUS™, as it is capable of analyzing large deformations and multiple loading steps. The properties selected for bone were of bovine bone, as they are comparable to that of human bone (Refer to Table III.1.) and it has been used as a substitute for human bone for in-vitro testing [Reilly and Burstein, 1974; An, 1999]. Bovine bone was modeled as a linear elastic, isotropic, homogeneous material [Schuller-Götzburg et al., 1999] with an elastic modulus and Poisson's ratio of 20 GPa and 0.3, respectively.

Material for the fastener was taken as high density polyethylene (HDPE), since it has properties comparable to biodegradable polymers [Middleton and Tipton, 2000; Claes, 1992; Gogolewski, 1992]. It is also cost effective for design verification and in-

vitro testing. It was modeled as linear elastic-perfectly plastic [Krevelen, 1990]. The thermophysical properties of HDPE are given in Table IV.1.

Table IV.1. Thermophysical properties of HDPE [ExxonMobil, 2005; *Krevelen, 1990]

Property	Value
Density (kg/m^3)	952
Meting Point (°C)	132
Flexural Modulus (MPa)	995
Tensile Yield Stress (MPa)	24.6
Tensile Break Elongation (%)	60
Poisson's ratio	0.45*

The symmetric finite element model of fastener and bone, having unit thickness is shown in Fig.IV.2. ABAQUS/Explicit solver was used to analyze this quasi-static model. Analysis was conducted in two steps, push-in step followed by pull-out step. The bone block being larger and stiffer than the fastener in the actual scenario, was assumed to be fixed at its outer periphery. The interface between the fastener and bone was modeled with kinematic contact algorithm. The coefficient of friction between HDPE and bovine bone was assumed to be 0.3, due to two reasons. Firstly, experiments to determine the coefficient of friction between HDPE and bovine bone were not completed, prior to these analyses. Secondly, the FE solver requires more extensive computations for coefficient of friction of 0.3 and above [ABAQUS, 2005]. The actual coefficient of friction between HDPE and bovine bone was experimentally determined (Refer to V.2.) and was used for subsequent FE analyses.
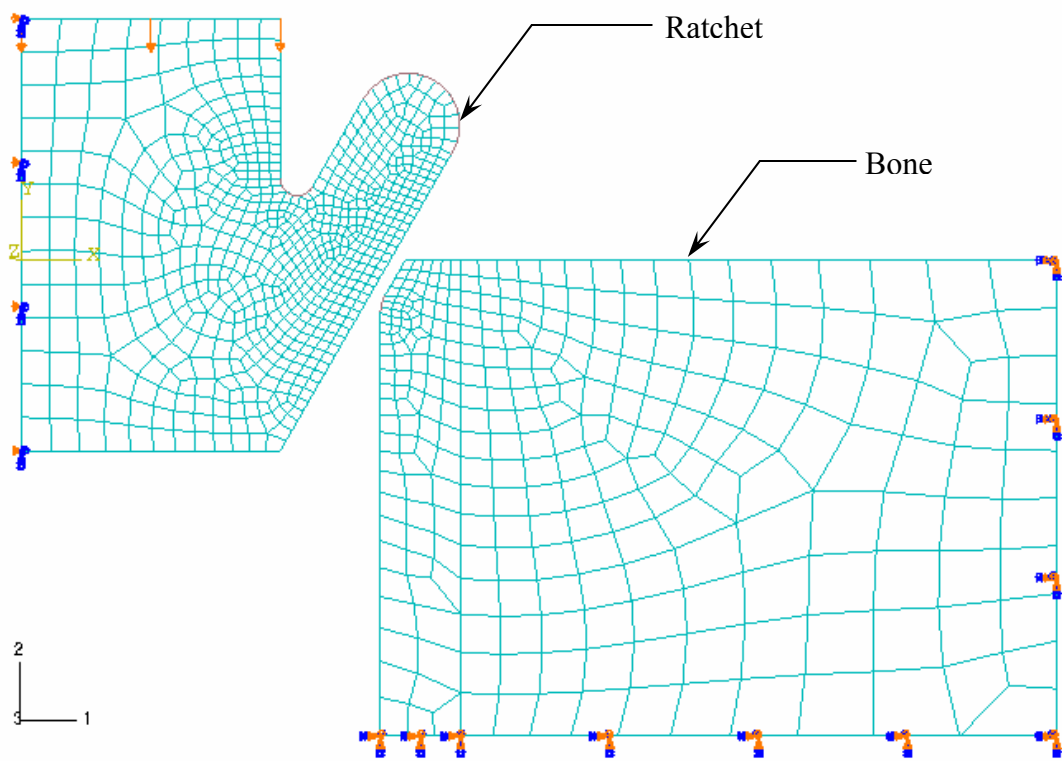
Fig.IV.2. FEA of ratchet design F and bone interaction

A displacement boundary condition in the appropriate direction was applied to the top of the fastener for the push-in and pull-out step. Plane stress quadrilateral reduced integration elements (CPS4R) were used to mesh the fastener bone geometry. Biased meshing was used to capture the intricate features of the profile. Mass scaling was used to reduce the computational time. The density of both the materials involved was adjusted, till the kinetic energy of the entire model was less than 10 % of the internal energy of deformation [ABAQUS, 2005]. The sum of the vertical reaction force at the top nodes of the fastener was recorded as push-in and pull-out force for the corresponding step.

IV.1.3. Design of spring element

Interfragmental compression provides effective reunion of bone fragments [Müller et al., 1991]. Tacks are able to hold bone fragments in place but are not as effective in subjecting them to interfragmental compression. Studies have compared the pull-out force for mini-screws and tacks and they have been found to be comparable. However, they do not illustrate whether they are able to provide interfragmental compression [Wouters et al., 2004; Leinonen et al., 2003]. To achieve this, head of the fastener was developed analogous to a Belleville spring. It would deflect under application of push-in force and will subsequently undergo elastic springback on removal of this force. On achieving equilibrium, it would get locked in place, subjecting the bone fragments to compression. The orientation and dimensions of the spring were selected such that, even after complete deflection, its tip would touch the top bone fragment and would not extend beyond it. This was done to ensure that the bone fragments are pressed against each other, even after springback. The final geometry of the fastener is as shown in Fig.IV.3.
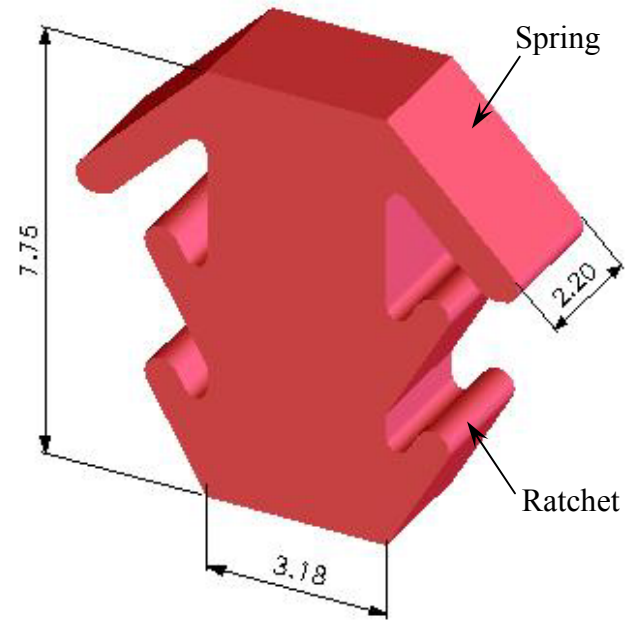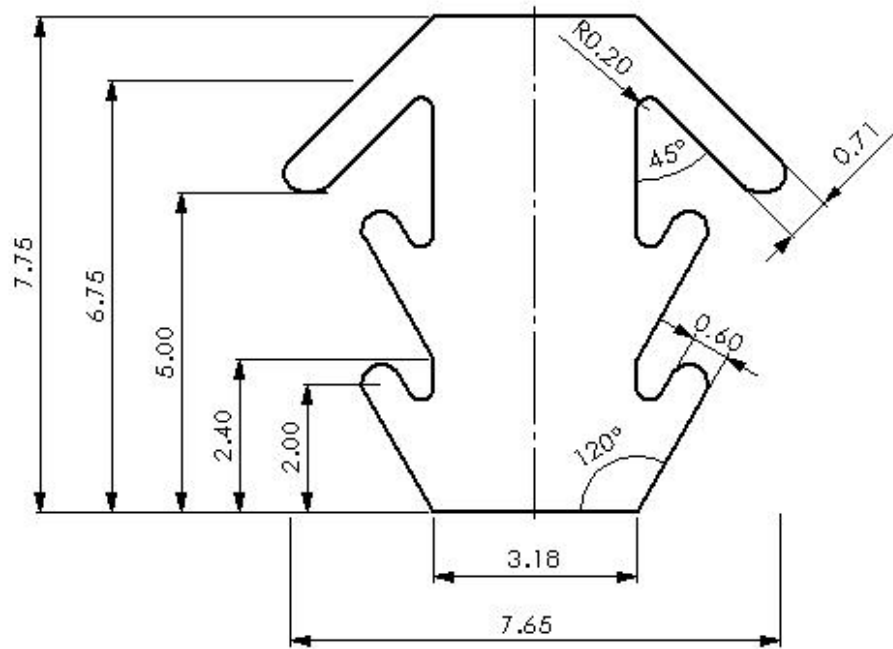
Fig.IV.3. Geometry and solid model of the fastener

IV.1.4. FEA of fastener

The actual fracture fixation scenario is shown in Fig.IV.4. The fastener is inserted in to the hole drilled inside the bone fragments. The FE model of the fastener and bone is shown in Fig.IV.5. Bone fracture was simulated by considering two bone fragments separated by the fracture plane. Analysis was conducted in three steps: push-in, springback and pull-out. The first and last steps were similar to the previous analysis. Following the push-in step, the deformed configuration was imported into ABAQUS/Standard for conducting the springback analysis. On completion of this step, the model was then exported back to ABAQUS/Explicit for the pull-out step (Refer to Appendix B for input files). The coefficient of friction was taken as 0.2, as determined from the friction experiments (Refer to V.2.). The push-in and pull-out force was recorded as mentioned previously. The average vertical compressive stress acting along the fracture plane was recorded as the interfragmental compression. The simulation was conducted for three levels of radial interference of 0.48, 0.50 and 0.52 mm. These values were selected to cover the entire range of the experimental interference levels.
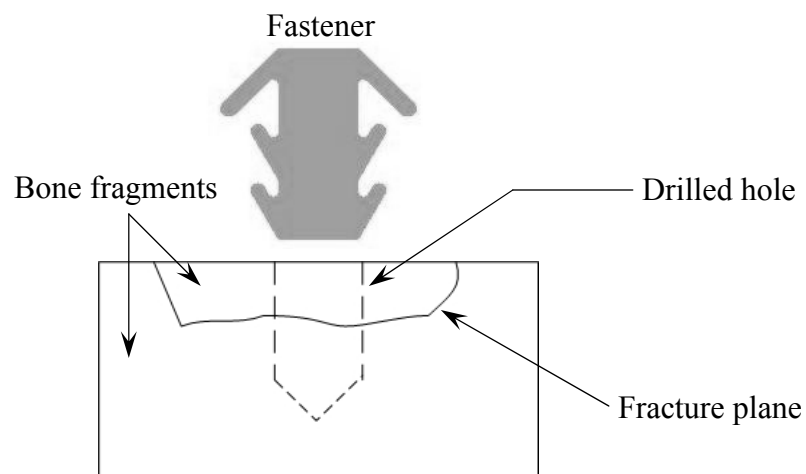

Fig.IV.4. Fracture fixation using fastener
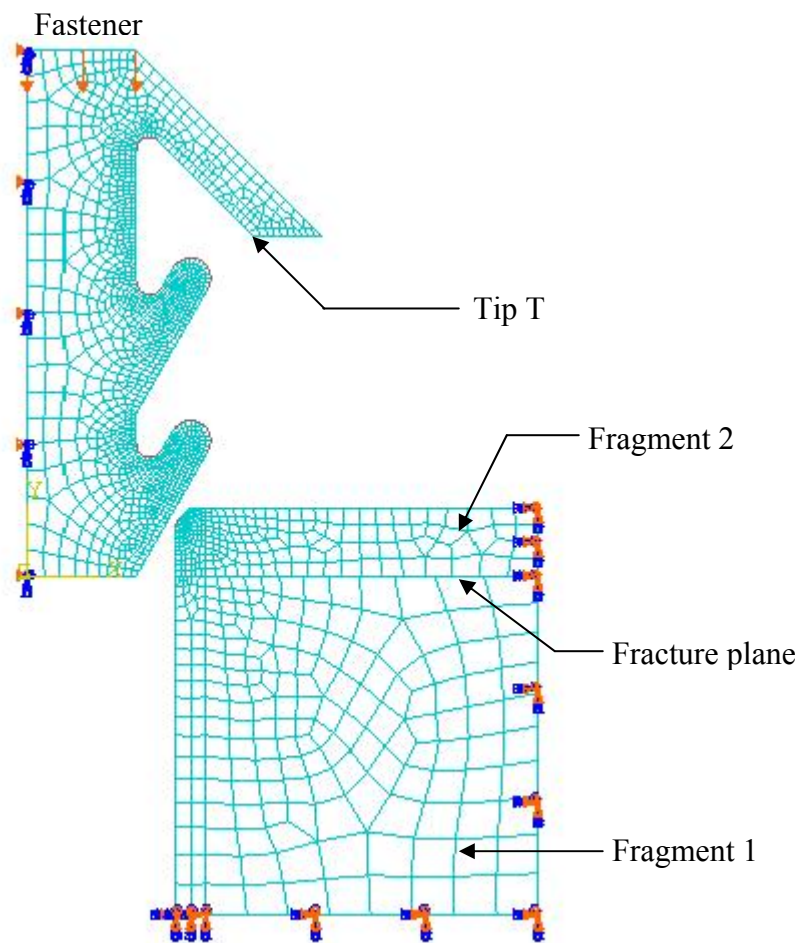
Fig.IV.5. Symmetric finite element model of fastener bone interaction

IV.2. Analytical model of fastener

An analytical model is proposed for explaining the variation in the push-in and pull-out force, when the fastener is inserted into the bone slot.

IV.2.1. Mechanics of the spring element

The spring element deflects on touching the bone surface. The deflection of the spring is governed by the displacement applied to the head of the fastener. The bone provides a reaction force to the tip of the spring causing it to deflect. It is necessary to evaluate this reaction force to determine the push-in force required for inserting the fastener.

The free body diagram of the spring is shown in Fig.IV.6. It is assumed as an inclined cantilever acted upon by a tip load. The tip load is the reaction force provided by the bone on the spring. Properties of bovine cortical bone are applied to the bone block and it is assumed to be an elastic, isotropic and homogeneous material. The material of the cantilever is HDPE, which is assumed to be elastic-perfectly plastic.
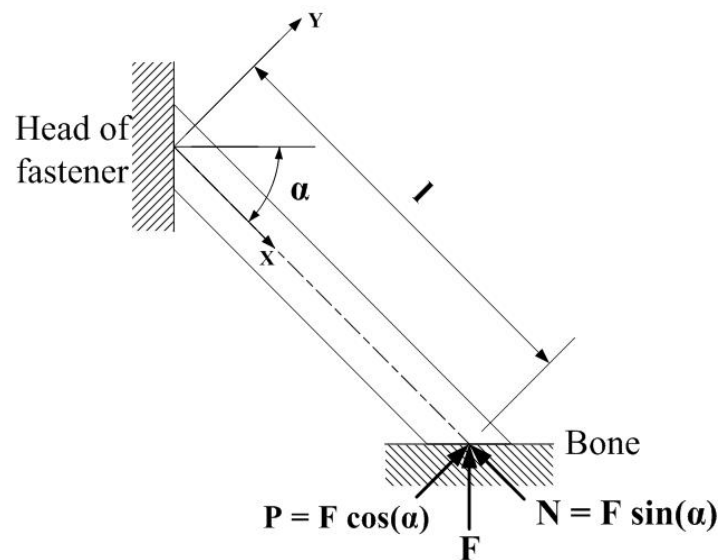
Fig.IV.6. Loading on the spring

Define:

b   width of spring

c   elastic region of spring cross-section

d   shift in center of gravity of spring cross-section

h   thickness of spring

l   length of spring along centroidal plane

m   dimensionless moment

m*   maximum dimensionless moment

n   dimensionless axial force

y   tip displacement of spring

E   Young's modulus

F   reaction provided by bone to the spring

F_S total spring force

M   moment acting at spring tip

M_e moment required for yielding

M_{max} maximum moment acting at root of spring

N   axial component of reaction F

N_e axial force required for yielding

P   transverse component of reaction F

α   orientation of longitudinal axis of spring

Δ   dimensionless shift in center of gravity of spring cross-section

γ   dimensionless elastic region of spring cross-section

κ   curvature of section

$κ_e$ curvature at yielding of section

Ø   dimensionless curvature

ξ   dimensionless location along spring

η   dimensionless tip displacement of spring

$σ_y$ yield strength

$σ_t$ tensile stress generated in spring

$σ_c$ compressive stress generated in spring

Deflection of the spring was analyzed analogous to deflection of an elastic-perfectly plastic cantilever, loaded with an inclined tip load. A previously developed methodology was used for determining the tip load [Yu and Johnson, 1982].

Following assumptions are made to analyze the problem:

1. Force F is assumed to be acting along the center of gravity of the cross-section of the beam.

2. Only the normal reaction F exerted by the bone is considered. As the spring is symmetric about the longitudinal axis, the friction forces between the spring and bone, on either sides of the longitudinal axis cancel each other. Hence, friction force is not considered in the analysis.

3. Plane sections remain plane after bending.

4. Direction and location of force F remain fixed in space.

5. Axial component of force F tends to shift the neutral axis away from the centroidal plane of the beam. Bending moment due to this is neglected as the length of the beam is greater than its deflection.

A prismatic elastic-perfectly plastic beam loaded with end moments M and an axial load N acting through center of gravity is shown in Fig.IV.7.
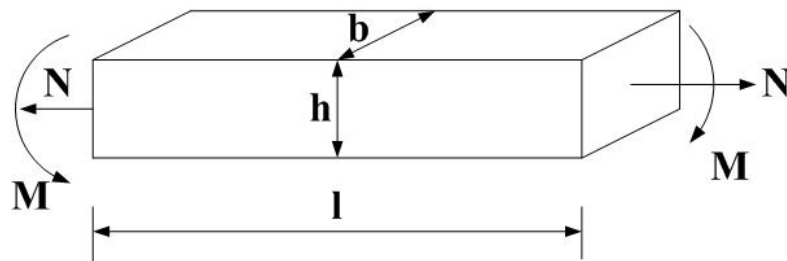
Fig.IV.7. Prismatic beam loaded with end moments and axial load [Yu and Johnson, 1982]

The magnitude and nature of loading could be such that, three different stress states (Fig.IV.8) are possible [Yu and Johnson, 1982].

1. Completely elastic distribution (E_R)
2. Primary plastic regime (P_I): One side of the beam is elastic while the other is plastic.
3. Secondary plastic regime (P_{II}): Both sides of the beam undergo yielding.
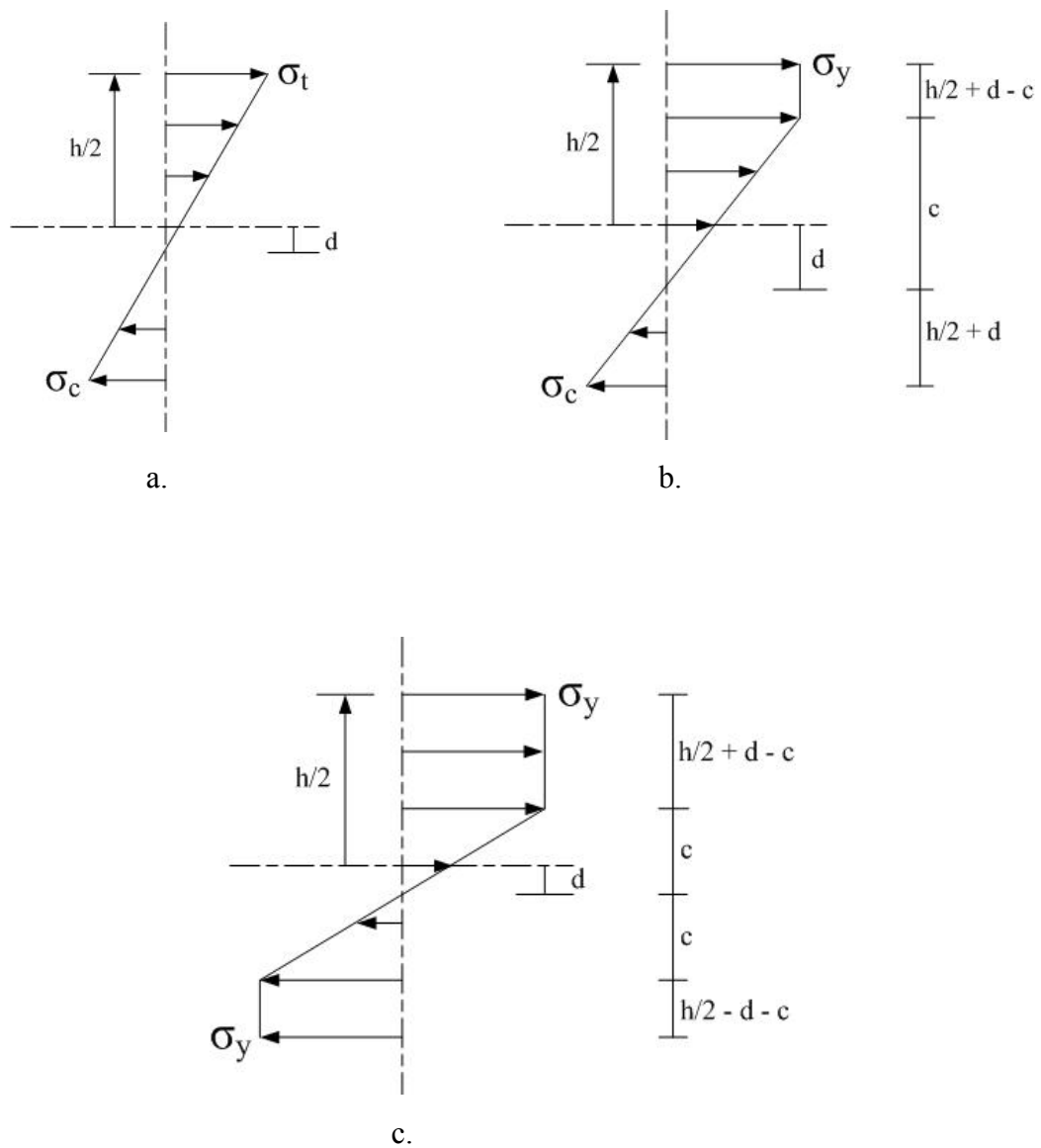
Fig.IV.8. a. Completely elastic regime (E_R); b. Primary plastic regime (P_I); c. Secondary plastic regime (P_{II}) [Yu and Johnson, 1982]

The moment, axial force and curvature of the section required to cause initial yielding of the section is given by:

$$M_e = \frac{\sigma_y bh^2}{6}; \ N_e = \sigma_y bh; \ \kappa_e = \frac{2\sigma_y}{hE}$$

(IV.1)

Dimensionless variables for moment, axial force and curvature are defined as:

$$m = \frac{|M|}{M_e}; \ n = \frac{|N|}{N_e}; \ \phi = \frac{|\kappa|}{\kappa_e}$$

(IV.2)

and

$$\gamma = \frac{c}{h/2}; \ \Delta = \frac{d}{h/2}$$

1. Boundary of elastic regime (E_R): $m + n = 1$

(IV.3)

2. Boundary of primary plastic regime (P_I): $m + n = 1; \ m = 1 + n - 2n^2$

(IV.4)

3. Boundary of secondary plastic regime (P_{II}): $m = 1 + n - 2n^2; \ m = \frac{3}{2}\left(1 - n^2\right)$ (IV.5)

The boundaries for the above three regimes can be plotted as shown in Fig.IV.9.
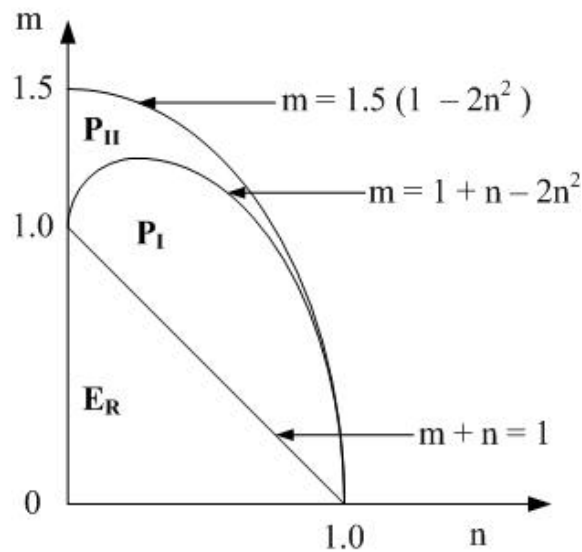
Fig.IV.9. Boundaries of the three stress regions [Yu and Johnson, 1982]

For a cantilever with an inclined tip load as shown in Fig.IV.6, the maximum bending moment at the root of the cantilever is given by

$$M_{max} = Pl$$

The maximum dimensionless bending moment is given by:

$$m^* = \frac{M_{max}}{M_e} = \frac{Pl}{M_e} \tag{IV.6}$$

The dimensionless location along the cantilever and tip displacement are given by

$$\xi = \frac{x}{l}; \quad \eta = \frac{y}{l^2 \kappa_e} = \frac{yhE}{2l^2 \sigma_y} \tag{IV.7}$$

During the subsequent analysis [Yu and Johnson, 1982], it is assumed that the loading is such that the cantilever experiences all the above three regimes along three different segments of the cantilever. The secondary plastic regime is experienced at the

root of the cantilever. The primary plastic regime is observed in the next segment away from the root. The elastic regime is experienced farthest away from the root of the cantilever. The corresponding tip deflection is given by:

$$\eta_{tip} = \frac{m^*}{6}\left[2-\xi_2^2\left(3-\xi_2\right)\right]+\left\{-\frac{m^*}{2}\left[1-\left(\frac{1-n}{m^*}\right)^2\right]+\left(\frac{d\eta}{d\xi}\right)_2\right\}\left(1-\xi_2\right)+\eta_2 \qquad \text{(IV.8)}$$

Where,

$$\eta_2 = A_2\ln\left(1-n\right)+\left\{\frac{2\left(1-n\right)}{m^*}+\left(\frac{d\eta}{d\xi}\right)_1\right\}\left(\frac{2n\left(1-n\right)}{m^*}\right)+\eta_1$$

$$\left(\frac{d\eta}{d\xi}\right)_2 = \frac{2n\left(1-n\right)}{m^*}+\left(\frac{d\eta}{d\xi}\right)_1$$

$$A_2 = \frac{4\left(1-n\right)^3}{m^{*2}}$$

$$\eta_1 = \frac{1}{3m^{*2}}\left[\left(1-n\right)^3 - A_1^{3/2} - 3m^*A_1^{1/2}\xi_1\right]$$

$$\left(\frac{d\eta}{d\xi}\right)_1 = \frac{1}{m^*}\left[1-n-A_1^{1/2}\right]$$

$$A_1 = 3\left(1-n^2\right)-2m^*$$

IV.2.2. Mechanics of the ratchet

The ratchet when inserted into the bone slot undergoes deflection due to the reaction provided by the bone wall. Also, if the level of radial interference is high enough such that the ratchet experiences compression between the bone wall and the shaft of the fastener, then it gives rise to pressure on account of interference. Both these forces act as normal forces acting on the ratchet. The friction force acting perpendicular to these normal forces is termed as push-in or pull-out force, depending upon direction of motion of the fastener.

IV.2.2.1. Deflection of the ratchet

The ratchet is treated as a short cantilever, with the reaction provided by the bone acting as a transverse load (Fig.IV.10). The dimensions of the ratchet ($l_R < 2h_R$) are such that the transverse shear forces would be dominant [Yu and Zhang, 1996]. However an initial approximation is made where in the moment-curvature relationship for pure bending (i.e. without shear load) is applied to the short cantilever ratchet under arbitrary transverse load. Plane sections are assumed to remain plane after bending. The direction and location of force F_R is assumed to remain fixed in space. The frictional forces acting parallel to the longitudinal axis of the ratchet are neglected for simplicity.
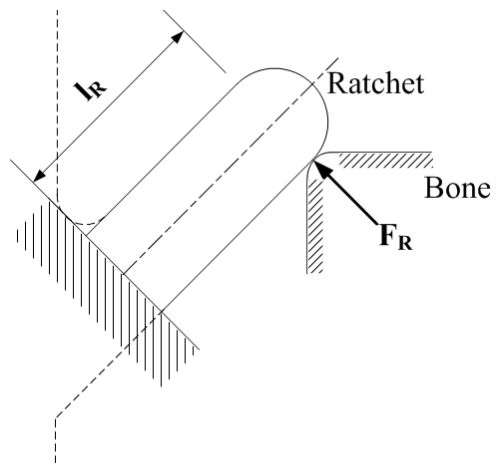
Fig.IV.10. Transverse load on the ratchet

Define:

b_R width of ratchet

h_R thickness of ratchet

l_R length of ratchet along centroidal plane

F_R transverse reaction provided by bone to the ratchet

M_e moment required for yielding

σ_y yield strength

Similar to the analysis of the spring element, the root of the cantilever will yield when the moment on account of the transverse reaction exceeds the maximum permissible moment required for yielding.

Moment required for yielding,

$$M_e = \int_{-h/2}^{h/2} \sigma_y b_R \, y \, dy = \frac{\sigma_y b_R h_R^2}{4} \qquad \text{(IV.9)}$$

The moment on account of the transverse load is

$$M = F_R l_R \qquad \text{(IV.10)}$$

The force required to cause yielding to the root of the cantilever from equations IV.9 and IV.10 is given by:

$$F_R = \frac{\sigma_y b_R h_R^2}{4 l_R} \qquad \text{(IV.11)}$$

IV.2.2.2. Interference of the ratchet

The ratchet will undergo interference when it gets compressed between the shaft of the fastener and the bone wall. The extent of interference will dictate the pressure exerted on the ratchet, which in turn would affect the friction force.

The interference fit problem between a cylindrical hub and shaft has been discussed [Timoshenko and Goodier, 1951]. However, the fastener has a rectangular cross-section and is assumed to be under plane stress state. The radial interference-pressure relation for a plane stress state (Fig.IV.11) is determined to evaluate the friction force.
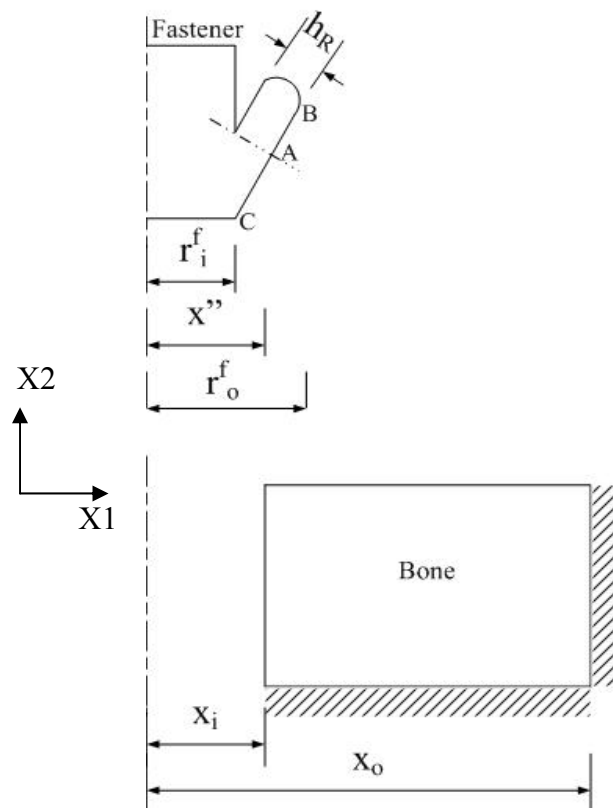
Fig.IV.11. Plane stress interference between fastener and bone

Define:

b_R width of ratchet

h_R thickness of ratchet

l_R length of ratchet along centroidal plane

r^f_i base radius of the fastener

r^f_o outer radius of the fastener

ų   displacement vector

x_i radius of slot in bone

x_o outer radius of bone

x' $r^f_i + h_R$

x'' intermediate radius of fastener in the Region AC

E   Young's modulus

G   shear modulus

P_i interference pressure

δ   effective radial interference

$\sigma_{\alpha\beta}$ stress tensor

$\varepsilon_{\alpha\beta}$ strain tensor

λ   material constant

υ   Poisson's ratio

Interference between the bone and fastener would occur under two scenarios:

1. When the ratchet (Region AB) is under interference.

$$\left(r_i^f + h_R \right) > x_i$$

$$i.e.\ x' > x_i$$

Thus the effective radial interference for Region AB would be: $\delta = \left(x' - x_i \right)$

2. When the shaft of the fastener (Region AC) is under interference.

Thus the effective radial interference for Region AC would be: $\delta = \left(x'' - x_i \right)$

Depending on the level of radial interference, either both scenarios together or only the second scenario might occur.

The above plane stress interference problem is formulated as follows:

For a plane stress state [Slaughter, 2002],

$$\sigma_{\alpha\beta} = \sigma_{\alpha\beta}(X1, X2); \qquad\qquad \alpha, \beta = 1, 2 ; \qquad\qquad \sigma_{13}, \sigma_{23}, \sigma_{33} = 0$$

Equilibrium equation in 2-D is: $\sigma_{\alpha\beta,\beta} = 0$

Equilibrium equation expressed in terms of displacement is:

$$(\lambda + 2G)\, grad\,(div\ \underline{u}) - G(curl(curl\ \underline{u})) = 0 \qquad\qquad (IV.12)$$

Where, $\underline{u} = u_x \hat{i} + u_y \hat{j}$ $\qquad\qquad\qquad\qquad\qquad\qquad\qquad\qquad$ (IV.13)

Substituting IV.13 into IV.12,

$$(\lambda + 2G)u_{x,\,xx} = 0$$

$$\therefore (\lambda + 2G)u_{x,\,x} = C_1'$$

$$\therefore (\lambda + 2G)u_x = C_1' x + C2'$$

$$\therefore u_x = C_1\, x + C2$$

Where,

$$\lambda = \frac{E\nu}{(1+\nu)(1-2\nu)}$$

$$G = \frac{E}{2(1+\nu)} \qquad\qquad\qquad\qquad\qquad\qquad\qquad (IV.14)$$

$$C_1 = \frac{C_1'}{\lambda + 2G}; \qquad C_2 = \frac{C_2'}{\lambda + 2G}$$

Similarly,

$$\therefore u_y = C_3 y + C_4$$

$$\varepsilon_{\alpha\beta} = \frac{1}{2}\left[u_{\alpha,\beta} + u_{\beta,\alpha}\right]$$

$$\therefore \varepsilon_{\alpha\beta} = \begin{bmatrix} C_1 & C_3/2 \\ C_3/2 & 0 \end{bmatrix}$$

(IV.15)

$$\sigma_{\alpha\beta} = 2G\varepsilon_{\alpha\beta} + \lambda\delta_{\gamma\gamma}\varepsilon_{\gamma\gamma}$$

$$\therefore \sigma_{\alpha\beta} = \begin{bmatrix} 2GC_1 + \lambda C_1 & GC_3 \\ GC_3 & \lambda C_1 \end{bmatrix}$$

Let superscript '**b**' and '**f**' and indicate the bone and fastener, respectively.

Thus the displacements are:

$$u_x^b = mx + n; \quad u_x^f = px + q$$

(IV.16)

Boundary Conditions:

1. As the fastener is symmetric there is no displacement along the line of symmetry.

$$@\, x = 0, \quad u_x^f = px + q = 0$$

$$\therefore q = 0$$

(IV.17)

$$\therefore u_x^f = px$$

2. There is continuity between the ratchet surface and the bone wall. Therefore, after the deformation due to interference, the two surfaces should be in contact.

$$\therefore x_i + u_x^b = x' + u_x^f$$

$$\therefore x_i + (mx_i + n) = x' + px' \qquad \text{(IV.18)}$$

$$\therefore \delta = (mx_i + n) - px'$$

3. The bone is assumed to be fixed at its outer surface

$$@\, x = x_o ; \quad u_x = 0$$

$$\therefore mx_o + n = 0 \qquad \text{(IV.19)}$$

$$\therefore n = -mx_o$$

4. At the interface, tractions are equal and opposite

$$\therefore \sigma_{xx}^b = \sigma_{xx}^f = -P_i \qquad \text{(IV.20)}$$

Where, P_i is the pressure generated due to interference.

From IV.15, IV.16 and IV.20

$$(2G_b + \lambda_b)m = (2G_f + \lambda_f)p = -P_i$$

$$\therefore m = \frac{-P_i}{(2G_b + \lambda_b)} \qquad \text{(IV.21)}$$

$$\therefore p = \frac{-P_i}{(2G_f + \lambda_f)}$$

Substituting IV.21 and IV.19 in IV.18,

$$\delta = \frac{-P_i}{(2G_b + \lambda_b)} x_i + \frac{P_i}{(2G_b + \lambda_b)} x_o + \frac{P_i}{(2G_f + \lambda_f)} x'$$

$$\therefore \delta = P_i \left[\frac{(x_o - x_i)}{(2G_b + \lambda_b)} + \frac{x'}{(2G_f + \lambda_f)} \right] \qquad \text{(IV.22)}$$

Similarly, for the second scenario,

$$\therefore \delta = P_i \left[\frac{(x_o - x_i)}{(2G_b + \lambda_b)} + \frac{x''}{(2G_f + \lambda_f)} \right] \qquad \text{(IV.23)}$$

CHAPTER V

EXPERIMENTS

The experiments that were conducted for prototype development and validation are enumerated below.

1. Friction test: It was conducted to determine the coefficient of friction between HDPE and bovine bone subjected to an interference fit.

2. Surface topography of drilled bone surface: Surface topography of the drilled bone surface was studied to examine the effect of drilling orientation on the roughness of the drilled surface.

3. Prototype manufacturing: Prototype of the fastener was manufactured from micromilling and micromolding techniques for in-vitro testing of the fastener.

4. In-vitro testing: The fasteners were subjected to in-vitro testing to determine their push-in and pull-out force and compare the results with the FEA and analytical predictions.

5. Cross-sectioning of fastener-bone interface: The fastener was sectioned in an inserted state to study its interaction with bone.

V.1. Equipment

The equipment that was used for conducting the above experiments is listed below.

1. Band saw: Doall Model V-36
2. CNC milling machine: HAAS VOP-B VF1
3. Micromolding system: Milacron BabyPlast
4. Microscope: Olympus STM6 3D measuring microscope
5. Milling machine: Bridgeport 8F
6. Polisher: Buehler Handimet Grinder

7. Profilometer: PocketSurf III-Federal

8. Tensile testing machine: Instron 4411

9. Ultrasonic bath: Struers Metason 200

10. Vibratory polisher: Buehler Vibromet 2

V.2. Friction test

The interference fit between the fastener and the bone wall would hold them together. The retention strength of a pin inserted inside a hub in an interference fit is directly proportional to the level of interference, area of contact and the coefficient of friction between the materials of the pin and the hub. The first two parameters depend upon the geometry of the fastener-bone block assembly, whereas the coefficient of friction is a material property. To achieve correct predictions of push-in and pull-out force by finite element analysis, it was necessary to determine the coefficient of friction between HDPE and cortical bovine bone.

The coefficient of friction of polymers is influenced by normal load, speed and temperature [Bely et al., 1982]. A variation in level of interference will change the interference pressure on the polymeric fastener. Hence it was deemed necessary to study the effect of interference pressure on the coefficient of friction of HDPE when in contact with cortical bone, for a constant speed and temperature.

V.2.1 Experimental set-up

The experimental setup was decided upon such that it would be able to determine the coefficient of friction between HDPE and cortical bone, and to simulate actual functioning of the fastener. A series of cylindrical pins of varying diameters were milled from HDPE sheet of 4.76 mm (3/16 in), using HAAS VOP-B VF1 CNC milling machine. Milling operation was used to manufacture the pins as it was also to be used for prototype development. One surface of the bone specimen was milled flat on a

Bridgeport 8F vertical milling machine before the drilling process. This was done so that the bone could be rested on the milled flat surface while drilling, to achieve a true hole. Holes were drilled inside the bone using a drill bit of diameter 3.175 mm (1/8 in) on a Bridgeport 8F vertical milling machine. Geometry of the pin and bone sample was as shown in Fig.V.1. and Fig.V.2., respectively. Average diameter of each pin was determined by measuring its diameters at five locations along its length. Similarly the average diameter of each hole was measured at four different angular orientations. All the measurements were done on an Olympus STM6 measuring microscope, which has a resolution of 0.1 μm. The radial interference was thus determined for each pair of pin and hole from the average radius of pin and hole as measured above.
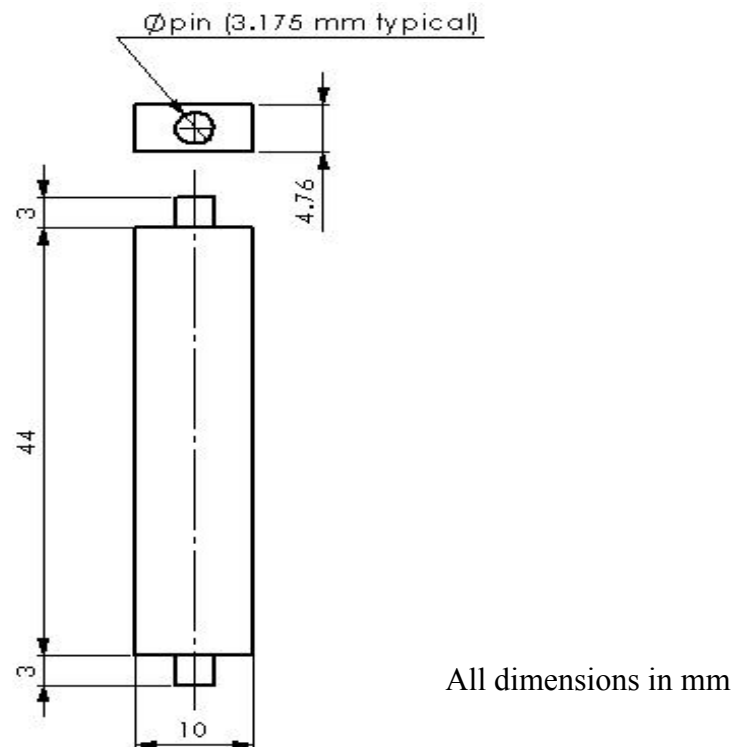

All dimensions in mm

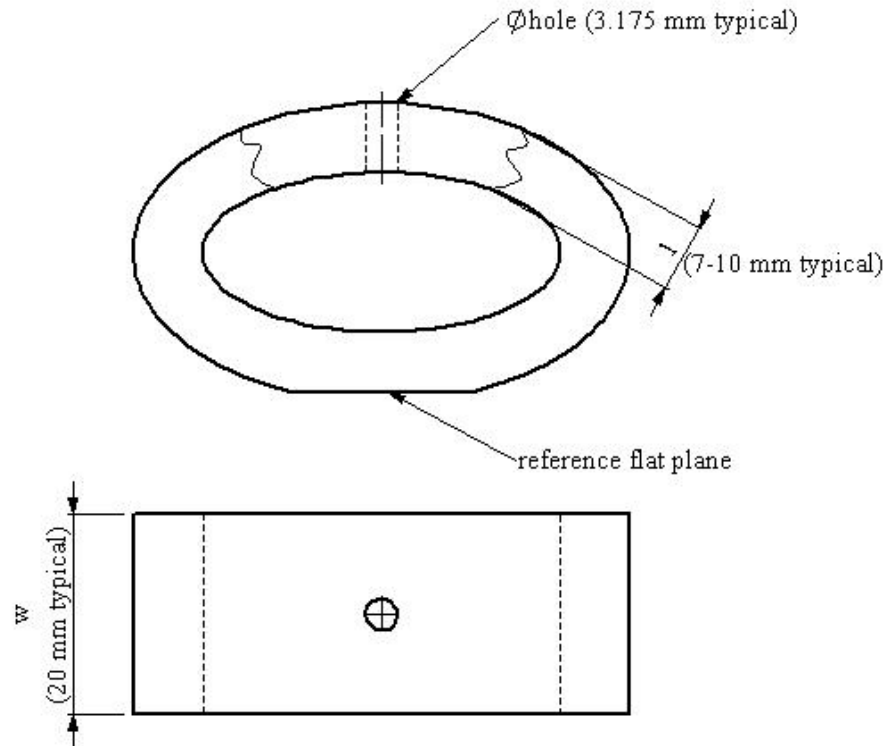Fig.V.1. Geometry of HDPE pin for friction test

Fig.V.2. Geometry of bovine femur bone for friction test

The methodology discussed in III.8. was used to determine the coefficient of friction between HDPE and bovine bone. However in the actual scenario, the configuration of the bone with a hole drilled inside it was different from the configuration of the hub. In the first case, the hole was drilled normal to the surface of the bone (Fig.V.2.), whereas the hub was a hollow cylinder.

The surface of the bone with the drilled hole was assumed as a flat plate with a centrally located hole, which is subjected to internal pressure due to interference. By application of Saint Venant's principle, it was approximated that, for a cylinder with a sufficiently large outer diameter (in comparison to the hole diameter), the stress field would be similar to that in a plate with a centrally located hole, at a far distance away

from it [Timoshenko and Goodier, 1951]. Thus the plate of width 'w' and thickness 'l' can be approximated to a cylinder of diameter 'w' and height 'l', inscribed in it. Hence the above stated relationship for a cylindrical pin and hub was used to determine the interference pressure.

To determine the coefficient of friction, it was necessary to experimentally determine the friction force. The experimental set-up was as shown in Fig.V.3. The bone specimen was clamped on the fixed cross head of an Instron 4411 tensile testing machine and the HDPE pin was held in the movable cross head. Axis of the HDPE pin was aligned with that of the hole drilled in the bone by visual inspection. The upper cross-head was given a downward displacement of 0.042 mm/sec (0.1 in/min). The HDPE pin was inserted into the hole till a depth of approximately 2.5 mm and the resulting force was recorded.

All the pins were used only once, but the holes were used on more than one occasion due to limitation on the availability and preparation of bone specimens. Hence, each bone specimen was cleaned with water, compressed air and Struers Metason 200 ultrasonic bath to remove any debris that might have been sticking to the surface of the hole.
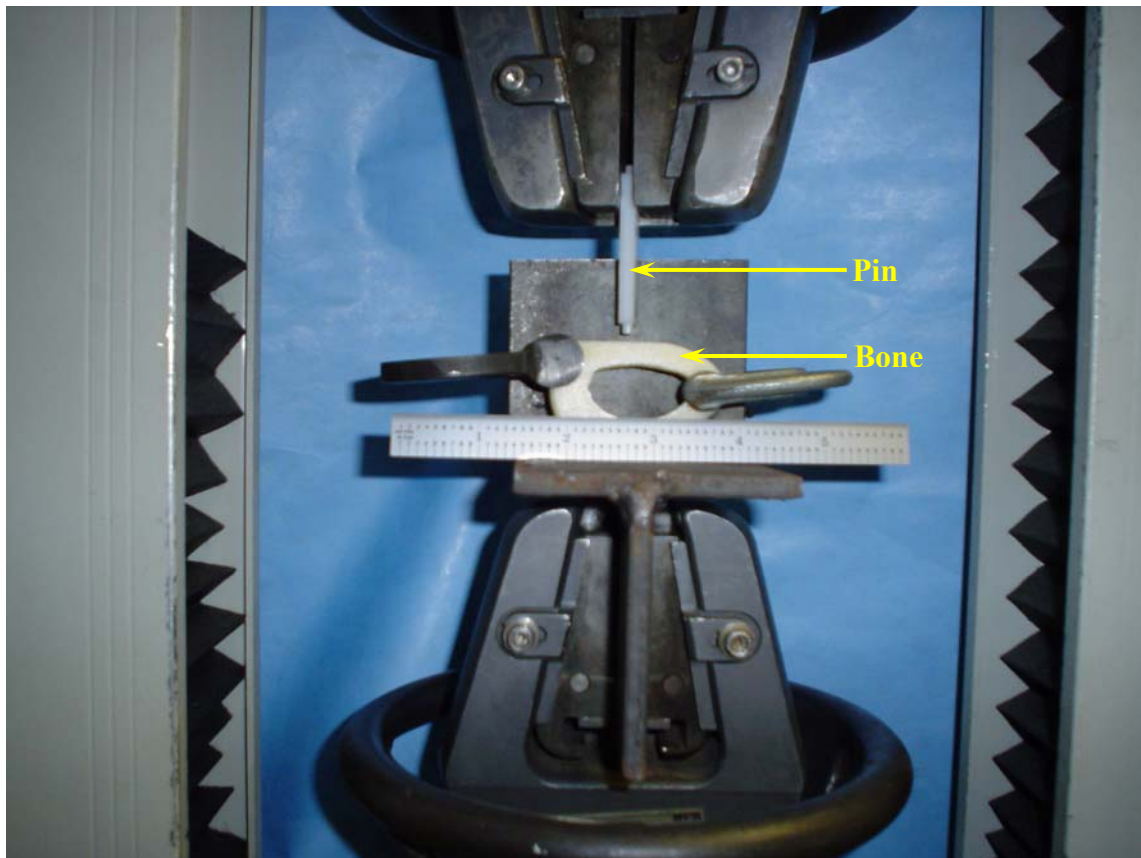
Fig.V.3. Set-up for friction measurement

V.2.2. Load cell calibration

The load cell on the Instron 4411 testing machine had a capacity of 4450 N (1000 lb) with an accuracy of ± 0.5 % up to 89 N (20 lb) and a resolution of 0.05 N (0.01 lb). As it was possible that the loads encountered during the tests might be lesser than 89 N, it was necessary to check the accuracy of the load cell below this load level. This was done prior to conducting the friction tests. Dead weights were suspended from the load cell and readings were noted and compared with the actual weights. The load cell was

found to have an accuracy of ± 2 % in the 0 to 89 N load range (Table V.1). Comparison of the actual and load cell measured load is shown in Fig.V.4.

Table V.1. Comparison of load cell readings and actual load

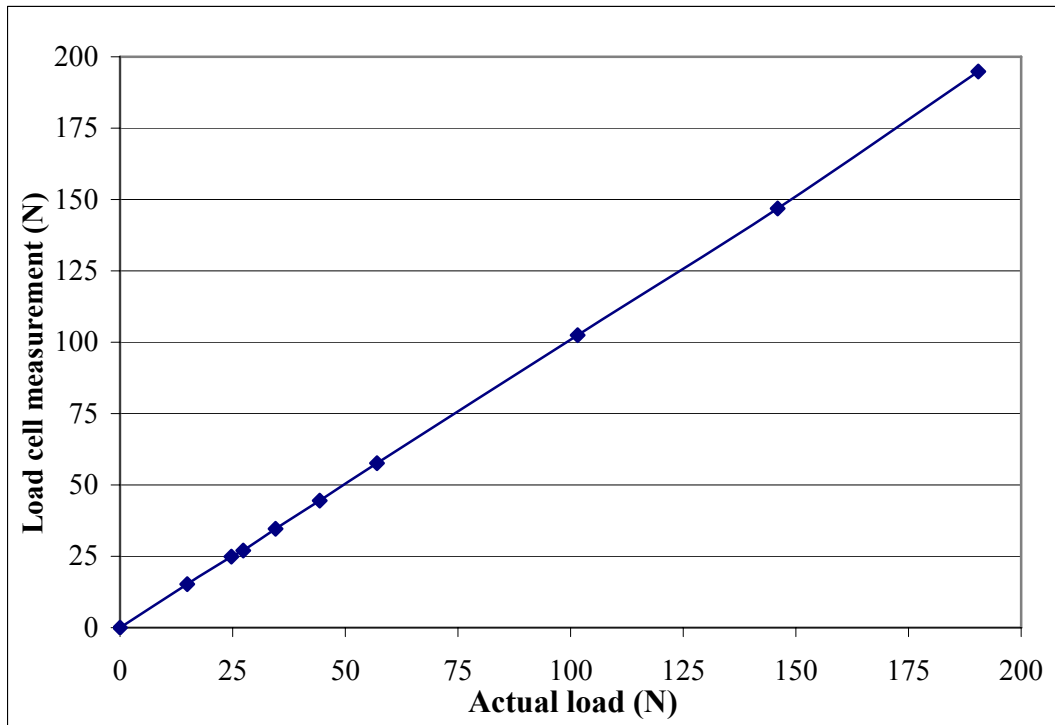| Instron tensile testing machine - Calibration		
Actual load (N)	Load cell measurement (N)	% error
0.00	0.000	0.00
14.91	15.21	1.97
24.72	24.92	0.79
27.37	26.98	-1.43
34.53	34.63	0.28
44.34	44.54	0.44
57.03	57.58	0.98
101.53	102.51	0.96
145.97	146.86	0.61
190.51	194.83	2.27

Fig.V.4. Load cell calibration

V.3. Surface topography of drilled surface of bone

Bone is an anisotropic, inhomogeneous material. Hence it exhibits different surface topography along different cutting planes [Jacobs et al., 1974]. During the initial stages of design of the fastener, it was thought necessary to study the topography of the drilled surface of the bone, as it might affect the functionality of the interference fit between the fastener and bone. As the material properties of bone vary with location and orientation, the roughness of the drilled surface of bone might vary accordingly. It was thought that a drastic difference in surface roughness might influence the strength of the fastener-bone joint.

V.3.1. Experimental set-up

      Direction of propagation of fracture depends on the nature of loading [Müller et al., 1991]. Hence implants for fixation need to be inserted at different angles with respect to the bone surface. The surface roughness was measured along three different drilling orientations: along the longitudinal axis (Axial), along the radius (Radial), and at an angle of 45° to it (Fig.V.5). Also, for the later two directions, the surface roughness was measured at two locations, closer to the inner radius and closer to the outer radius.
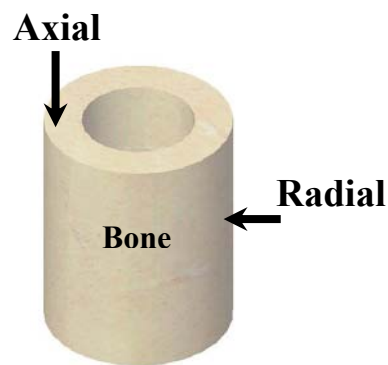

Fig.V.5. Drilling orientations for surface topography of bone

      To begin with, the planar ends of the cylindrical bone pieces were milled on a Bridgeport Model 8F milling machine to get flat and parallel surfaces. This was done to ensure that the pieces could be clamped rigidly while drilling. The bone specimens were stored in saline solution before and after each machining step. For drilling, the specimens were clamped between the flat ends and mounted on an indexing vice. Guidelines provided by Jacobs et al. [1976] and Saha et al. [1982] were used for drilling

the bone. A drill of diameter 3.175 mm with a helix angle of 24° to 36° and point angle of 118° was used. Spindle speed was set at 500 rpm and manual feed was given.

Specimens were sectioned with a Doall V-36 band saw along the centroidal plane of the drilled hole. Final geometry of the sectioned specimens is shown in Fig.V.6. The lower surface of the sectioned specimen was polished with a 150 grit sand paper to make it flat and parallel to the ground. Average roughness of the drilled surface was measured with a PocketSurf III-Federal profilometer. As the thickness of the bone pieces were 7 to 10 mm thick along the radial direction (Refer to Fig.V.5.), the traverse length for the stylus was kept at 3.5 mm. Thus at least two non overlapping regions, one closer to the inner radius (I.R.) and other closer to the outer radius (O.R.) of the bone could be measured.
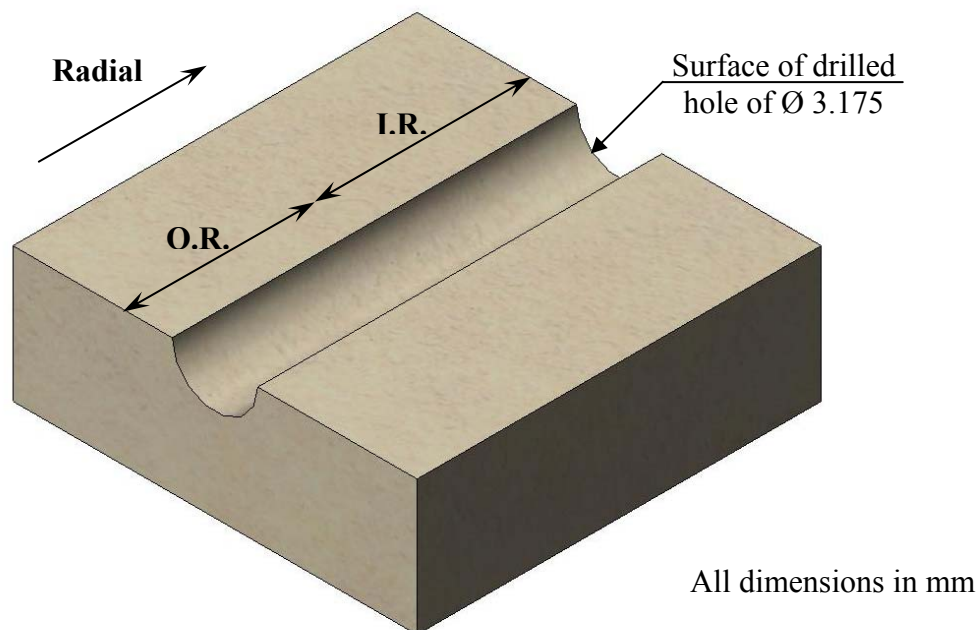

Fig.V.6. Specimen for measurement of roughness of drilled surface of bone

V.4. Manufacturing of fastener prototype

To test the functioning of the fastener and compare it with the finite element predictions, it was necessary to develop a prototype of the fastener.

V.4.1. Micromilling

The fastener was machined on a HAAS VOP-B VF1 CNC milling machine. A HDPE sheet of thickness 4.7625 mm (3/16 in) was used as the raw material. To support the sheet during machining, it was placed in a pocket milled inside an aluminum block. The geometry of the block with the HDPE coupon placed inside it is shown in Fig.V.7.
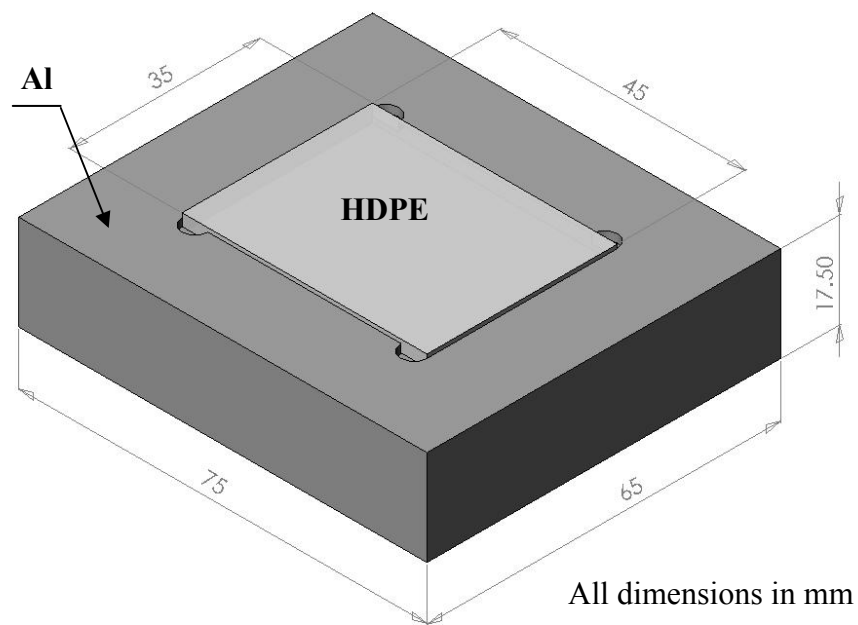

Fig.V.7. HDPE set in aluminum block for micromilling prototype

The coupon was prevented from moving during machining by adhering it to the base of the pocket milled inside the aluminum block. The adhesive used was Crystalbond™ 509, manufactured by Electron Microscopy Sciences. The block was heated to the flow temperature of the adhesive (77 °C) and a uniform layer of adhesive was applied on the base of the pocket. The HDPE coupon was then placed inside the pocket and pressed against it to ensure uniform adhesion. The coupon could be detached by heating up the block to the flow point of the adhesive.

It was necessary to overcome the drawback of the low aspect ratio of the end mills and achieve a higher thickness for the fastener. A thickness twice as that of the exposed length of the smallest end mill used, was made possible by machining the HDPE coupon from both sides. The HDPE coupon was adhered to the block and face milled to achieve a thickness of 2.2 mm, which is less than twice the exposed length of the smallest end mill used. Profile of the fastener was milled till a depth of 1.1 mm. Following this, the coupon was detached from the block, flipped over and the machined surface was adhered to the pocket. The top half of the thickness of the coupon was then machined. The CNC code was developed such that the profile of the fastener was located centrally on the coupon and the flipping action would not affect the location of the fastener with respect to the axis of the cutting tool.

V.4.2. Micromolding

The mold was aluminum based and the cavities were made by micromilling. To overcome the drawback of the low aspect ratio of the end mills, a split cavity mold was used (Refer to Appendix C for NC codes). A shrinkage factor of 2.5 % was used while milling the cavity [Menges and Mohren, 1993]. The molding process parameters were set as in Table V.2. The geometry of the mold with the mold inserts is shown in Fig.V.8.

Table V.2. Molding process parameters

Molding Process Parameters		
Parameter	**Value**	**Units**
Injection time	5.0	sec
Cooling time	10.0	sec
Ejection time	0.1	sec
Ejection pause	1.0	sec
2nd shot load time	2.0	sec
Load material	10.0	mm
Piston diameter	10.0	mm
Minimum operating stroke	15.0	mm
Injection pressure	6.5	MPa
Oil temperature	< 50.0	°C
Plasticizer	200.0	°C
Injection chamber	200.0	°C
Nozzle	210.0	°C
Mold	175.0	°C

The water supply was switched on before starting the molding system. Subsequently, the mold along with the injection chamber, plasticizer and nozzle were heated to their specified temperature. The mold cavity was filled in two shots. On completion of injection, the machine was stopped and the mold was allowed to cool down to ambient temperature. The fasteners were then separated from the sprue.
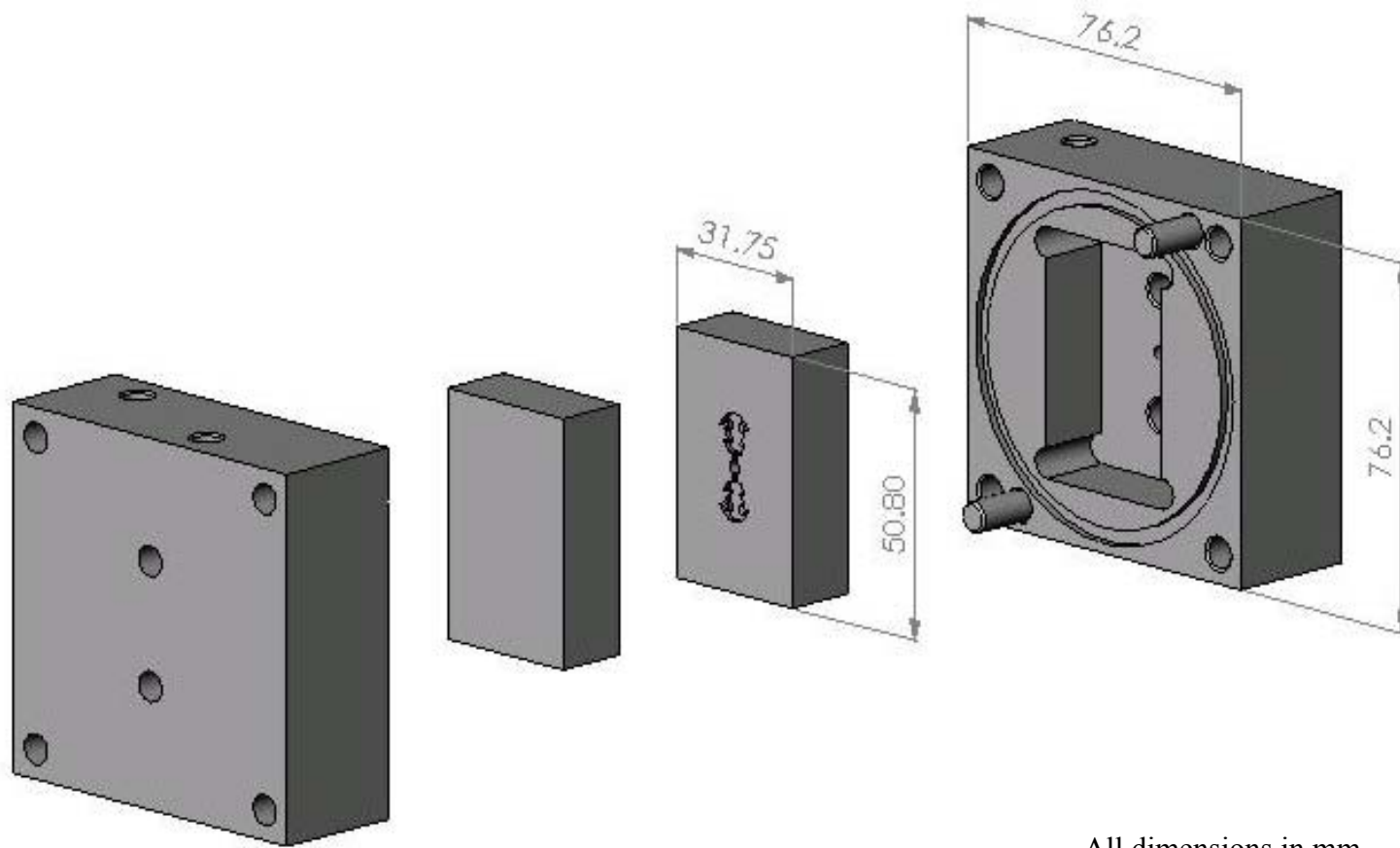
All dimensions in mm

Fig.V.8. Mold tool with mold inserts for micromolding prototype

V.5. In-vitro testing

In-vitro testing of the fastener was necessary to determine the push-in and pull-out force under varying levels of interference. The experimental set-up was similar to ASTM F 1540 – 95 test set-up for a non threaded implant. This test is meant to determine the pull-out force but was adapted to provide the push-in force as well.

V.5.1. Experimental set-up

Molded samples were used for in-vitro testing. The bone specimens were refrigerated in saline water prior to testing. The experimental set-up was similar to that used for the friction test. However some changes were necessary to account for the geometry of the fastener. The fastener has a 2-D profile and is assumed to be under plane-stress state. Hence the fastener could not be inserted into a circular hole drilled inside the bone as it would have violated the above assumption. It was necessary to ensure that the entire thickness of the fastener was in uniform contact with the bone wall and the planar surfaces of the fastener were stress free. Thus the fastener was inserted in an oblong slot milled inside the bone. As the length of the slot had to be greater than the thickness of the fastener, bending or toppling of the fastener was observed during insertion. To avoid this, guide pins were inserted inside the slot, one on each side of the fastener. A centrally located pin hole was made inside the fastener prior to the test. This was done so that a string could be passed through it to form a loop. This was hung from a metallic hook held in the movable cross head of the testing machine, to facilitate pull-out.

V.5.2. Push-in test

A punch held in the movable cross head of the testing machine was used to push the fastener inside the bone slot (Fig.V.9). The center of the slot, axis of the fastener and axis of the punch were aligned by visual inspection, prior to insertion. The cross head speed was set at 0.0423 mm/sec (0.1 in/min). The cross head was given a downward displacement and the fastener was inserted into the bone block till its head deformed and became flat. The change in push-in force with cross-head displacement was recorded.
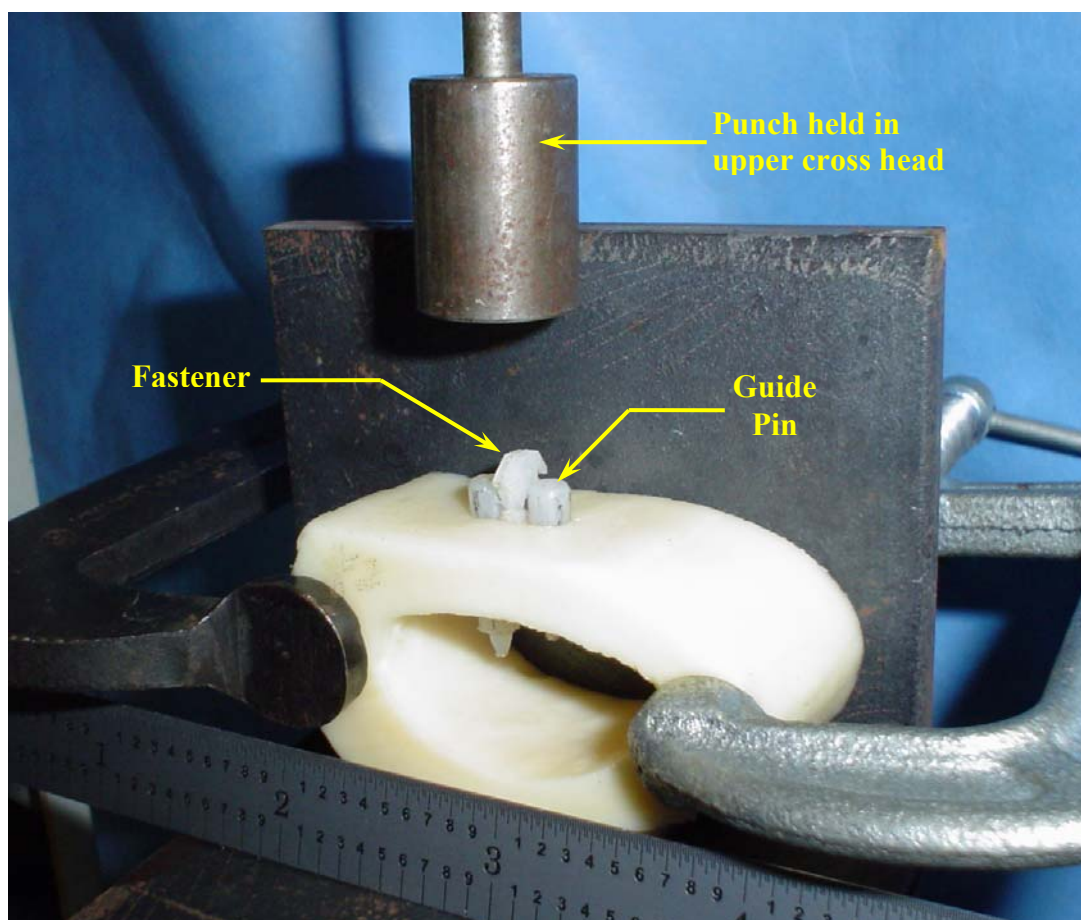

Fig.V.9. Set-up for push-in test

V.5.3. Pull-out test

After the fastener was completely inserted, the cross head was raised and the punch was replaced by a metallic hook (Fig.V.10). The hook was aligned with the axis of the fastener. A nylon string was passed through the pin hole in the fastener and a loop was made around the hook. The cross head was provided an upward displacement with the same speed of 0.0423 mm/sec (0.1 in/min) as in push-in, till the fastener was completely pulled-out from the bone block. The variation in force with the cross head displacement was recorded.
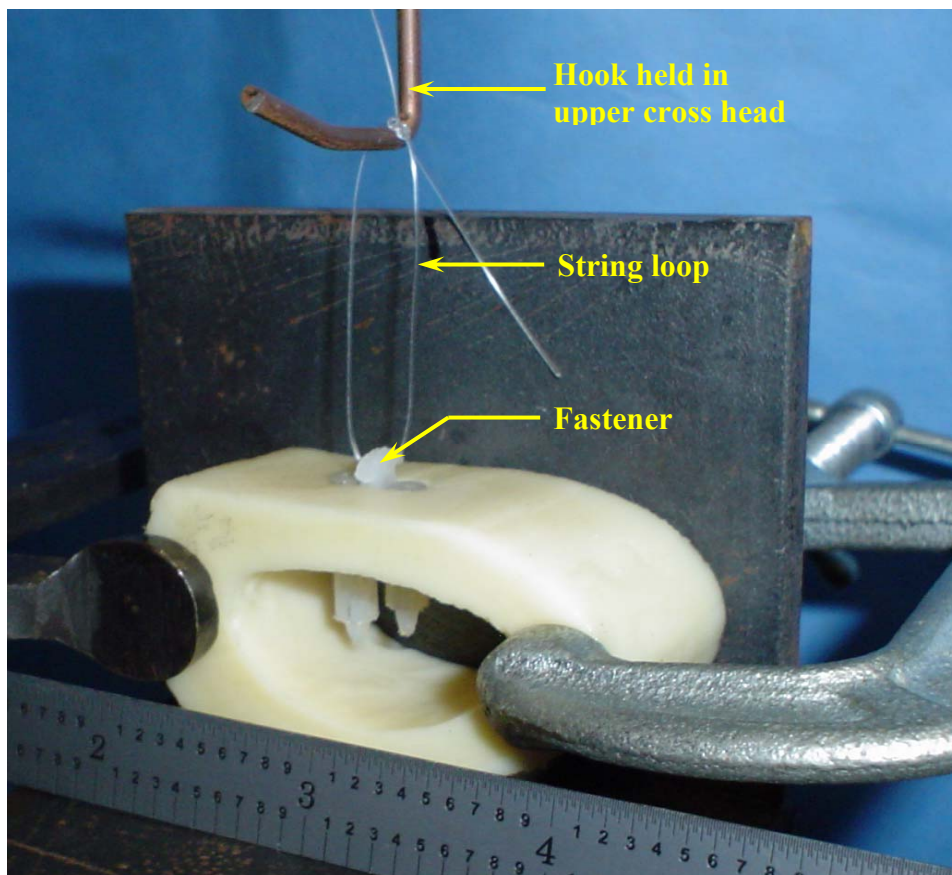

Fig.V.10. Set-up for pull-out test

V.5.4. Cross sectioning of inserted fastener

As the fastener is inserted inside the bone, the ratchets deform and slide against the bone wall. Hence it was essential to study the fastener-bone wall interface to get a better understanding of the fastener-bone interaction such as spring deflection, ratchet deformation and interference.

After the fastener was inserted inside the bone slot, the bone was sectioned on either sides of the slot with a Doall V6 band saw to get a coupon sized specimen. Two such specimens with different levels of radial interference were prepared. These were then set in EPO-FIX™ embedding resin. On room temperature curing of the resin, the specimens were sectioned with the band-saw along the mid-plane of the fastener. The sectioned surface was then manually, sequentially polished till 600 grit size, on a Buehler Handimet grinder. Following this diamond metallographic compound of roughness 15 μm, 9 μm, 5 μm and 1 μm were used sequentially for manually polishing the surface on a Buehler Vibromet 2 vibratory polisher.

CHAPTER VI

RESULTS AND DISCUSSION

VI.1. Ratchet design

The variation in push-in and pull-out force with insertion depth for design F is shown in Fig.VI.1. From the push-in plot it can be seen that, as the fastener was inserted into the bone, a sudden rise in force (F_{imax}) was observed due to initiation of contact with the edge of the slot. As the push-in force was compressive in nature, it was indicated by a negative sign. Subsequently, the force reduced and became constant as the ratchet was completely in contact with the bone wall. This constant value was taken as the push-in force (F_i) required for the fastener. The pull-out force was tensile in nature and indicated by a positive sign. The pull-out force (F_o) was highest to initiate separation between the fastener and the bone. It subsequently reduced with reducing contact between the fastener and bone, and finally dropped to zero indicating complete separation. The push-in and pull-out force values for different designs were as given in Table VI.1.
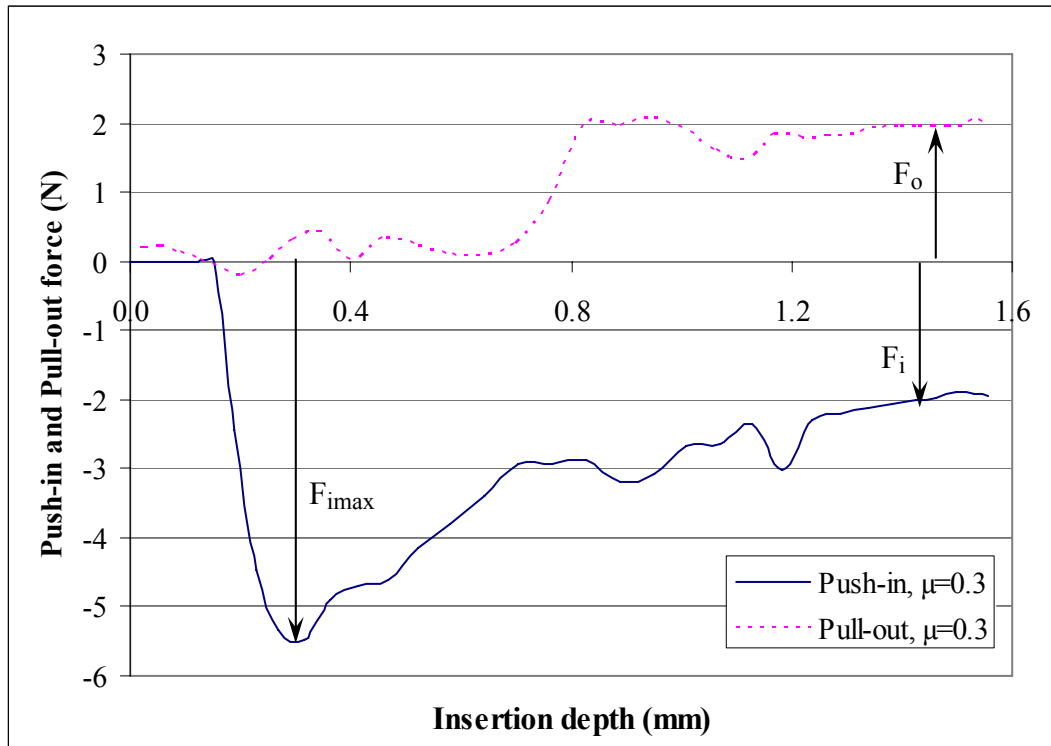
Fig.VI.1. FEA prediction of push-in and pull-out force with insertion depth

Table VI.1. Push-in and pull-out force for different designs

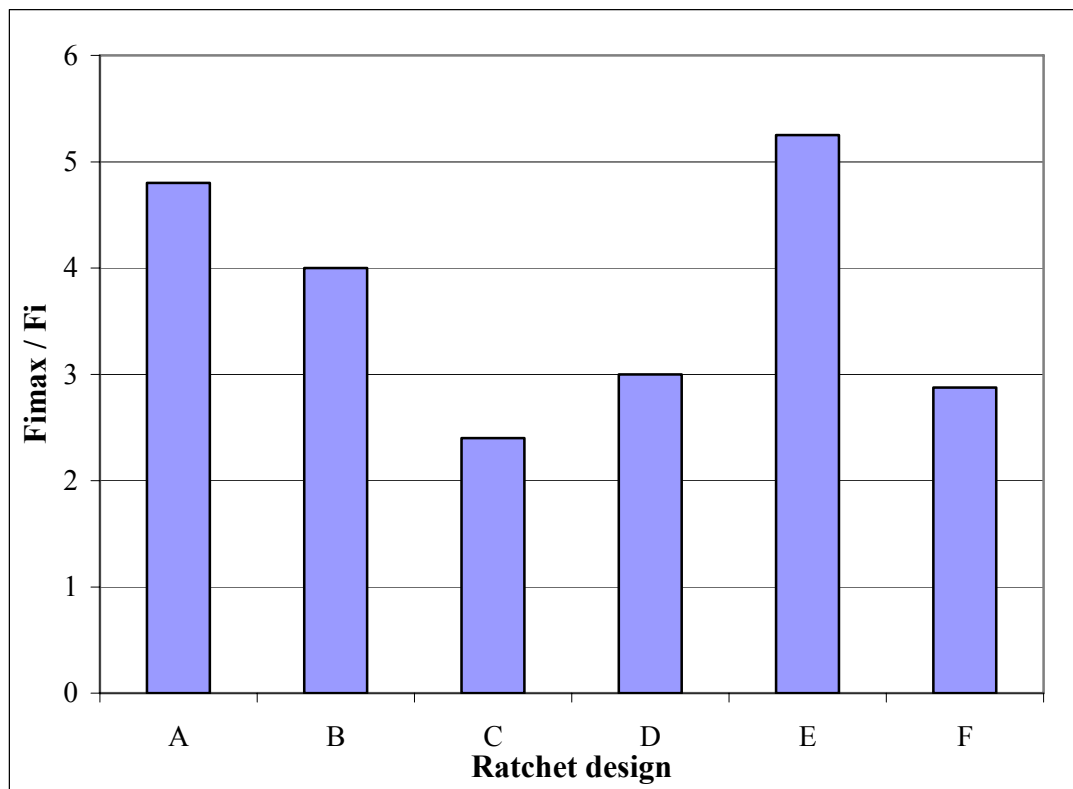| Design	Push-in force F_i (N)	Max. Push-in force F_{imax} (N)	F_{imax} / F_i	Pull-out force F_o (N)	F_o / Insertion depth (N/mm)
A	0.25	1.20	4.80	0.25	0.25
B	0.75	3.00	4.00	0.75	0.46
C	2.50	6.00	2.40	2.5	0.69
D	1.75	5.25	3.00	1.75	0.60
E	1.00	5.25	5.25	1.00	0.63
F	2.00	5.75	2.88	2.00	0.91

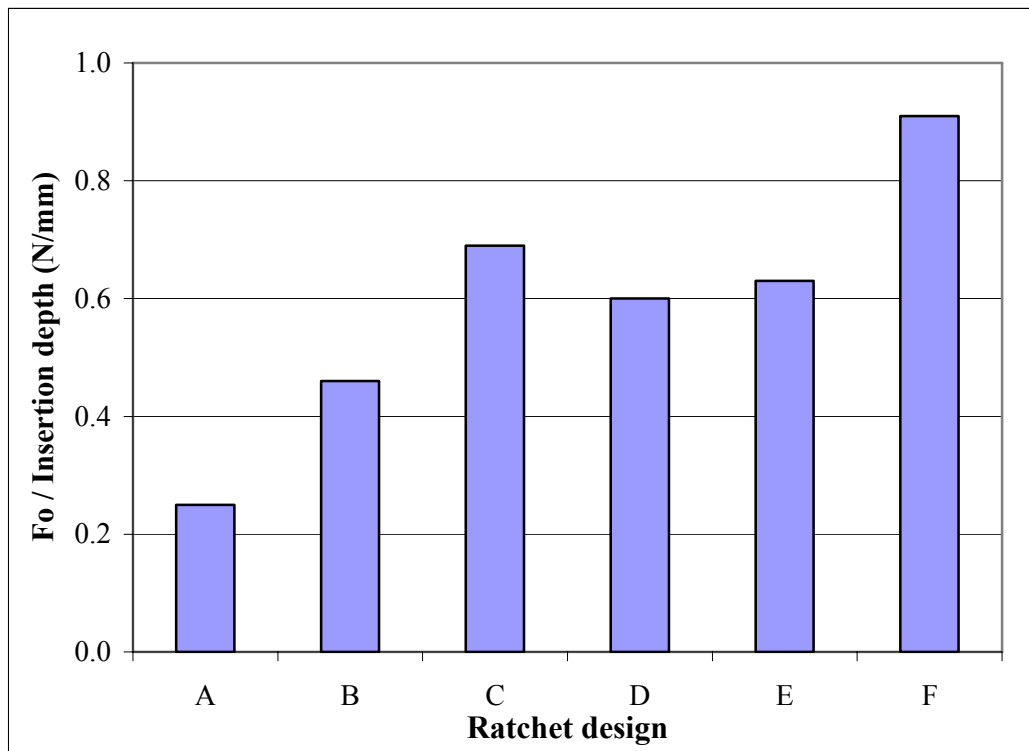Fig.VI.2. Ratio of maximum to constant push-in force for different designs

Fig.VI.3. Pull-out force per unit length of insertion for different designs

From Fig.VI.2 it can be seen that for Design C, the ratio of maximum to constant push-in force was the least amongst all designs. Design F had a slightly higher value. This ratio indicates the peak force that the ratchet would need to sustain, while being pushed inside the bone. A higher peak force would be damaging not only to the ratchet but also to the bone fragment that is to be fixated.

For stability of the fracture site, it is necessary that the fastener hold the fragments together under the application of external load. Hence a higher pull-out force per unit length of interference would be able to sustain higher external load acting on the fastener-bone joint. Design F provided the highest pull-out force per unit length of interference (Fig.VI.3); therefore it was selected for prototype development.

VI.2. Coefficient of friction between HDPE and bovine cortical bone

The push-in force required to push the HDPE pin inside the hole was plotted against the insertion depth. A typical plot of push-in force against insertion depth is shown in Fig VI.4.
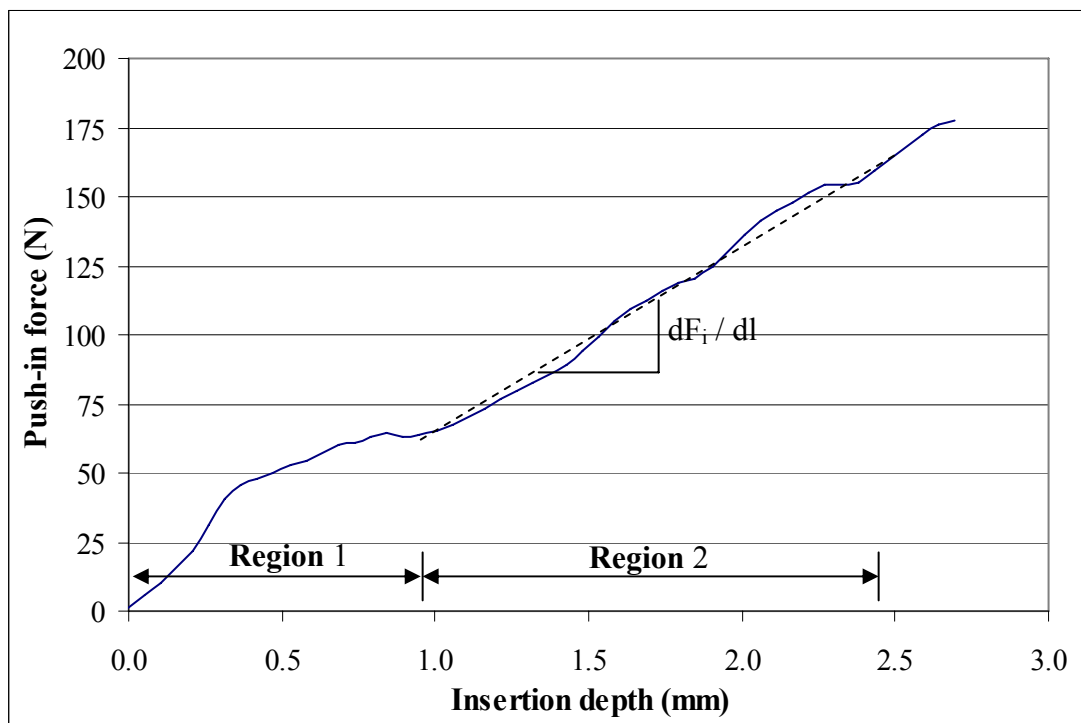

Fig.VI.4. Variation of push-in force with insertion depth

The plot was divided into two regions. In Region 1, an initial sharp rise in force was observed due to initiation of contact between the pin and the hole. Subsequently, the slope of the curve reduced as contact got uniformly established. In Region 2, an almost

linear increase in push-in force with insertion depth was observed. As seen from equation III.2, the push-in force directly varies with the length of contact. The slope of the plot in Region 2 gives the change of push-in force with insertion depth. This was used in equation III.4 to determine the coefficient of friction. Results of friction tests have been summarized in Table VI.2.

The relationship between the radial interference and interference pressure as given by equation III.1 is valid only for linear elastic, isotropic materials. HDPE was assumed to be elastic-perfectly plastic. Hence at higher levels of interference, the pressure evaluated from the above expression was greater than the yield strength of HDPE. Hence, instead of correlating the coefficient of friction with interference pressure, a dimensionless parameter which was a ratio of radial interference (δ) to radius of the hole (r) was considered. For a hole radius (r) of 1.5875 mm and plate width (w) of 20 mm, the relationship between the radial interference and interference pressure given by equation III.1 was:

$P_i = 1019.96\ \delta$

For interference pressure equal to the yield strength of HDPE, the radial interference required is:

$\delta = 24.6/1019.96 = 0.0241$ mm.
$\delta/r = 0.0241/1.5875 = 0.0152$

Table VI.2. Coefficient of friction between HDPE and bovine bone for varying levels of radial interference

| Test #	$\emptyset_{hole}$ (mm)	$\emptyset_{pin}$ (mm)	Radial Interference δ (mm)	Dimensionless Interference δ/r	Coefficient of friction μ
1	3.1620	3.1890	0.0135	0.0085	0.264
2	3.1785	3.2070	0.0142	0.0090	0.265
3	3.1700	3.2010	0.0155	0.0098	0.211
4	3.1700	3.2090	0.0195	0.0123	0.170
5	3.1720	3.2210	0.0245	0.0154	0.213
6	3.1720	3.2390	0.0335	0.0211	0.215
7	3.1650	3.2370	0.0360	0.0227	0.296
8	3.1700	3.2510	0.0405	0.0256	0.320
9	3.1620	3.2480	0.0430	0.0272	0.344
10	3.1700	3.2790	0.0545	0.0344	0.300
11	3.1785	3.2940	0.0578	0.0363	0.183
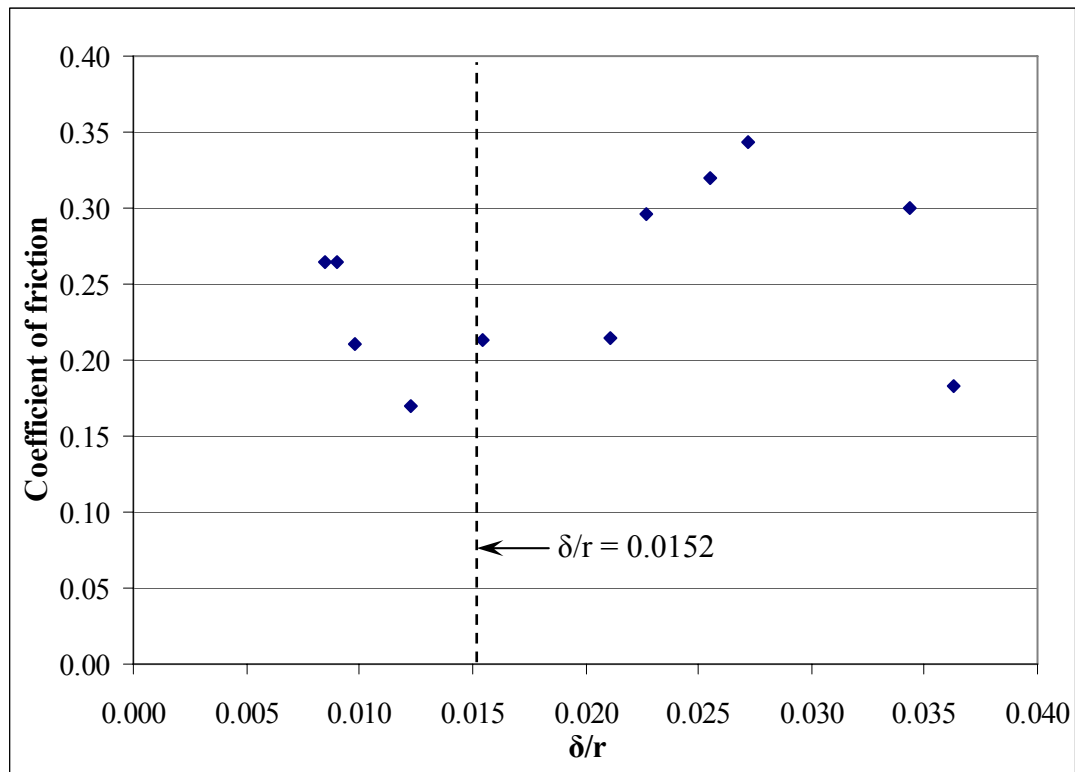
Fig.VI.5. Variation of coefficient of friction with dimensionless interference

The coefficient of friction was found to be in the range of 0.17 and 0.344 (Fig.VI.5). From the functional perspective of the fastener, a smaller coefficient of friction would mean a lower pull-out force for the fastener and a weaker fastener-bone joint. Hence to simulate the worst case scenario, the coefficient of friction was assumed to be 0.2 in the finite element analysis.

VI.3. Surface topography of drilled surface of bone

The surface roughness of the drilled surface of the bone for three different orientations was measured. The profilometer results were plotted in Fig.VI.6.
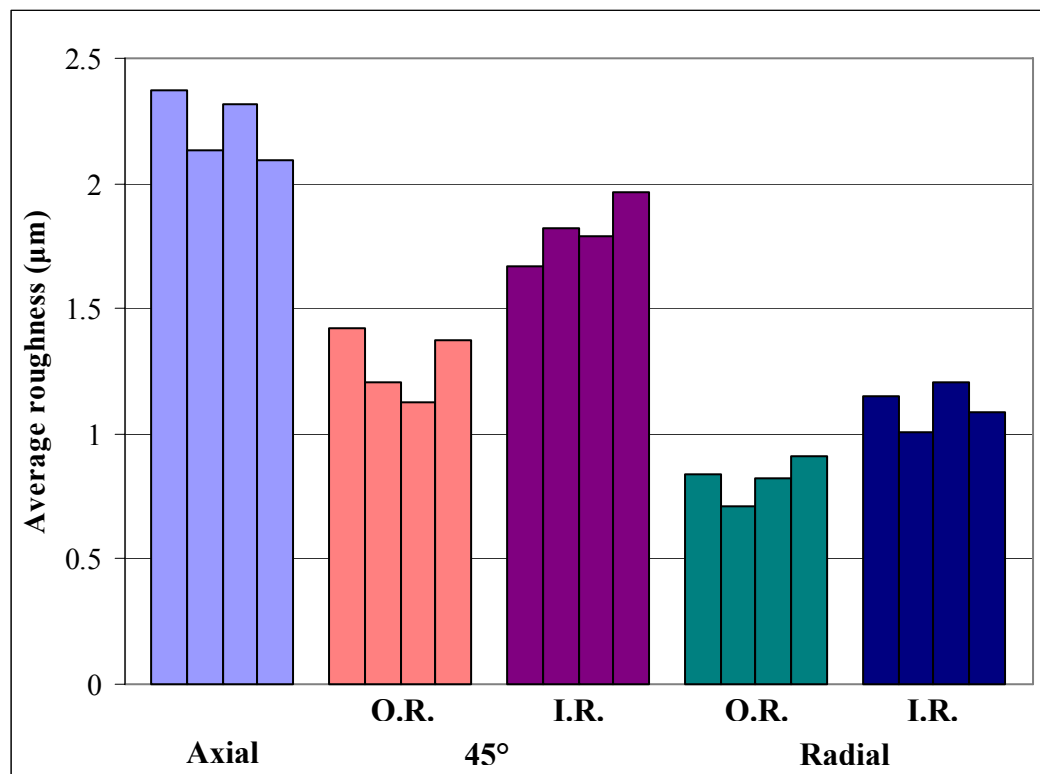

Fig.VI.6. Surface roughness along the three different orientations
(O.R.: Closer to outer radius; I.R.: Closer to inner radius of bone)

It was observed that the roughest surface was obtained along the axial direction while the smoothest was attained for the radial direction (Refer to FigV.5.). Also for the radial orientation and the one inclined at 45° to it, the surface roughness was found to be higher in the inner region (I.R.) of the bone than the outer region (O.R.). For the axial orientation, the hole had to be drilled at the center of the thickness of the bone. Hence the surface roughness could not be classified as outer or inner region.

Axial direction was along the direction of the osteons (Refer to Fig.III.1.). It has been shown that a crack prefers to propagate between the osteons due to a weak interface between them [Jacobs et al., 1974]. Along the radial direction, the osteons are bound together by dense and strong collagen fibers. As the tool encountered a weaker and less dense material along the axial direction, it resulted in a rougher surface as compared to the radial direction.

Cortical bone which is stronger and denser compared to cancellous bone, is found on the outer periphery of bone. The density and strength reduces towards the center as the soft cancellous bone is found in the inner region of the bone. Higher density of the cortical bone resulted in a smoother surface finish in the outer region for the radial orientation and 45° to it.

VI.4. Prototype development by micromilling

Micromilling was used to develop a prototype of the fastener. A magnified image of a fastener produced by this technique is shown in Fig.VI.7. Mid-plane of the fastener was seen to have burrs sticking from it, resulting in a poor surface finish. Due to the small exposed length of the end mills, the mid-plane could not be machined properly. The top edges of the fastener had tool scratch marks on them at some locations. Also the profile could not be replicated accurately. Because of these drawbacks, this technique was not pursued further.
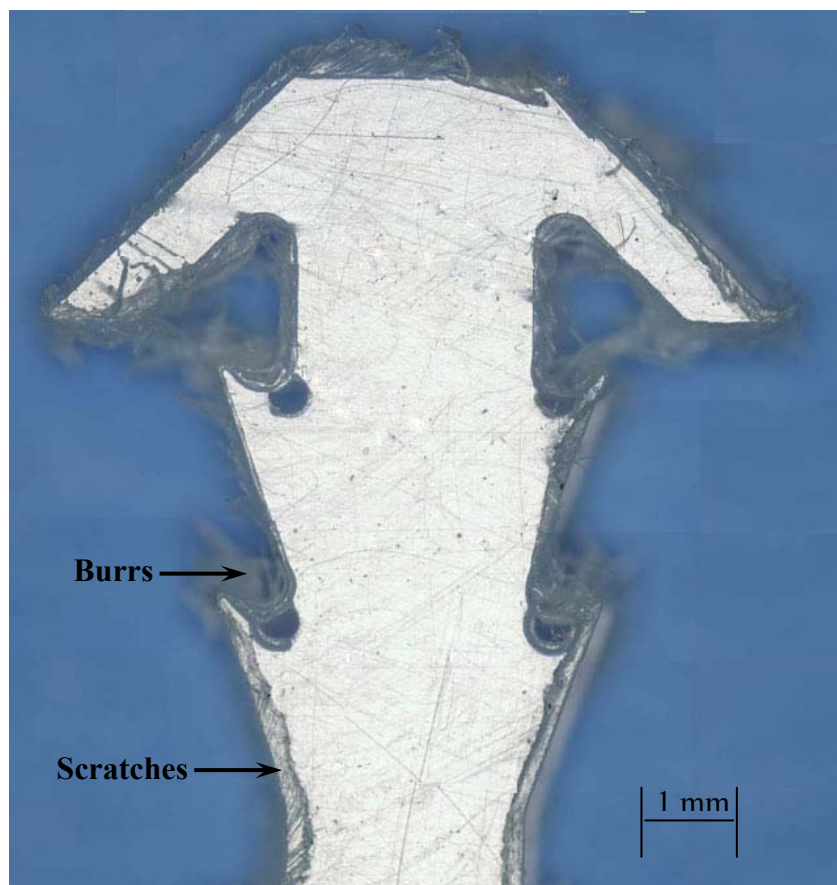

Fig.VI.7. A micromilled prototype

VI.5. Prototype development by micromolding

The micromolding process was able to replicate the features of the fastener with greater precision than the micromilling technique. The prototype developed by this process was seen to have a better surface finish, less flash and better adherence to the specified profile (Fig.VI.8). The flash was removed by a miniature deburring tool. Micromolded fasteners were subsequently used for conducting in-vitro tests to determine the push-in and pull-out forces.
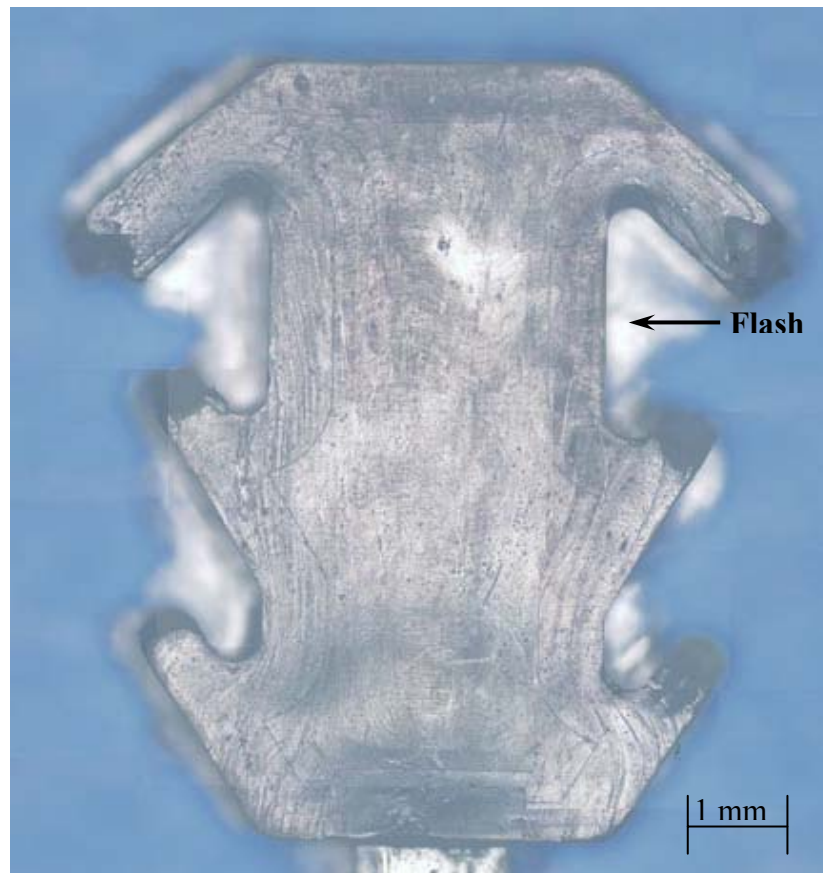

Fig.VI.8. A micromolded prototype

VI.6. Study of the fastener bone interface

An optical microscopy specimen of a fastener completely inserted inside the bone slot is shown in Fig.VI.9.
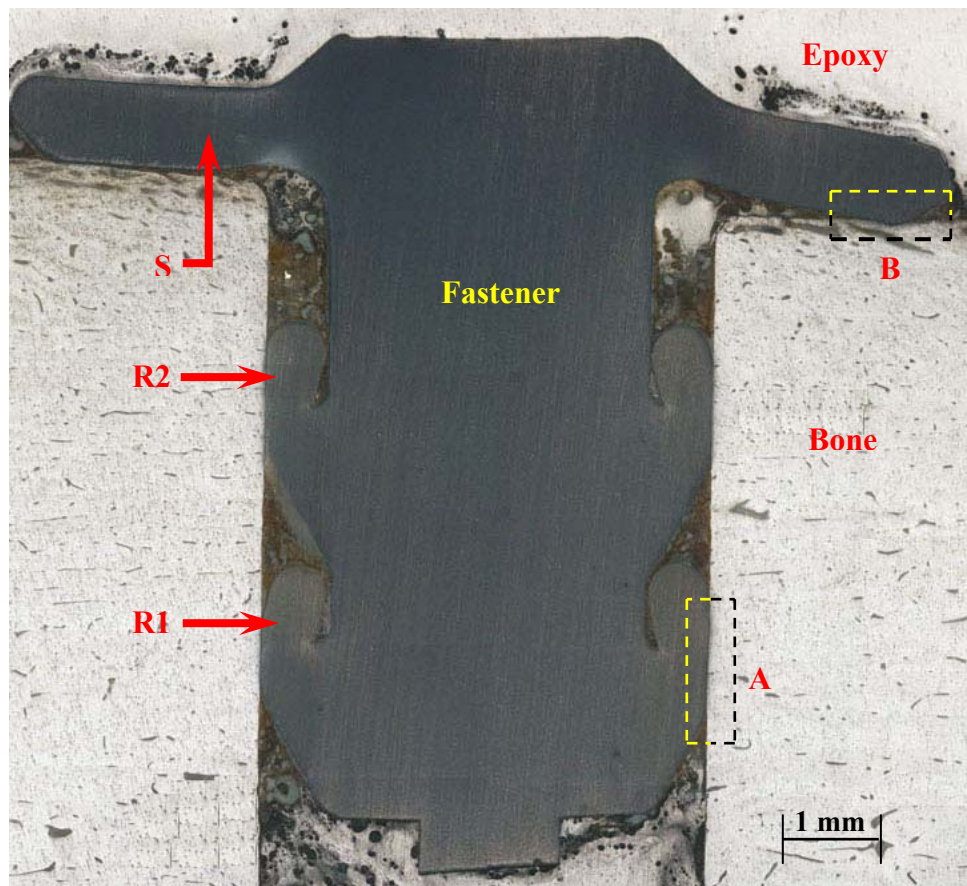

Fig.VI.9. Cross-section of a fastener inserted inside a bone slot

(The first and second pair of ratchets is denoted by R1 and R2, respectively. The spring element integrated into the head of the fastener is denoted by S)

The fastener-bone interface was studied at two locations, namely A and B as shown in Fig.VI.9.

The interface between the ratchets and the bone wall, indicated by Region A, would have a bearing on the push-in and pull-out force of the fastener. As the fastener was pushed into the bone slot, the ratchets undergo deflection and deform such that the surface of the ratchet in contact with the bone matches the surface profile of the bone.
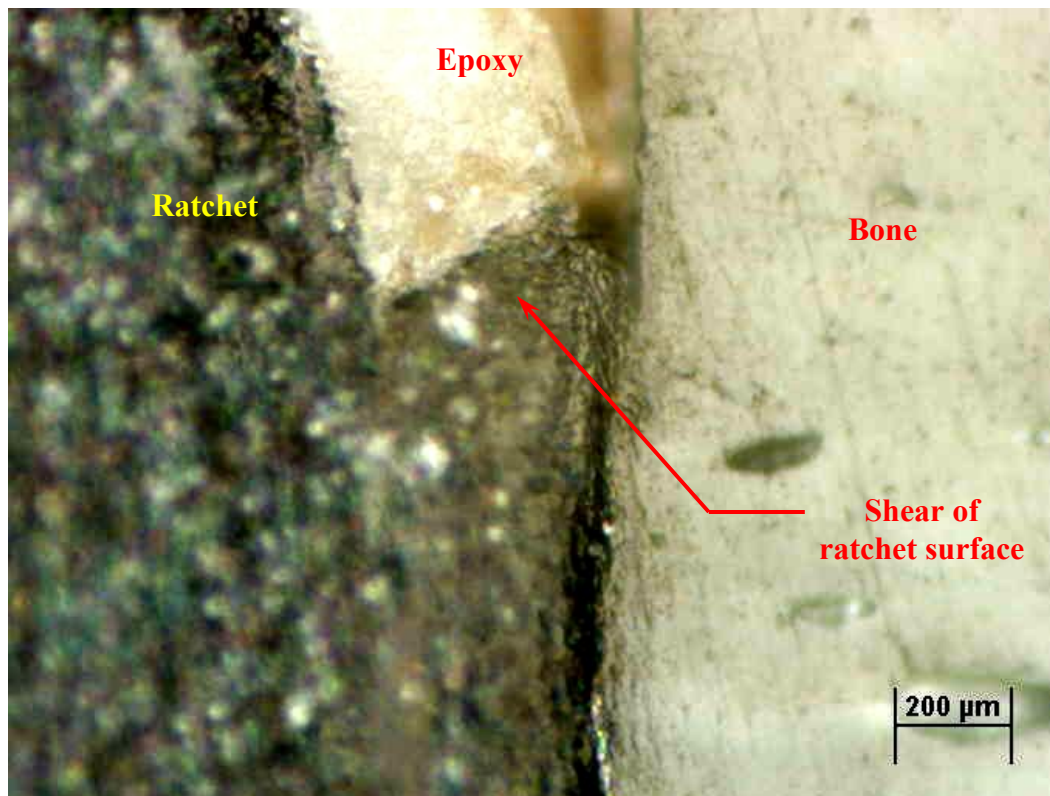

Fig.VI.10. Region A: Shearing of ratchet surface

Due to interference, the ratchet in contact with the bone was found to undergo shear deformation as shown in Fig.VI.10. When the ratchet was pressed into the bone slot, the abrasive edge of the bone tends to shear off the ratchet surface in contact with it. Such shearing of the ratchet surface would have reduced the effective interference between the fastener and bone. Hence, the strength of the fastener-bone interface must have reduced, leading to a reduction in the pull-out force as compared to the push-in force.
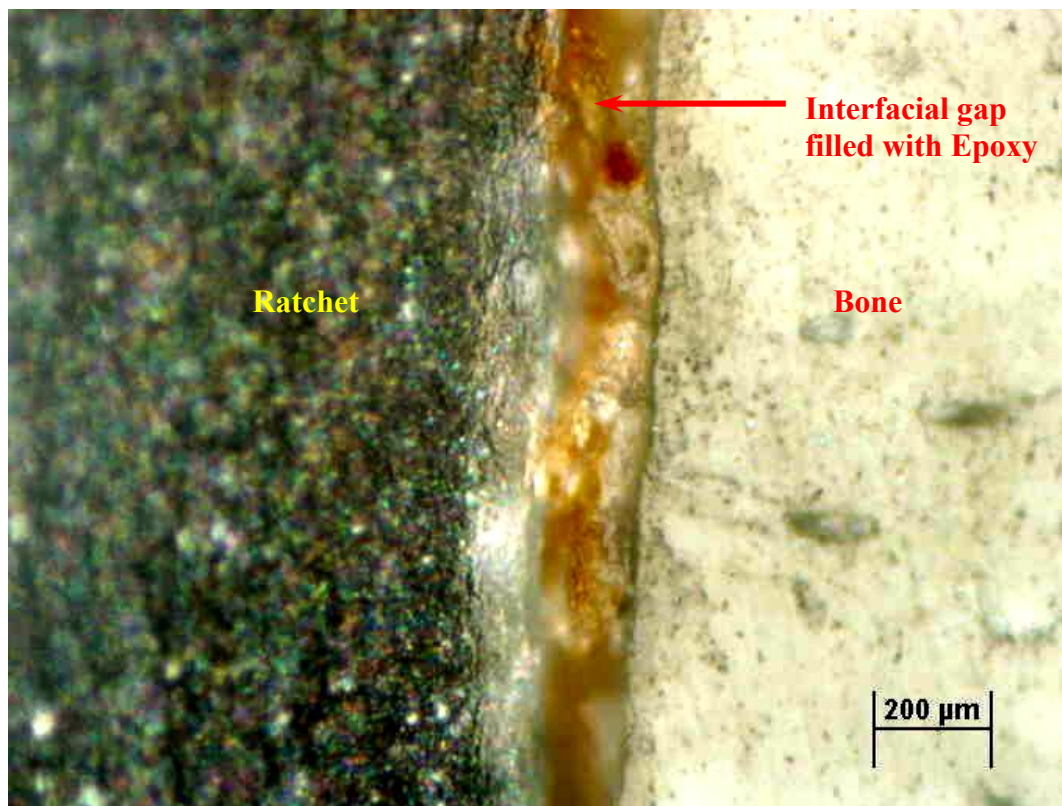

Fig.VI.11. Region A: Interfacial gap between ratchet and bone

A gap was observed between the ratchet and bone along the interface (Fig.VI.11). During initiation of contact between fastener and bone, the abrasive edge of the bone slot causes plastic deformation of the ratchet and produces a dent in it. As the ratchet further slides inside the slot, the dent no longer maintains contact with the bone surface. Such a gap over an isolated region of the fastener-bone interface would have caused a reduction in the area of contact between the ratchet and fastener, leading to a reduced pull-out force.

The other region of interest was the spring–bone interface, highlighted as Region B. It is observed that the tip of the spring remains in contact with the bone surface even after springback and helps to maintain the interfragmental compression. In comparison to the ratchet surface no shearing of the spring surface is observed (Fig.VI.12.)
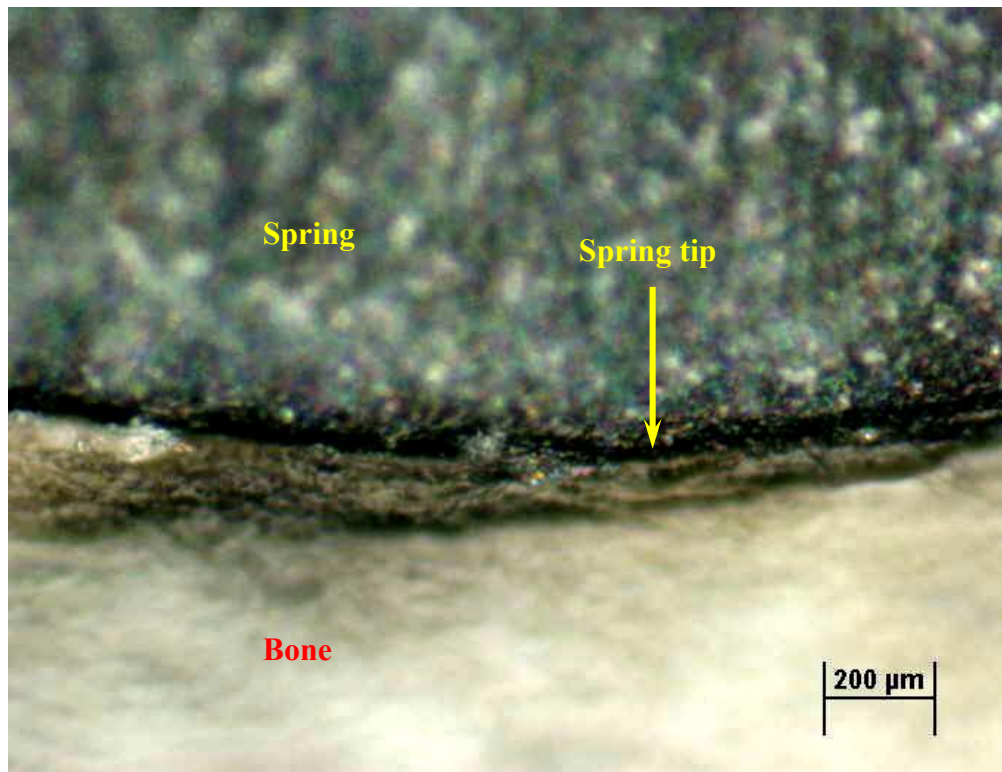

Fig.VI.12. Region B: Spring tip in contact with bone

VI.7. FEA stress plots

The deformation of the fastener during the push-in, springback and pull-out step, along with the resulting stresses was examined with the help of FEA. The Von Mises stress contours are shown in Fig.VI.13. After completion of push-in (Fig.VI.13.b), the root of ratchets and spring were subjected to high stress. Also ratchet bone interface was highly stressed due to interference pressure and shearing due to friction force. Springback of the head of the fastener caused stress redistribution (Fig.VI.13.c). Tip 'T' of the spring element maintained contact with top bone fragment. After pull-out (Fig.VI.13.d), residual stresses and deformation was observed in ratchets and spring element due to plastic deformation.
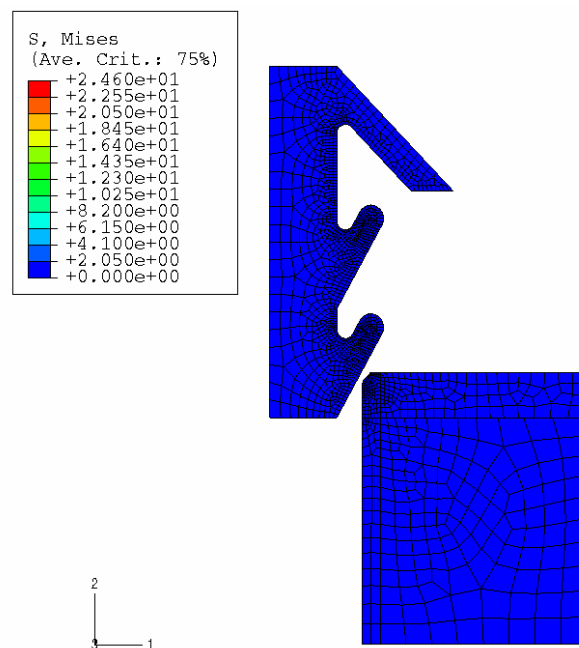

Fig.VI.13. Deformation and Von Mises stress contour plot of fastener and bone (Radial interference, δ = 0.50 mm) a: Prior to insertion
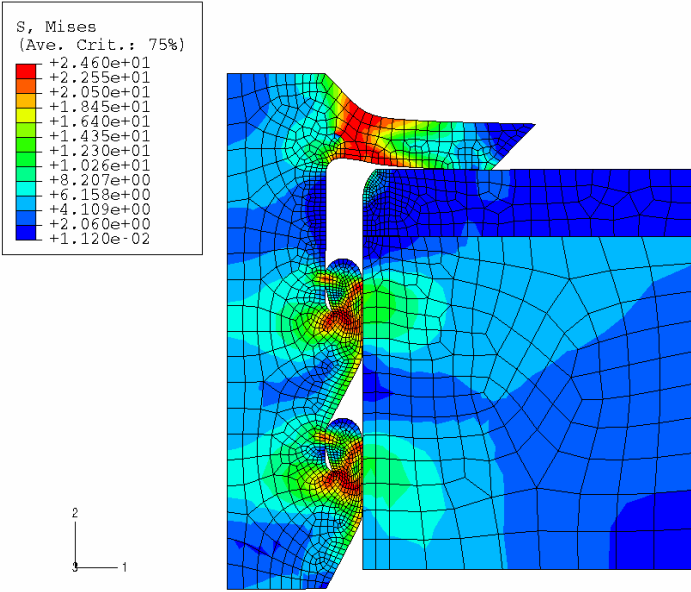
Fig.VI.13. (continued) b: After push-in
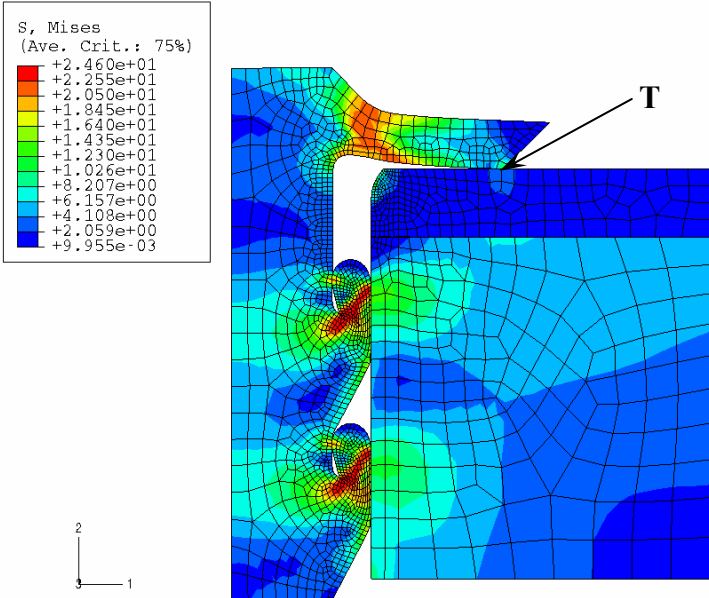
Fig.VI.13. (continued) c: After spring-back
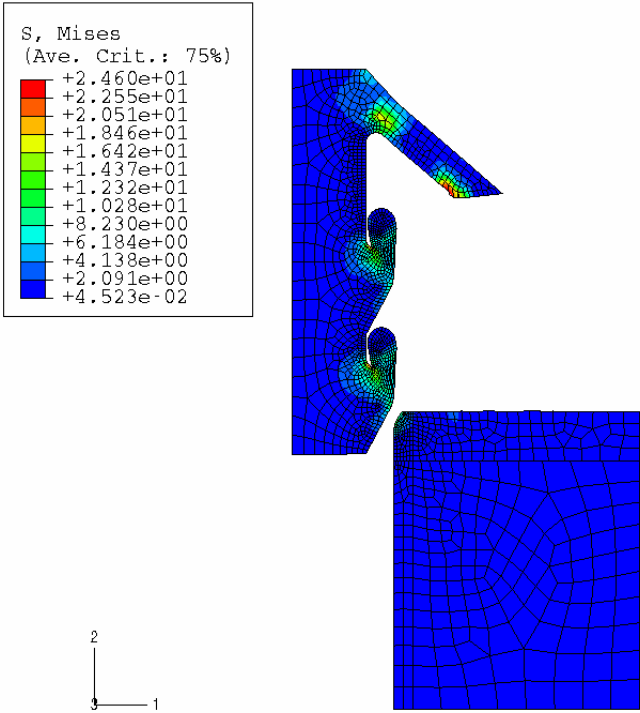
Fig.VI.13. (continued) d: After pull-out

VI.8. Analytical model

The predictions given by the analytical model for the push-in and pull-out force are given below.

VI.8.1. Spring force

For the spring element incorporated into the head of the fastener:

$\alpha = 45°$

Length of spring (l) = 3 mm

Height of spring (h) = 0.707 mm

Width of spring (b) = 2.2 mm

Thus,

$$M_e = \frac{\sigma_y bh^2}{6} = 4.51 \text{ Nmm}$$

$$N_e = \sigma_y bh = 38.26 \text{ N}$$

$$\kappa_e = \frac{2\sigma_y}{hE} = 0.0696 \text{ mm}^{-1}$$

$$P = N = F \sin(45) = 0.707F$$

$$M_{max} = Pl = 2.121F$$

$$m^* = \frac{M_{max}}{M_e} = \frac{Pl}{M_e} = 0.47F$$

$$n = \frac{|N|}{N_e} = 0.0185F$$

Entire cross-section at the root of the cantilever will undergo yielding when the equation IV.5 is satisfied.

$$m^* = \frac{3}{2}\left(1 - n^2\right)$$

$$\therefore 0.47F = \frac{3}{2}\left[1 - \left(0.0185F\right)^2\right]$$

$$\therefore F = 3.18\ N \tag{VI.1}$$

At this tip load, entire cross section at the root of the cantilever will yield. The corresponding tip displacement given by equation IV.8 is,

$$y = 0.245\ mm$$

During the finite element analysis and experiments, the displacement given to the tip of the spring is 1.3 mm, which is greater than the displacement produced on complete yielding of the cross section. As the material does not work harden, the force encountered by the spring element to undergo the above displacement can be assumed to be 3.18 N. As this force is for a symmetric model, the total force required to deflect the spring element would be twice of the above calculated force. The total spring force is given by:

$$\therefore F_S = 6.36\ N \tag{VI.2}$$

VI.8.2. Ratchet deflection force

The dimensions of the ratchet are:

Length of ratchet (l_R) = 0.75 mm

Height of ratchet (h_R) = 0.6 mm

Width of ratchet (b_R) = 2.2 mm

The force required to deflect one ratchet from equation IV.11 is given by:

$$\therefore F_R = 6.49 \text{ N} \tag{VI.3}$$

VI.8.3. Ratchet interference force

The dimensions considered for analysis are:

Base radius of the fastener (r^f_i) = 1.5875 mm

Outer radius of the fastener (r^f_o) = 2.688 mm

Height of the ratchet (h_R) = 0.6 mm

Radius of slot in bone (x_i) = 2.188 mm

Outer radius of bone (x_o) = 7.5 mm

Scenario 1:

$x' = r^f_i + h_R = 2.1875$ mm

As $x' < x_i$, there is no interference between the ratchet and bone.

Scenario 2:

In the Region AC (Fig.VI.14), interference will occur when the intermediate radius x''
exceeds x_i. The maximum interference pressure that can be generated is limited to the

yield strength of HDPE as it is assumed to be an elastic-perfectly plastic material. The intermediate radius x" at which this pressure is experienced is given by:

$$\therefore \delta = P_i \left[\frac{\left(x_o - x_i\right)}{(2\mu_b + \lambda_b)} + \frac{x"}{(2\mu_f + \lambda_f)} \right]$$ [From IV.23]

$$\therefore (x" - 2.188) = 24.6 \left(\frac{5.312}{26923.06} + \frac{x"}{3793.11} \right)$$
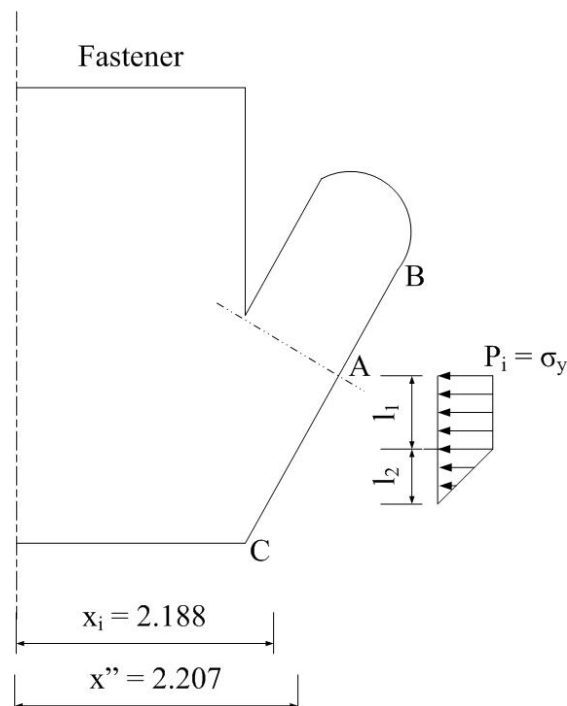
$$\therefore x" = 2.207 \text{ mm}$$

Fig.VI.14. Stresses on fastener due to interference

The normal force on account of interference on Region AC is given by:

$$F_N = \left(\sigma_y\right)\left(l_1 b_R\right) + \int_{y=0}^{y=l_2} \sigma_y \left(b_R\right)\left(1 - \frac{y}{l_2}\right) dy \qquad \text{(VI.4)}$$

Where, l_1 and l_2 are determined from the geometry of the fastener and bone.

The normal force experienced by one ratchet due to interference is:

$$\therefore F_N = 17.4 \text{ N} \qquad \text{(VI.5)}$$

VI.8.4. Fastener push-in force

The push-in force (F_i) for a coefficient of friction of 0.2 is given by:

$$F_i = F_S + \mu_f \left(\text{no. of ratchets}\right)\left(F_R + F_N\right) \qquad \text{(VI.6)}$$

$$\therefore F_i = 6.36 + 0.2*(4)*(6.49 + 17.4)$$

$$\therefore F_i = 25.47 \text{ N}$$

VI.8.5. Fastener pull-out force

The pull-out force (F_o) for a coefficient of friction of 0.2 is given by:

$$F_o = \mu_f \left(\text{no. of ratchets}\right)\left(F_R + F_N\right) \qquad \text{(VI.7)}$$

$$\therefore F_o = 0.2*(4)*(6.49 + 17.4)$$

$$\therefore F_o = 19.112 \text{ N}$$

The pull-out force (F_o) for a coefficient of friction of 0.07 is given by:

$$\therefore F_o = 0.07*(4)*(6.49 + 17.4)$$

$$\therefore F_o = 6.374 \text{ N} \qquad \text{(VI.8)}$$

VI.9. Push-in tests

The variation in push-in force with insertion depth given by FEA and experimental tests is shown in Fig.VI.15. As the fastener was pushed into the bone slot, a sharp rise in force was observed. This was due to the initiation of contact between the edge of the bone slot and the ratchet pair R1 (Refer to Fig.VI.9.). As contact was established, this force reduced due to reduction in the influence of contact stresses as seen in Region 1. The interference between the fastener and the bone slot caused the deflection of ratchet pair R1. Once the entire length of the ratchet R1 was in contact with the bone wall, the area in contact between the ratchet and bone remained constant with no further deflection. This resulted in the push-in force remaining constant over Region 2. This force was denoted by Fr_1.

The same variation in force was observed as ratchet pair R2 (Refer to Fig.VI.9.) came in contact with the bone. The ratchet force Fr_2 is the sum of forces required for pushing in both ratchet R1 and ratchet R2.

Subsequently, as the spring element S came in contact with the bone, there was a rise in force, as observed in Region 4. The force required to deflect the spring and push-in both the pair of ratchets was denoted by Fi.

The push-in force determined analytically using equation VI.6 was found to be greater than that predicated by FEA or experimental results. This could be due to the difference in the area under interference, for analytical method as compared to the other two methods.
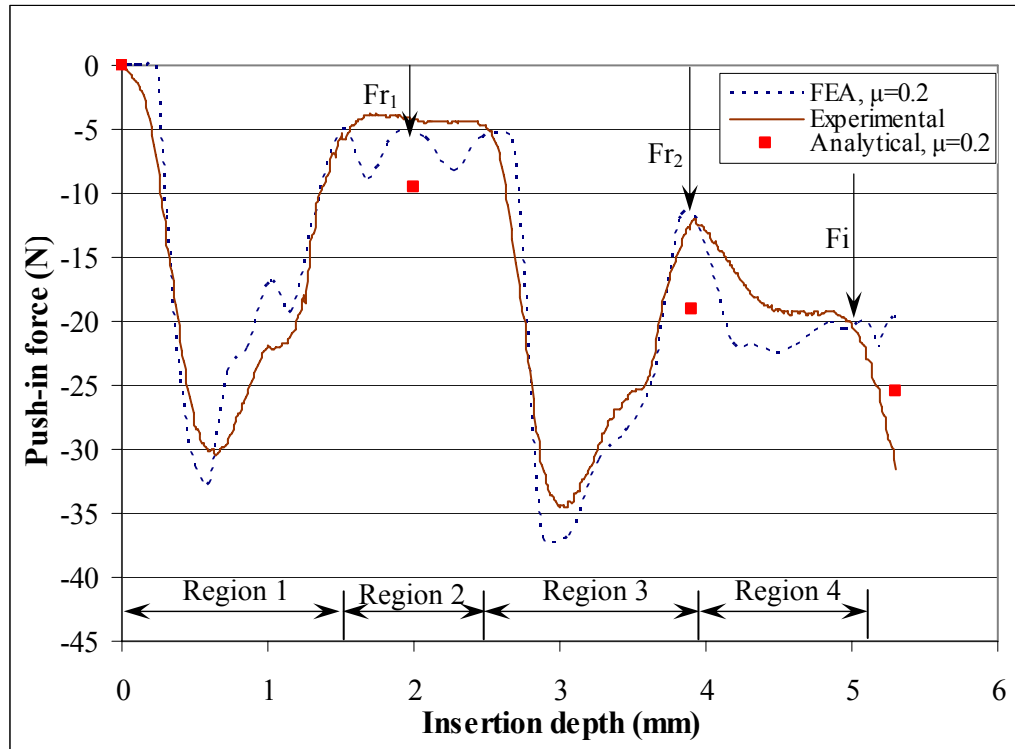
Fig.VI.15. Variation in push-in force with insertion depth
(Radial interference, $\delta = 0.50$ mm)

The experimental values of push-in force for different levels of radial interference were comparable to those obtained from FEA. Push-in force was found to increase with increasing levels of interference (Fig.VI.16.). An increased interference generated a higher interference pressure. This resulted in an increased push-in force for higher levels of interference. The analytical results compared well with the FEA and experimental results for lower levels of interference. With increase in interference, a significant difference was observed. This could be attributed to the assumption of small deformation for the analytical model. With increased interference, the deformation of the

ratchet could not be predicted properly by the analytical model which in turn affected the area under interference and the push-in force. Also, as observed in Fig.VI.8 the fastener bone interface is not continuous but has a gap along it. Hence the actual area in contact between the fastener and bone is lesser than that assumed in the analytical model. So the analytical model predicted higher push-in force as compared to the FEA and experimental results.
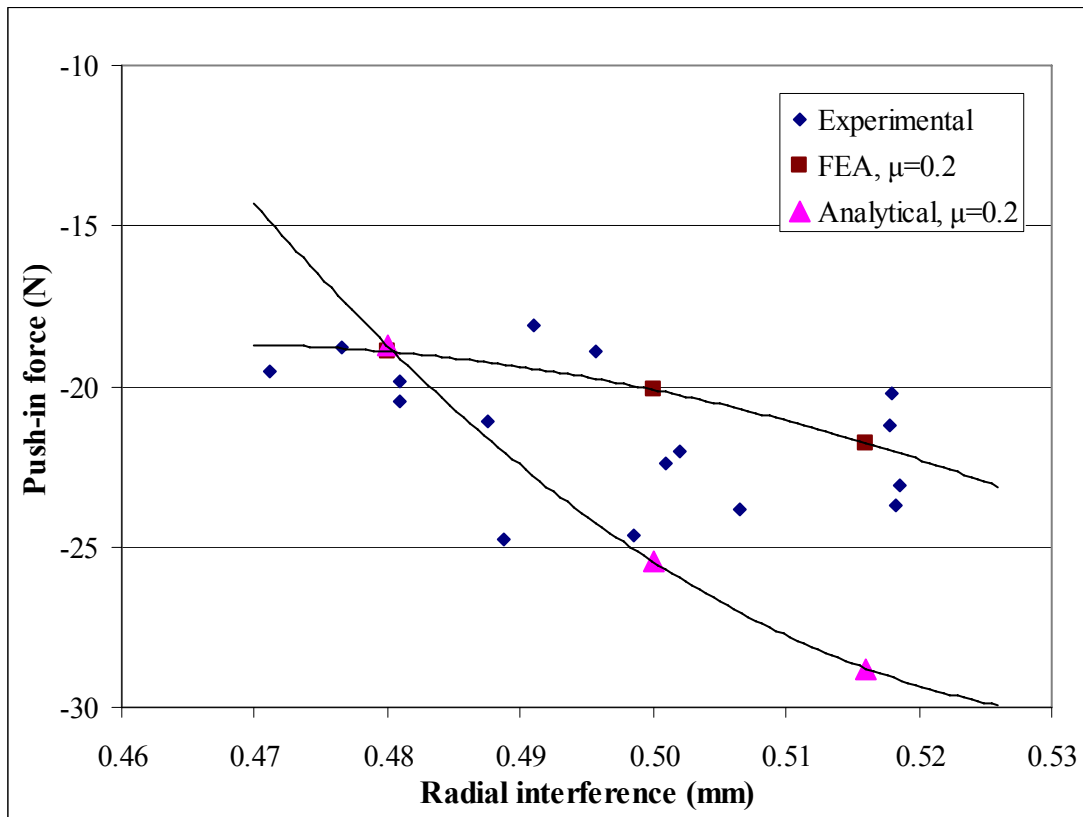
Fig.VI.16. Variation in push-in force with radial interference

VI.10. Pull-out tests

From the finite element analysis it was found that maximum force was required to initiate separation between the fastener and bone. This force was denoted by Fo. Once the fastener began to slide with respect to the bone, the pull-out force gradually decreased till zero, indicating no contact between the two (Fig.VI.17). In the experiment, the slack and further tensioning of the string required a higher cross head displacement, as compared to the FEA specified displacement. The force required for tensioning the string was assumed to be negligible.

The experimental values of pull-out force were found to be lower than those projected by the FEA for a coefficient of friction of 0.2 (Fig.VI.17). This could be attributed to breakage of asperities on the polymer surface during insertion leading to smoothening of the surface and a reduction in coefficient of friction. Shearing of polymer which lies at the interface of the bone and the fastener could also contribute to this reduction in pull-out force. A smaller coefficient of friction of 0.07 was then assumed instead of the experimentally determined value of 0.2 and the pull-out force predicted in this case was comparable to the experimental values.

However, the pull-out force determined analytically using equations VI.7 and VI.8 for both the coefficients of friction 0.2 and 0.07, was found to be higher than the corresponding FEA predictions.
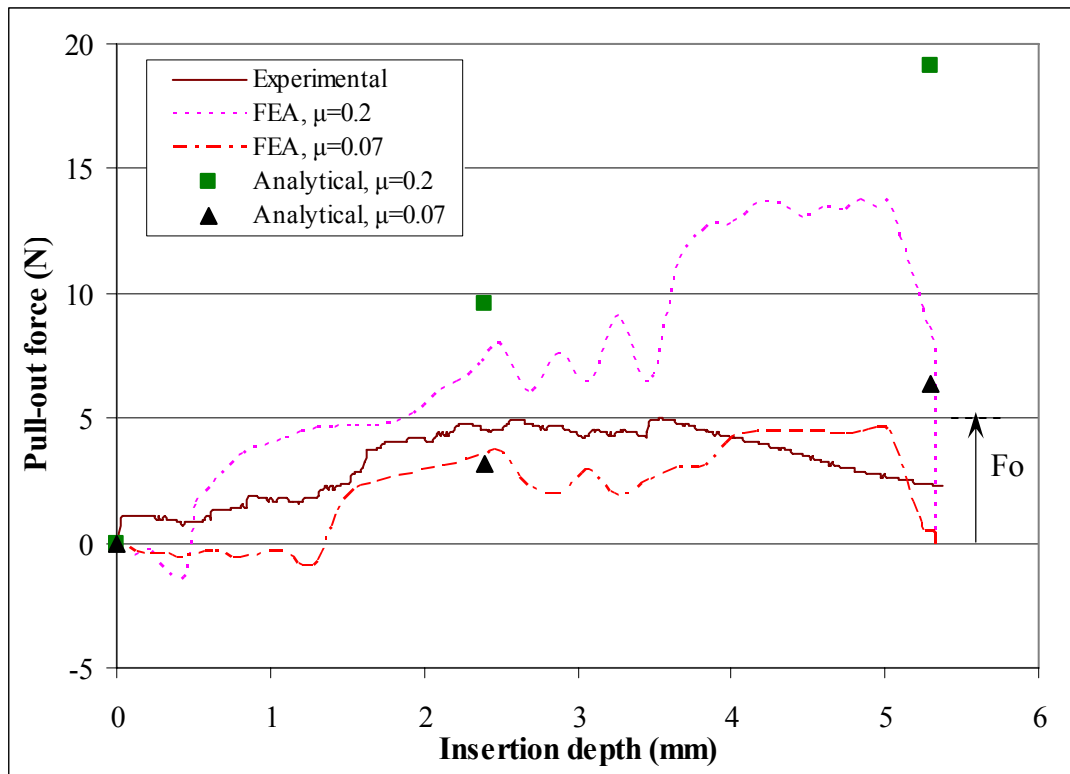
Fig.VI.17. Variation in pull-out force with insertion depth
(Radial interference, $\delta = 0.50$ mm)

The variation in the pull-out force with radial interference was as shown in Fig. VI.18. FEA results for a coefficient of friction of 0.07 matched well with the experimental results over the whole range of interference values. Analytical results were comparable to the FEA and experimental results for the lower range of interference. With increasing interference, they were found to be higher than the corresponding FEA and experimental results.
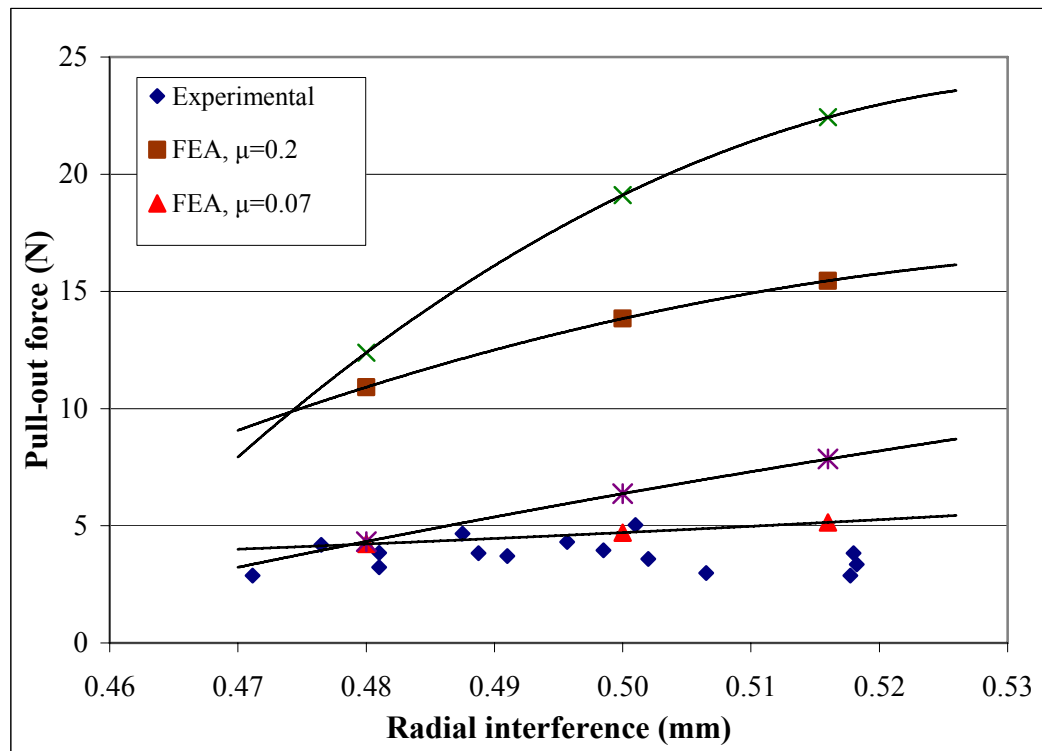
Fig.VI.18. Variation in pull-out force with radial interference

VI.11. Interfragmental compression

Interfragmental compression generated along the fracture plane (Refer to Fig.IV.5.) was determined from the FEA (Fig.VI.19). During insertion of the fastener, the spring underwent deflection and resulted in pressing the fragments together. Upon removal of the push-in force, the spring undergoes elastic springback. As springback tends to unload the system to achieve equilibrium, its effect on interfragmental compression was examined through FEA. The springback step was conducted for both the coefficients of friction i.e. 0.2 and 0.07.

The displacement of the tip T of the spring along the top surface of Fragment 2 (Refer to Fig.IV.5.) on removal of the push-in force was taken as a measure of the

springback. As expected, increasing springback reduced the interfragmental compression. Coefficient of friction was not seen to have a significant effect on the interfragmental compression.

Fig.VI.19: Variation in interfragmental compression with springback

(Radial interference, $\delta = 0.50$ mm)

CHAPTER VII

CONCLUSIONS AND RECOMMENDATIONS

VII.1 Conclusions

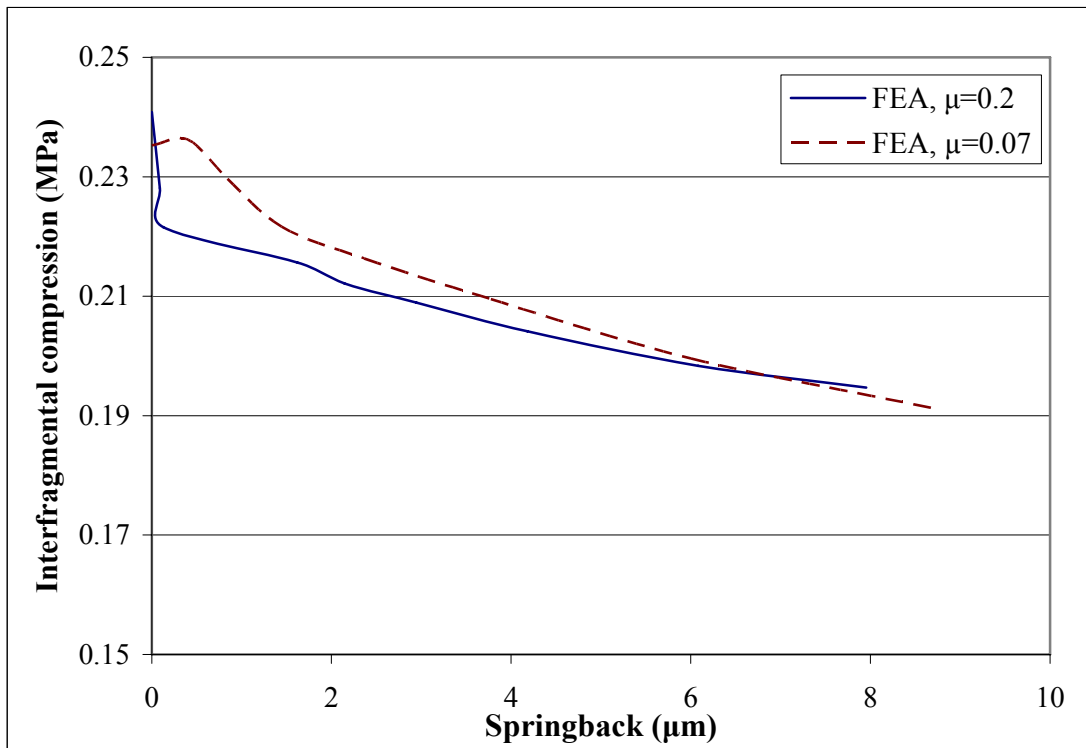A prototype orthopedic fastener was developed for fixation of small bone fragments. The first constraint on the design of the fastener was that it had to be threadless in order to fixate small bone fragments without damaging them, unlike with threaded fasteners which require tapping of the bone fragment. The second constraint required it to provide interfragmental compression to the fracture site to aid in its healing. Also it had to be polymer based so that the same design methodology could then be applied towards the development of a biodegradable prototype of the fastener.

The first constraint was satisfied by providing ratchets on the shaft of the fastener. Due to interference between the fastener and the drilled hole, these ratchets would deflect during insertion into the drilled hole and subsequently stiffen to hold the bone fragments in place. Different ratchet profiles were analyzed by finite element method. Their performance was compared on the basis of their push-in and pull-out force per unit length of interference. The profile that provided the highest ratio of pull-out to push-in force per unit length of interference was selected.

The interfragmental compression was achieved by incorporating a spring element into the head of the fastener, analogous to a Belleville washer. During insertion of the fastener, the spring would deflect and press the bone fragments against each other.

High Density Polyethylene (HDPE) was used to mold prototype of the designed fastener. Coefficient of friction between HDPE and bovine bone was measured to be varying between 0.17 and 0.344 under interference fit. It was assumed to be 0.2 for subsequently FEA.

The push-in force predicted by FEA and experimental results for varying levels of interference were found to be in good agreement. The pull-out force predicted by FEA

was found to be higher than the experimental results for a coefficient of friction of 0.2. However, for a lower coefficient of 0.07, the two results were comparable. An analytical model was proposed to explain the functioning of the fastener. The results for push and pull-out force predicted by this model were comparable to the FEA and experimental results for lower radial interference but deviated for higher radial interference. This could be attributed to higher deformation encountered by the fastener at higher interference levels. The interfragmental compression at the fracture plane was determined from FEA. With increasing springback of the spring element of the head, the interfragmental compression went on reducing. However on completion of springback, the fragments were still subjected to interfragmental compression.

VII.2 Recommendations

1. The proposed analytical model fails to provide an accurate prediction for the push-in and pull-out force at higher levels of interference. By incorporating the effect of large deformations and shearing of the ratchet surface, the model might be able to predict more precise results.

2. A 3-D prototype (Fig.VII.1) of the fastener needs to be developed to ensure that the fastener is easily inserted into a drilled hole without buckling or bending as might be the case with a 2-D prototype. Also, a 3-D profile would provide a higher contact area resulting in an increased pull-out force for the fastener.
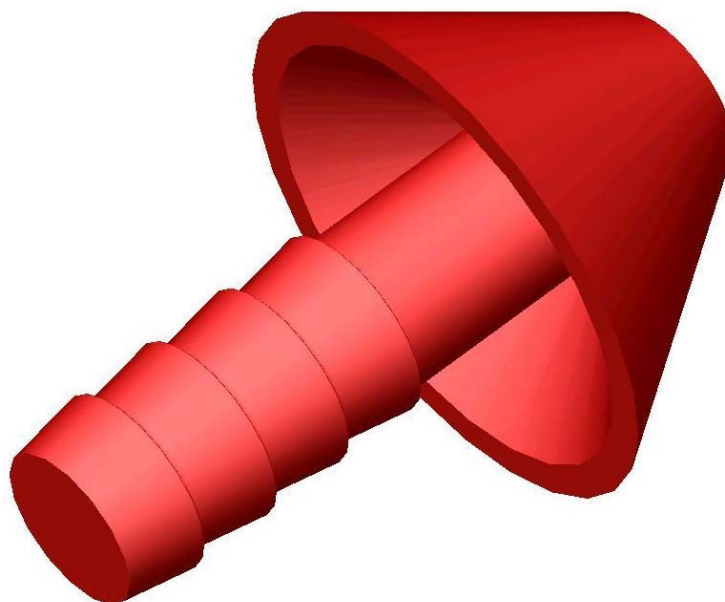
Fig.VII.1. 3D fastener model

3. The fastener needs to be manufactured from biodegradable polymers and composites so that its performance can be compared with the available literature pertaining to commercial fixation methods developed from biodegradable polymers and composites.

REFERENCES

ABAQUS, 2005. ABAQUS Version 6.4 Documentation. http://sc.tamu.edu/softwareDocs/abaqus64/ (Accessed on 06/01/2004)

ASTM, 2000. Annual Book of ASTM Standards. 13.01., 826-1063.

Amecke B., Bendix D., Entenmann G., 1992. Resorbable Polyesters: Composition, Properties, Applications. Clinical Materials 10, 47-50.

An Y.H., 1999. Mechanical Properties of Bone. In: An Y.H., Draughn R., (Eds.), Mechanical Testing of Bone and Bone-Implant Interface. CRC Press, Boca Raton, FL.

Beiser I.H., Kanat I.O., 1990. Biodegradable Internal Fixation. Journal of American Podiatric Medical Association 80 (2), 72-75.

Bely V.A., Sviridenok A.I., Petrokovets M.I., Savkin V.G., 1982. Friction and Wear in Polymer-Based Materials. Pergamon Press, New York.

Caborn D.N.M., Urban W.P., Johnson D.L., Nyland J., Pienkowski D., 1997. Biomechanical Comparison between Bioscrew and Titanium Alloy Interference Screws for Bone-Patellar Tendon-Bone Graft Fixation in Anterior Cruciate Ligament Reconstruction. Arthroscopy: The Journal of Arthroscopic and Related Surgery 13 (2), 229-232.

Carter D.R., Beaupré G.S., 2001. Skeletal Function and Form. Cambridge University Press, New York.

Chao E.Y.S., Aro H.T., Inoue N., 1995. Engineering Principles for Bone Fracture Fixation and Repair. In: Hollinger J.O. (Ed.), Biomedical Applications of Synthetic Biodegradable Polymers. CRC Press, Boca Raton, FL, 145-172.

Claes L.E., 1992. Mechanical Characterization of Biodegradable Implants. Clinical Materials 10, 41-46.

Cohen J., 1983. Metal Implants: Historical Background and Biological Response to Implantation. In: Rubin L.R. (Ed.), Biomaterials in Reconstructive Surgery. The C.V. Mosby Company, St. Louis, MO.
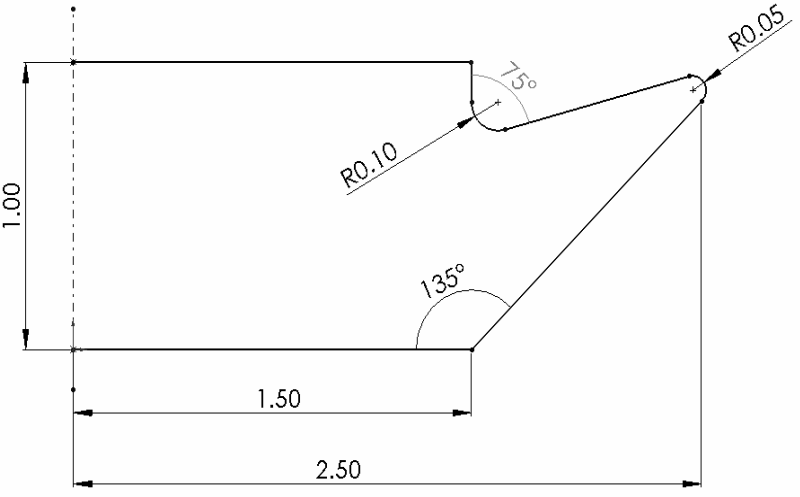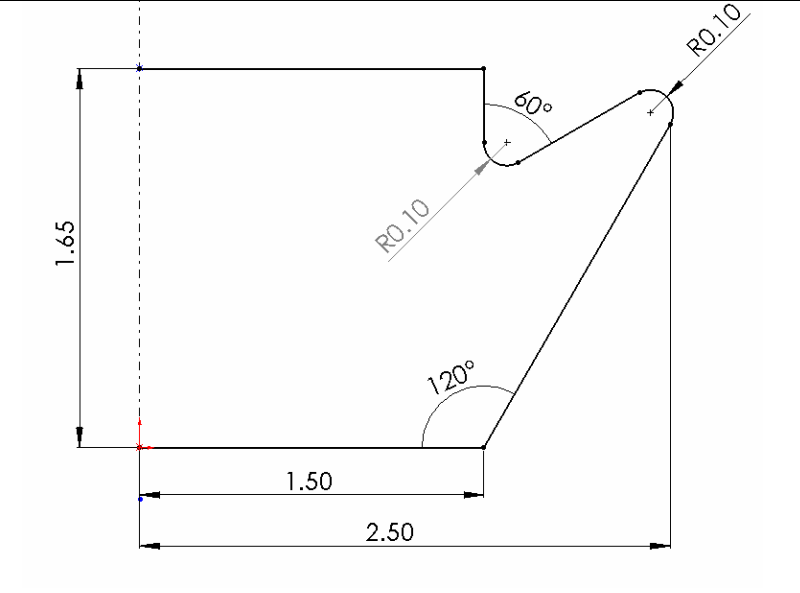
Cohen S.R., Holmes R.E., Amis P., Fitchner H., Shusterman E.M., 2001. Tacks: A New Technique for Craniofacial Fixation. Journal of Craniofacial Surgery 12 (6), 596-602.

Collinge C.A., Stern S.H., Cordes S.D., Lautensclager E., 1999. The Mechanical Properties of Small Fragment Orthopedic Screws. American Academy of Orthopaedic Surgeons 1999 Annual Meeting Scientific Exhibits.
http://www.aaos.org/wordhtml/anmeet99/sciexh/se067.html
(Accessed on 10/21/03)

Colton C.L., 2003. The History of Fracture Treatment. In: Browner B.D. (Ed.) Skeletal Trauma: Basic Science, Management, and Reconstruction. 3rd ed., Elsevier, St. Louis, MO.
http://home.mdconsult.com/das/book/50281319-2/view/1217/8.html/top
(Accessed on 08/06/05)

Costi J.J., Kelly A.J., Hearn T.C., Martin D.K., 2001. Comparison of Torsional Strengths of Biodegradable Screws for Anterior Cruciate Ligament Reconstruction. American Journal of Sports Medicine 29 (5), 575-580.

Department of Mechanical Engineering, University of California, Berkeley, 2005. Fracture Fixation and Corrosion in Long Bone Fractures.
http://www.me.berkeley.edu/ME117/S05/finalproject/pdf/Fracture_Fixation.pdf
(Accessed on 08/06/05)

ExxonMobil, 2005. ExxonMobil HDPE, HD 6706 Injection Molding Resin Data Sheet.
http://www.exxonmobilpe.com/Public_Files/Polyethylene/Polyethylene/NorthAmerica/Data_Sheet_ExxonMobil_HDPE_HD_6706.pdf (Accessed on 10/05/05)

Ford, T.C., 1994. The Herbert Screw and Its Applications in Foot Surgery. Journal of Foot Ankle Surgery 33, 346-354.

GMReis, 2005. PDR – Cannulated Double Thread Compression Screws.
http://gmreis.com.br/html/pdr.htm (Accessed on 08/06/05)

Gogolewski S., 1992. Resorbable Polymers for Internal Fixation. Clinical Materials 10, 13-20.

Hamblen D.L., 1989. What Is the Biological Reaction to Implant Materials? In: Proceedings of the Institute of Mechanical Engineers – The Changing Role of Engineering in Orthopedics. Professional Engineering Publishing, London, 7-8.

Herstik J.G., Pelletier J.P., Kanat I.O., 1990. Pin Tract Infections, Incidence and Management in Foot Surgery. Journal of American Podiatric Medical Association 80, 135-144.

Hughes A.W., Jordan B.A., 1972. The Mechanical Properties of Surgical Bone Screws and Some Aspects of Insertions Practice. Injury 4, 25-38.

Jacobs C.H., Berry J.T., Pope M.H., Hoaglund F.T., 1976. A Study of the Bone Machining Process - Drilling. Journal of Biomechanics 9, 343-349.

Jacobs C.H., Pope M.H., Berry J.T., Hoaglund F., 1974. A Study of the Bone Machining Process - Orthogonal Cutting. Journal of Biomechanics 7, 131-136.

Johnson L.L., Eda vanDyk G., 1996. Metal and Biodegradable Interference Screws: Comparison of Failure Strength. Arthroscopy: The Journal of Arthroscopic and Related Surgery 12 (4), 452-456.

Koranyi E., Bowman C.E., Knecht C.D., Janssen M, 1970. The Holding Power of Orthopedic Screw in Bone. Clinical Orthopedics 72, 283-286.

Krevlen D.W. van, 1990. Properties of Polymers: Their Correlation with Chemical Structure, Their Numerical Estimation and Prediction from Additive Group Contributions. Elsevier, New York.

Lavi, A., 2002. Anatomy of Screws and Fixation. In: Proceedings of the Fixation Workshop, New York State Podiatric Medical Association (NYSPMA), New York City, NY, 1-12.
http://www.vilex.com/docs/Anatomy%20Paper.pdf (Accessed on 12/20/2003)

Leinonen S., Tiainen J., Kellomäki M., Törmälä P., Waris T., Ninkovic M., Ashammakhi N., 2003. Holding Power of Bioabsorable Self-Reinforced Poly-L/DL-Lactide 70/30 Tacks and Miniscrews in Human Cadaver Bone. Journal of Craniofacial Surgery 14 (2), 171-175.

Menges G., Mohren P., 1993. How to Make Injection Molds. Hanser Publishers, New York.

Middleton J.C., Tipton A.J., 2000. Synthetic Biodegradable Polymers as Orthopedic Devices. Biomaterials 21 (23), 2335-2346.

Müller, M.E., Allgöwer M., Schneider R. and Willenegger H., 1991. Manual of Internal Fixation, 3rd ed. Springer-Verlag, Berlin.

Orthopaedic-Implants, 2005. Orthopaedic Implants – Screws.
www.orthopaedic-implants.com/orthopedic-implants/bone-screws.html
(Accessed on 08/06/05)

Reilly, D.T. and Burstein, A. H., 1974. The Mechanical Properties of Cortical Bone. Journal of Bone Joint Surgery 56 (A), 1001-1022.

Rokkanen P.U., 1991. Absorbable Materials in Orthopaedic Surgery. Annals of Medicine 23, 109-115.

Saha S., Pal S., Albright J.A., 1982. Surgical Drilling: Design and Performance of an Improved Drill. Journal of Biomechanical Engineering, Transactions of the ASME 104 (3), 245-252.

Schatzker J., Sanderson R., Murnagham J.P., 1975. The Holding Power of Orthopedic Screws in Bone. Clinical Orthopedics 108, 115-126.

Schuller-Götzburg P., Krenkel Ch., Reiter T.J., Plenk H., 1999. 2D-Finite Element Analysis and Histomorphology of Lag Screws with and without a Concave Washer. Journal of Biomechanics 32, 511-520.

Shier D, Butler D, Lewis R., 1996. Hole's Human Anatomy & Physiology, 7th ed. Wm C Brown Publishers, Dubuque, IA.

Shigley J.E., Mischke C.R., Budynas R., 2004. Mechanical Engineering Design, 7th ed. McGraw-Hill Higher Education, New York.

Simon J.A., Ricci J.L., Di Cesare P.E., 1997. Bioabsorbable Fracture Fixation in Orthopedics: A Comprehensive Review. Part I. Basic Science and Preclinical Studies. American Journal of Orthopedics 26 (10), 665-671.

Slaughter W.S., 2002. The Linearized Theory of Elasticity. Birkhaüser, Boston.

Timoshenko S., Goodier J.N., 1951. Theory of Elasticity, 2nd ed. McGraw-Hill Book Company, New York.

Törmälä P., 1992. Biodegradable Self-Reinforced Composite Materials; Manufacturing Structure and Mechanical Properties. Clinical Materials 10, 29-34.

Tunc D.C., 1991. Body-Absorbable Osteosynthesis Devices. Clinical Materials 8, 119-123.

Weiler A, Windhagen H.J., Raschke M.J., Laumeyer A., 1998. Biodegradable Interference Screw Fixation Exhibits Pull-Out Force and Stiffness Similar to Titanium Screws. American Journal of Sports Medicine 26 (1), 119-128.

Wouters D.B., Rudolf R.M., Mouton L. J., Horn J. R., 2004. The Meniscus Arrow or Metal Screw for Treatment of Osteochondritis Dissecans? In-vitro Comparison of Their Effectiveness. Knee Surgery, Sports Traumatology, Arthroscopy 12 (1), 52-57.

Yu T.X., Johnson W., 1982. Influence of Axial Force on the Elastic-Plastic Bending and Springback of a Beam. Journal of Mechanical Working Technology 6, 5-21.

Yu T.X., Zhang L.C., 1996. Plastic Bending, Theory and Applications. World Scientific, Singapore.

APPENDIX A

RATCHET DESIGNS
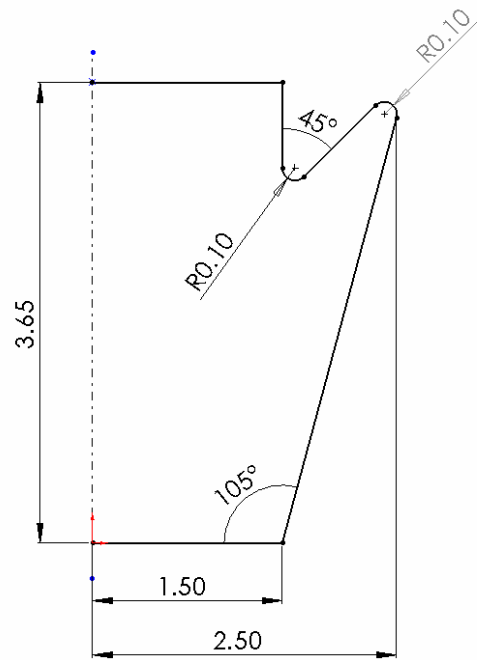
	Design **A**
	Design **B**
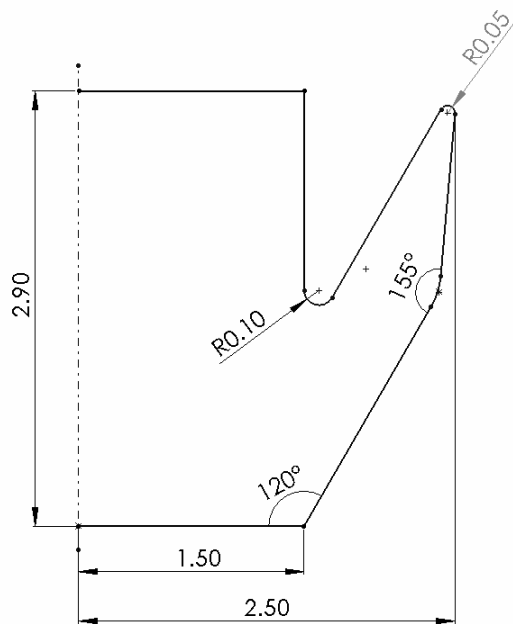
	Design **C**
	Design **D**
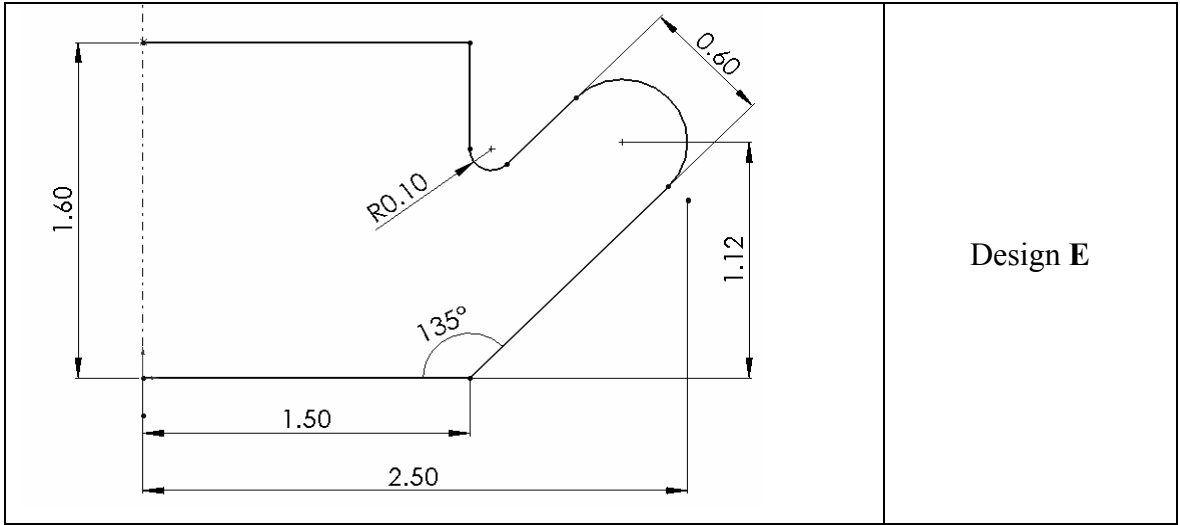
Design **E**

APPENDIX B
INPUT FILES FOR FEA

1. Push-in step

*Heading

** Job name: tofindes2 Model name: model1

**Node files, Element files and Surface definitions have been omitted for brevity

*Preprint, echo=NO, model=NO, history=NO, contact=NO

** --

** PART INSTANCE: bone1-1

** Region: (bsec:Picked), (Controls:EC-1)

*Elset, elset=bone1-1, generate

** Section: bsec

*Solid Section, elset=bone1-1, controls=EC-1, material=bone

2.2,

** --

** PART INSTANCE: fastener-1

** Region: (fsec:Picked), (Controls:EC-1)

*Elset, elset=fastener-1, generate

** Section: fsec

*Solid Section, elset=fastener-1, controls=EC-1, material=polyethylene

2.2,

** --

** PART INSTANCE: bone2-1

** Region: (fsec:Picked), (Controls:EC-1)

*Elset, elset=bone2-1, generate

** Section: fsec

*Solid Section, elset=bone2-1, controls=EC-1, material=polyethylene

2.2,

*System

*Nset, nset=axis

*Elset, elset=axis

*Nset, nset=bone1, generate

*Elset, elset=bone1, generate

*Nset, nset=bone2, generate

*Elset, elset=bone2, generate

*Nset, nset=fixed1

*Elset, elset=fixed1

*Nset, nset=spring

*Nset, nset=fixed2

*Elset, elset=fixed2

*Nset, nset=fixed3

*Elset, elset=fixed3

*Nset, nset=top

*Elset, elset=top

*Surface, type=ELEMENT, name=bone1top

*Surface, type=ELEMENT, name=bone2bottom

*Surface, type=ELEMENT, name=bone2surf

*Surface, type=ELEMENT, name=bone2top

*Surface, type=ELEMENT, name=fsurf

*Surface, type=ELEMENT, name=selfcontact1surf

*Surface, type=ELEMENT, name=selfcontact2surf

*Surface, type=ELEMENT, name=springsurf

*Surface, type=ELEMENT, name=bone1surf

**

** ELEMENT CONTROLS

*Section Controls, name=EC-1, hourglass=ENHANCED

1., 1., 1.

*Amplitude, name=push-in, definition=SMOOTH STEP

0., 0., 500., 1.

** MATERIALS

*Material, name=bone

*Density

1.900,

*Elastic

20000., 0.3

*Material, name=polyethylene

*Density

0.952,

*Elastic

1000., 0.45

*Plastic

 24.6,   0.

 24.6, 0.2

 24.6, 0.48

** INTERACTION PROPERTIES

*Surface Interaction, name=friction

*Friction

 0.2,

*Surface Interaction, name=selfcontact

*Friction

0.,

** --

** STEP: push-in

*Step, name=push-in

*Dynamic, Explicit

, 500.

*Bulk Viscosity

0.06, 1.2

** BOUNDARY CONDITIONS

** Name: fixed1 Type: Symmetry/Antisymmetry/Encastre

*Boundary

fixed1, ENCASTRE

** Name: fixed2 Type: Symmetry/Antisymmetry/Encastre

*Boundary

fixed2, ENCASTRE

** Name: fixed3 Type: Symmetry/Antisymmetry/Encastre

*Boundary

fixed3, ENCASTRE

** Name: push-in Type: Displacement/Rotation

*Boundary, amplitude=push-in

top, 2, 2, -5.3

** Name: xsymm Type: Symmetry/Antisymmetry/Encastre

*Boundary

axis, XSYMM

** INTERACTIONS

** Interaction: bonecontact

*Contact Pair, interaction=selfcontact, mechanical constraint=KINEMATIC,

cpset=bonecontact

bone2bottom, bone1top

** Interaction: interference 1

*Contact Pair, interaction=friction, mechanical constraint=KINEMATIC,

cpset=interference 1

bone1surf, fsurf

** Interaction: interference 2

*Contact Pair, interaction=friction, mechanical constraint=KINEMATIC,

cpset=interference 2

bone2surf, fsurf

** Interaction: selfcontact1

*Contact Pair, interaction=selfcontact, mechanical constraint=KINEMATIC,

cpset=selfcontact1

selfcontact1surf,

** Interaction: selfcontact2

*Contact Pair, interaction=selfcontact, mechanical constraint=KINEMATIC,

cpset=selfcontact2

selfcontact2surf,

** Interaction: springsurf

*Contact Pair, interaction=friction, mechanical constraint=KINEMATIC,

cpset=springsurf

bone2top, springsurf

** OUTPUT REQUESTS

*Restart, write, overlay, number interval=1, time marks=NO

** FIELD OUTPUT: F-Output-1

*Output, field, variable=PRESELECT, number intervals=50

** HISTORY OUTPUT: H-Output-1

*Output, history, variable=PRESELECT, frequency=50

*End Step

2. Springback step

*Heading
**Surface definitions are not included for brevity as they are the same as in push-in step.
*IMPORT, STEP=1, STATE=YES, UPDATE=NO
fastener-1,bone1-1, bone2-1
*IMPORT ELSET
axis,top,fixed1,fixed2,fixed3,
bone1surf_S4,bone1surf_S1,bone1surf_S3,
bone1top_S1,bone1top_S3,bone1top_S4,
bone2bottom_S2,bone2bottom_S1,bone2bottom_S4,bone2bottom_S3,
bone2surf_S2,bone2surf_S4,bone2surf_S3,
bone2top_S2,bone2top_S1,bone2top_S4, bone2top_S3,
fsurf_S1,fsurf_S3,fsurf_S4,fsurf_S2,
selfcontact1surf_S4,selfcontact1surf_S2,selfcontact1surf_S1,selfcontact1surf_S3,
selfcontact2surf_S2,selfcontact2surf_S4, selfcontact2surf_S1,
springsurf_S1,springsurf_S3,springsurf_S2,springsurf_S4,
**
*IMPORT NSET
axis,spring,fixed1,fixed2,fixed3,top
**
*Surface, type=ELEMENT, name=bone1surf
*Surface, type=ELEMENT, name=bone1top
*Surface, type=ELEMENT, name=bone2bottom
*Surface, type=ELEMENT, name=bone2surf
*Surface, type=ELEMENT, name=bone2top
*Surface, type=ELEMENT, name=fsurf
*Surface, type=ELEMENT, name=selfcontact1surf
*Surface, type=ELEMENT, name=selfcontact2surf

*Surface, type=ELEMENT, name=springsurf

** Name: Xsymm Type: Symmetry/Antisymmetry/Encastre

*BOUNDARY, FIXED

axis, XSYMM

*BOUNDARY, FIXED

fixed1, ENCASTRE

*BOUNDARY, FIXED

fixed2, ENCASTRE

*BOUNDARY, FIXED

fixed3, ENCASTRE

*BOUNDARY, FIXED

spring, 2,2

** INTERACTION PROPERTIES

*Surface Interaction, name=friction

1.,

*Friction, slip tolerance=0.005

0.2,

*Surface Interaction, name=selfcontact

1.,

*Friction

0.,

** INTERACTIONS

** Interaction: bonecontact

*Contact Pair, interaction=selfcontact

bone1top, bone2bottom

** Interaction: interference 1

*Contact Pair, interaction=friction

fsurf, bone1surf

** Interaction: interference 2

```
*Contact Pair, interaction=friction
fsurf, bone2surf
**Interaction: selfcontact1
*Contact Pair, interaction=selfcontact
selfcontact1surf,
** Interaction: selfcontact2
*Contact Pair, interaction=selfcontact
selfcontact2surf,
** Interaction: springsurf
*Contact Pair, interaction=selfcontact
springsurf, bone2top
*RESTART, WRITE, OVERLAY, FREQ=10
*STEP, name=springback, NLGEOM, INC=100
*STATIC
.05,1
** OUTPUT REQUESTS
** FIELD OUTPUT: F-Output-1
*Output, field, variable=PRESELECT
** HISTORY OUTPUT: H-Output-1
*Output, history, FREQ=99
*ENERGY OUTPUT, VAR=ALL
*End Step
```

3. Pull-out step

*Heading

**Surface definitions are not included for brevity as they are the same as in push-in step.

*IMPORT, STATE=YES, UPDATE=NO

fastener-1,bone1-1, bone2-1

*IMPORT ELSET

axis,top,fixed1,fixed2,fixed3,

bone1surf_S4,bone1surf_S1,bone1surf_S3,

bone1top_S1,bone1top_S3,bone1top_S4,

bone2bottom_S2,bone2bottom_S1,bone2bottom_S4,bone2bottom_S3,

bone2surf_S2,bone2surf_S4,bone2surf_S3,

bone2top_S2,bone2top_S1,bone2top_S4, bone2top_S3,

fsurf_S1,fsurf_S3,fsurf_S4,fsurf_S2,

selfcontact1surf_S4,selfcontact1surf_S2,selfcontact1surf_S1,selfcontact1surf_S3,

selfcontact2surf_S2,selfcontact2surf_S4, selfcontact2surf_S1,

springsurf_S1,springsurf_S3,springsurf_S2,springsurf_S4,

**

*IMPORT NSET

axis,spring,fixed1,fixed2,fixed3,top

**

*Surface, type=ELEMENT, name=bone1surf

*Surface, type=ELEMENT, name=bone1top

*Surface, type=ELEMENT, name=bone2bottom

*Surface, type=ELEMENT, name=bone2surf

*Surface, type=ELEMENT, name=bone2top

*Surface, type=ELEMENT, name=fsurf

*Surface, type=ELEMENT, name=selfcontact1surf

*Surface, type=ELEMENT, name=selfcontact2surf

```
*Surface, type=ELEMENT, name=springsurf
*Amplitude, name=Pull-out, definition=SMOOTH STEP
0., 0., 500., 1.
** INTERACTION PROPERTIES
*Surface Interaction, name=friction
*Friction
 0.07,
*Surface Interaction, name=selfcontact
*Friction
0.0,
** BOUNDARY CONDITIONS
*BOUNDARY, FIXED
axis, XSYMM
*BOUNDARY, FIXED
fixed1, ENCASTRE
*BOUNDARY, FIXED
fixed2, ENCASTRE
*BOUNDARY, FIXED
fixed3, ENCASTRE
*BOUNDARY, FIXED
spring, 2,2
** STEP: Pull-out
*Step, name=pull-out
*Dynamic, Explicit
, 500.
*Bulk Viscosity
0.06, 1.2
** BOUNDARY CONDITIONS
** Name: Pull-out Type: Displacement/Rotation
```

*Boundary, amplitude=pull-out

top, 2, 2, 5.3

** INTERACTIONS

** Interaction: bonecontact

*Contact Pair, interaction=selfcontact, mechanical constraint=KINEMATIC,

cpset=bonecontact

bone2bottom, bone1top

** Interaction: interference 1

*Contact Pair, interaction=friction, mechanical constraint=KINEMATIC,

cpset=interference 1

bone1surf, fsurf

** Interaction: interference 2

*Contact Pair, interaction=friction, mechanical constraint=KINEMATIC,

cpset=interference 2

bone2surf, fsurf

** Interaction: selfcontact1

*Contact Pair, interaction=selfcontact, mechanical constraint=KINEMATIC,

cpset=selfcontact1

selfcontact1surf,

** Interaction: selfcontact2

*Contact Pair, interaction=selfcontact, mechanical constraint=KINEMATIC,

cpset=selfcontact2

selfcontact2surf,

** Interaction: springsurf

*Contact Pair, interaction=friction, mechanical constraint=KINEMATIC,

cpset=springsurf

bone2top, springsurf

** OUTPUT REQUESTS

*Restart, write, overlay, number interval=1, time marks=NO

** FIELD OUTPUT: F-Output-1

*Output, field, variable=PRESELECT, number intervals=50

** HISTORY OUTPUT: H-Output-1

*Output, history, variable=PRESELECT, frequency=50

*End Step

VITA

Name: Mukul Mukund Agnihotri

Address: 27/2, Parvati Apartments, Erandawane, Pune 411004
                   India

Forwarding   MnM Lab, Texas A&M University
Address: MS 3367, College Station, Texas 77843-3367, USA

Email address: mukul.agnihotri@gmail.com

Education: M.S., Mechanical Engineering, Texas A&M University,
                   December 2005
                   B.Eng., Mechanical Engineering, University of Pune, India
                   July 2003

Experience: Graduate Teaching Assistant, Department of Engineering
                   Technology, Texas A&M University
                   (September 2004-May 2005)